SCUOLA DI DOTTORATO
UNIVERSITÀ DEGLI STUDI DI MILANO-BICOCCA

Department of

INFORMATICA, SISTEMISTICA E COMUNICAZIONE

PhD program in COMPUTER SCIENCE
Cycle 29°

A Biophysically Detailed Cerebellar Stellate Neuron Model Optimized with Particle Swarm Optimization Algorithm

MARTINA FRANCESCA RIZZA

Registration number 068430

Supervisor: Professor Egidio D'Angelo

Supervisor: Professor Marco Antoniotti

Tutor: Professor Giancarlo Mauri

Coordinator: Professor Stefania Bandini

Reader: Ph.D. Alex Graudenzi

Reader: Ph.D. Stefano Masoli

ACADEMIC YEAR 2016/2017

Index

List of abbreviations

aa - Ascending Axon

AIS - Axon Initial Segment

AMPA - α-amino-3-hydroxy-5-methyl-4-isoxazolepropionic acid

BC - Basket Cell

Ca^{2+} - Calcium

CNS - Central Nervous System

cf - Climbing Fiber

CPU - Central Processing Unit

DCN - Deep Cerebellar Nuclei

E_{rev} - Reversal Potentials

ECM - Extracellular Matrix

eFEL - Electrophys Feature Extraction Library

EGL - External Granular Layer

GA – Genetic Algorithm

GABA - Gamma-Aminobutyric Acid

GCL - Granular Cell Layer

GoC - Golgi Cell

GPU - Graphic Processing Unit

GrC - Granule Cell

HCN - Hyperpolarization-Activated Cyclic Nucleotide-Gated

HH - Hodgkin and Huxley

HPC - High Performing Computing

I/O – Input-Output Relationship Curve

IF - Integrate and Fire

IGL - Internal Granular Layer

IO - Inferior Olive

K^+ - Potassium

KO – Knock Out

LC - Lugaro Cell

LRL - Lower Rhombic Lip

LTD - Long- Term Depression

LTP – Long-Term Potentiation

$G_{i\text{-}max}$ - Maximum Ionic Conductance

mf - Mossy Fiber

ML - Molecular Layer

MLI - Molecular Layer Interneuron

MPI - Message Passing Interface

Na^{+} - Sodium

Na_t - Sodium Transient Current

Na_p - Sodium Persistent Current

Na_r - Sodium Resurgent Current

NMDA - N-methyl-D-aspartate

NTZ - Nuclear Transitory Zone

ODE - Ordinary Differential Equations

P – Postnatal Day

PC - Purkinje Cell

PCL - Purkinje Cell Layer

PCN - Pre-Cerebellar Nuclei

PCP - Purkinje Cell Plate

PE - Parameter Estimation

pf - Parallel Fiber

PNS - Peripheral Nervous System

PSO - Particle Swarm Optimization

RLS - Rhombic Lip Migratory Stream

SC - Stellate Cell

Shh - Sonic Hedgehog

SI - Swarm Intelligence

SS - Simple Spike

θ - Parameterization

UBC - Unipolar Brush Cell

URL - Upper Rhombic Lip

VZ - Ventricular Zone

List of Figures

List of Tables

Introduction

The primary focus of my research is the modeling and simulation of some of the key biophysical properties of cerebellar neurons.
Chapter 1 includes a brief overview of the different types of models of (i) single neuron and (ii) network of neurons, based on different mathematical formalisms. Computational models of neurons are used to describe and simulate complex biological processes, which can be investigated both from the qualitative and from the quantitative perspective via powerful computational infrastructures, hence providing a valuable support for neuroscientists and experimentalists in general. In particular, I will focus on conductance-based models, based on *Hodgkin and Huxley* (HH) mathematical description and spiking neuron models, based on *Integrate and Fire* (IF) theory. Then, I will report the results of my research on models of the cerebellar neurons, which have a broad range of potential applications.

The first part of the thesis describes the reconstruction of the multi-compartmental model of the cerebellar S*tellate Cell* (SC). Chapter 2 provides the details on the development of a new single neuron model, which is the first reconstruction of a SC neuron modeled with the HH notation. The model is a multi-compartment, conductance-based model composed by a 3D reconstructed morphology divided in several sections (i.e., soma, axon, *Axon Initial Segment* (AIS), proximal dendrites and distal dendrites). The kinetics of each ionic channel, located on the cellular membrane, are based on experimental data. The model reproduced the main electrophysiological properties of the SC, and allowed to achieve relevant results. Moreover, the model provided a novel description of the gap junctions functioning and the synaptic activity, which are fundamental to regulate the SC firing properties and the synaptic transmission.

Yet, the most advanced models to reproduce the correct neuronal dynamics are based on the HH theory and require the fine-tuning of a large number of parameters, which are the *Maximum Ionic Conductance* ($G_{i\text{-}max}$). The definition of appropriate $G_{i\text{-}max}$ values, for each section of the morphology, is, in fact, a complex task, as they cannot be experimentally determined. Therefore, the value of the parameters must be assigned during the modeling phase and accurately validated afterwards. Accordingly, the creation of conductance-based models requires a lot of information about the location and nature of ionic channels (i.e., *Sodium* (Na^+), *Calcium* (Ca^{2+}), *Potassium* (K^+) and others ionic species). It is also a time-consuming and error-prone task, because of the manual calibration of $G_{i\text{-}max}$ parameters for each channel. In order to explore the huge parameter space of single-neuron models, it is possible to exploit numerical optimization techniques, which are able to automatically estimate the most fitting $G_{i\text{-}max}$ values, with the goal of obtaining neuron models that can reproduce the desired electro-physiological behavior. Therefore, the second part of the thesis, described in Chapter 3, investigates the approach based on an automatic *Parameter Estimation* (PE) method, which exploits the *Swarm Intelligence* (SI) optimization technique known as *Particle Swarm Optimization* (PSO). PE of the $G_{i\text{-}max}$ values of a neuron model is a fundamental and very complex task in Computational Neuroscience, and the interest of neuroscientist in this area has progressively increased in the last decade. The investigation of this complex problem is

made possible by the recent development of *High Performing Computing* (HPC) techniques that allows development of specific procedures aimed at the automated fine calibration of the parameters.

PSO was applied to the cerebellar SC neuron model to estimate the $G_{i\text{-}max}$ parameters by designing different fitness functions based on target traces. The efficiency of the method was tested by evaluating the correct balance of parameters that were able to reproduce spontaneous firing behavior of the neurons, and this lead to very promising results. The methodology proposed relies on the execution of a massive number of simulations, whose computational costs are relevant. To reduce the overall running time, the methodology was implemented on a parallel architecture (i.e., a cluster) and by developing sophisticated and efficient software architectures.

The third part of the thesis, in Chapter 4, aims at reviewing a challenging area of neuronal development, focusing on the primary stages of the cerebellar neuronal development. The cerebellar development is a complex biological process that requires the interaction between biochemical and biophysical mechanisms. Many aspects of development, such as neurons differentiation, proliferation and migration, axon and dendritic growth as well as synapses formation and stabilization, were extensively described with experiments in both the brain and the cerebellum, but only some of these aspects were described with computational models. Many models describe specific neurogenesis and axonal connectivity in the cerebral cortex, hippocampus, olfactory bulb and spinal cord. Currently, there are no single models which are specifically built to explain the cerebellar neurogenesis and synaptogenesis. The frameworks used to build the aforementioned methods could be applied to the cerebellum. Therefore, in this chapter, I will review the latest experimental discoveries about the cerebellum, the available models and the latest tools to model the development of the cerebellar network as a self-constructing process. These will be applied to the creation of a new framework, which will model all key properties of the cerebellum structure and dynamics.

Chapter 1

1. Computational Models of Neuronal Activity

Neurons, from a biochemical and biophysical point of view, are the most complex cells of the entire human body. Neuronal functions depend critically on their ionic channels, membrane proteins expressed in hundreds of subtypes and selectively distributed in specific sections of their cell body. As with all the other cell types, their cytoplasm is endowed with an intricate network of intracellular regulatory systems (Koch et al., 1999).

A model can be defined as a representation of the reality or part of it, but with an extensive range of limitations. The typical biological model, the animal model, used to understand physiological, biochemical and biophysical processes in a laboratory is based on the use of mice, rats and in some cases cats and monkeys. This is supported by the assumption that these animals are so similar to humans to offer a comparable model of what can be seen in humans, since the latter cannot be studied in all the possible variations (Seok et al., 2013). To overcome some of the limitations imposed by the use of the animal models, it was decided to increase and take advantage of the computational power to build more accurate models of cells and additionally to experiment in a controlled environment, reducing the dependency on the animal models.

My research thesis focuses on the modeling of biophysical properties of cerebellar neurons. The computational models of single neurons are mathematical descriptions used to describe specific biological processes, for example, how action potentials are initiated and propagated. The models are used: 1) to reproduce the electrophysiological properties of a specific neuron; 2) to describe properties that are not observable with experiments (for example, recording from axon and dendrites); 3) to predict properties that can be reproduced with experiments at a later time (D'Angelo et al., 2001a; Masoli et al., 2015; Masoli and D'Angelo, 2017; Solinas et al., 2007a; Subramaniyam et al., 2014); 4) to build networks with millions of neurons connected with spatial and connectivity rules (Lennon et al., 2014; Solinas et al. 2010; Yamazaki and Igarashi, 2013).

Detailed mathematical models of neurons are valuable means for the investigation of these cells. The model described in this work is a complex non-linear system for which simple, intuitive analytical solutions are not readily available. A computational model is an optimal tool to afford the analysis of this kind of complexity. The model proposed in this thesis, the SC neuron model, is described with systems of differential equations able to reproduce the dynamics of the ion flowing through the cellular membrane, reproducing the HH mathematical scheme (**Para. 1.1**). These equations are used to describe how the currents, generated by the ion flow, can produce action potential and its ability to propagate along a cable. The computational model represents the mathematical model, allowing a computer to construct numerical solutions of the cell response to injected currents or synaptic activity. Due to the complexity of the model, the study of simulated SCs electrophysiological behaviors requires potent computational resources.

The quality and accuracy of a neuronal computational model, versus the time/power to calculate it, is the main unresolved problem in this new field. Every detail added to a model requires more processing power and time to obtain results; so many modelers have decided to do a smaller reconstruction or to add fewer details to each neuron model. This has resulted in models only able to reproduce a limited number of behaviors.

Computational models, in the neuroscience field, represent an indispensable approach to test hypotheses and theories on the subject of interest and the range of feasible simulations directly depends on the accessible computational resources. Modeling systems at different scales of complexity, with different computational methodologies, is computationally challenging.

The SC neuron model requires an appropriate computational power, which could be limited to a single *Central Processing Unit* (CPU). The creation of a rich computational model capable of reproducing many different behaviours, is achieved with good quality data available (**Ch. 2**). Whereas the computational power required for the PE problem, applied to the SC model, is an important issue that regards the automatic estimation of unknown parameters. To understand the emergent behavior of a neuron, computational analyses generally require the inference of unknown $G_{i\text{-}max}$ values (not measurable with laboratory experiments). To respond to the huge computational power request for the PE problems and for the construction of neuronal networks composed by millions of neurons, the application of HPC techniques in the computational neuroscience field is necessary.

The thesis will describe the use of a distributed architecture for the PE of the SC model (**Ch. 3**). Parallel infrastructures can be used to strongly reduce the prohibitive running times required by these methods, by distributing the workload over multiple computing units. The design and development of parallel and distributed algorithms is a still a challenge to fully exploit the parallel infrastructures.

Since the most advanced models based on the HH theory require the fine-tuning of a large number of parameters, which are the $G_{i\text{-}max}$ values, and since this activity is generally performed by hand, in a time-consuming and error-prone process, approaches based on automatic procedures to estimate the unknown parameters were developed. Several studies used traditional optimization techniques based on *Genetic Algorithms* (GA) to estimate the unknown parameters of neuronal models (Druckmann et al., 2007, 2008, 2011).
In my project, I investigated a SI technique known as PSO to estimate the parameters of the cerebellar SC neuronal model, which showed promising results. Furthermore, thanks to HPC techniques, to reduce the computational costs, the fitness evaluations were accelerated with a cluster (**Ch. 3**).

Parallel and distributed computing is also necessary for the generation of large-scale computational models that allow studying the functional interaction of millions of neurons in a network. In this way, it is possible to contribute toward the achievement of real-time performance for neuronal network models, to study the network dynamics, understanding mechanisms that underlie

fundamental neuronal functions and processes, such as learning, memory consolidation and neuronal development. HPC techniques and *Graphic Processing Unit* (GPU) techniques, thanks to their high computational power, are required to achieve this goal.

1.1 Mathematical Models Description

The core mathematical framework for modern biophysically based neural modeling was developed by Hodgkin and Huxley (Hodgkin and Huxley, 1952) that unveiled the key properties of the $G_{i\text{-}max}$ values underlying the nerve action potential. The electrical properties of a neuron are represented in terms of an electrical equivalent circuit: capacitors are used to model the charge storage capacity of the cell membrane, resistors for the various types of ion channels embedded in membrane, and batteries to represent the electrochemical potentials established by differing intra and extracellular ion concentrations (**Fig. 1**).

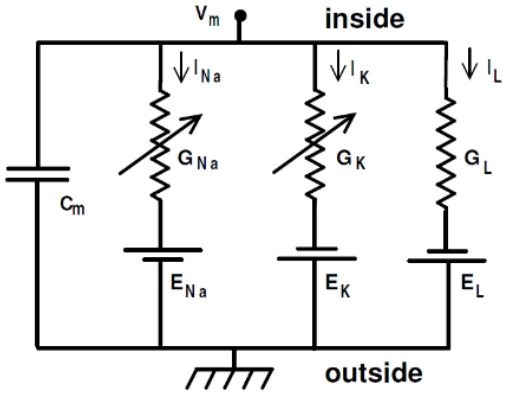

Fig. 1. Electrical equivalent circuit that represents the neuronal membrane (Hodgkin and Huxley, 1952).

The HH model is a conductance-based model, which describes, with a system of *Ordinary Differential Equations* (ODE), the behavior of each single channel and their interaction to generate and propagate action potentials.

Ionic channel activity was usually modeled following the HH formulation where, in each compartment, membrane voltage was obtained as the time integral of the equation:

$$\frac{dV}{dt} = -\frac{1}{C_m} * \left\{ \sum [g_i * (V - V_i)] + i_{inj} \right\} \quad (1)$$

Where V is the membrane potential, C_m the membrane capacitance, g_i are the ionic conductances, V_i the *Reversal Potentials* (E_{rev}) (the subscript i indicates different channels), and i_{inj} is the injected current.

The simulator NEURON uses cylindrical structures to define the geometry of each section. In this way, it can solve the cable equation for the membrane passive currents, and integrate the ionic channels and synaptic currents. A multi-compartmental neuron model is reconstructed with multiple compartments, to characterize the soma, the dendritic and the axonal trees with theirs

collaterals. The number of compartments depends on the dimension and morphological resolution of the neuron.

Adjacent compartments communicating through an internal coupling resistance. For each ionic channel *i*, the conductance g_i is:

$$g_i = Gmax_i * x_i^{zi} * y_i \quad (2)$$

Where $Gmax_i$ is the maximum ionic conductance, x_i and y_i are state variables (probabilities ranging from 0 to 1) for a gating particle, and z_i is the number of such gating particles. The gating particles are part of the conformational structure of the ionic channel and control the ion flow through the channel. When the ion flow moves in response to a change of membrane voltage, it causes conformational changes in the protein, opening and closing these gating particles.

The energy for channel gating comes from changes in the electrical potential difference across the membrane, and, these changes can open and close the voltage dependent channels.

These channels respond to the change in membrane potential by first going from a closed resting state to a transient open state, then they enters a prolonged refractory or inactivated state in which they are closed and incapable of being activated. Only after the potential difference across the membrane is restored to its original value, the channel recover from inactivation, returning to the resting state.

The gating particles of HH ionic channels have activation and inactivation time constants (τ) in ms. An example of activation and inactivation gating curves is shown for Ca^{2+} and K^+ channels in the Fig. 1 of the work of (Masoli et al., 2015).

The **Table 4** in the **Ch.2** reports the equations to calculate the rate constants, the conductances and the time constants of each ionic channel, following the HH scheme (D'Angelo et al., 2001a; Masoli et al., 2015; Masoli and D'Angelo, 2017; Solinas et al., 2007a; Subramaniyam et al., 2014).

The simplest model of a channel opening and closing has two states, closed (C) and open (O), and two rate constants, α and β, as shown the following scheme:

$$C \underset{\beta}{\overset{\alpha}{\rightleftharpoons}} O$$

The time constant (τ) is calculated as $\tau = \frac{1}{\alpha+\beta}$.

Real channels have more than two states and the general rule is that τ equals the reciprocal of the sum of all rate constants leaving the state (Armstrong, 1992; Armstrong and Hille, 1998; Kandel et al., 2013; Simms and Zamponi, 2014).

The theory developed by Lapique (Abbott, 1999; Brunel and van Rossum, 2007) was, instead, the base for the definition of IF models, also defined spiking neuron models. These models describe a system composed of a resistance and a capacitance, mimicking the cell membrane behavior. One of the advantages is the simplicity and computational efficiency (Burkitt, 2006), as the IF models are

simplified description of neurons, many details of the electrophysiology of neurons could be missed. This type of model is highly investigated and often used to study aspects of neural coding, memory, or network dynamics.
The total current that flows through the membrane is defined by the following equation:

$$I(t) = \frac{u(t)}{R} + C\frac{du}{dt} \tag{3}$$

The driving current can be split into two components $I(t) = I_R + I_C$. The first component is the resistive current I_R that passes through the linear resistor R. It can be calculated from Ohm's law as $I_R = u/R$ where u is the voltage across the resistor. The second component I_C charges the capacitor C. From the definition of the capacity as $C = q/u$ (where q is the charge and u the voltage), we find a capacitive current $I_C = C\,\mathrm{d}u/\mathrm{d}t$.

The neuron firing is defined by a threshold condition, in fact the model fires whenever the variable u reaches a threshold μ. After the firing, the membrane potential of the model is reset to a value u_{reset}. If the value u reaches the value μ, the neuronal dynamics is interrupted and the integration restarts with the new initial condition u_{reset}.

1.2 Software

To build a neuronal computational model it is necessary to have capable programs containing specific tools to construct complex 3D morphology of SCs, the connection between every section of the neuron, the location of specific ion channels on the membrane and the connectivity between the neurons to form a network. The fundamental characteristic of a model is the simulation of what occurs over time. Therefore, to see if a model is generating the required behaviours, the environment allows the simulations to be performed accurately, for example, when the injection of a current into the soma causes changes in the action potential generation.

The simulation environment used in this thesis is NEURON (version 7.3 and 7.4) (Hines et al., 2007, 2009). NEURON is described on the official site as “a simulation environment for modelling individual neurons and networks of neurons”. It provides tools for conveniently building, managing, and using models in a way that is numerically sound and computationally efficient. It is particularly well suited to problems that are closely linked to experimental data, especially those that involve cells with complex anatomical and biophysical properties (http://www.neuron.yale.edu/neuron/). The program is offered as an open source, which means that the code can be modified by anyone who wants to contribute to it. The program offers an integrate graphic interface but the most can be obtained only with the script language provided with it. The built-in programming language allows one to define every constituent of a model but it is difficult to learn, compared to other script languages. To resolve this problem, the author of NEURON, in 2009, decided to add Python support as an optional programming language and Python is now the main language for NEURON code development.

Python can be described as a general-purpose, interpreted high-level programming language whose design philosophy emphasizes code readability. Its' syntax is clear, expressive and has a large and comprehensive standard library. Python is a script language, which is highly extendible, simple and easy to use.

The model created in Python takes advantage of the many additional modules like Numpy and Scipy, which permit a better management of the mathematical part, to load and save files and to analyze the results.

The *Message Passing Interface* (MPI) for Python, named mpi4py, was used to support parallel simulations of the PSO optimizations, to estimate automatically the unknown parameters of the neuron models. Thanks to MPI it is possible to implement a methodology that can be used both on multi-core CPUs as well as on clusters.

1.3 Models of Biological Processes Applied to the Cerebellar Neurons

The models that describe the neuronal electrical activity are the most commonly studied models concerning the cerebellar activity. To explore the cerebellar neuron functioning I have studied the use of IF models and HH models to describe single neurons activity or complex network of multiple neurons respectively.

The IF approach is the most effective to reconstruct the extensive network composed of hundreds of thousands of simplified neuron models, capable of reproducing a large range of neuronal complex behaviors. Examples of this approach are the descriptions of the *Granule Cell* (GrC) model (Bezzi et al., 2004) and the *Purkinje Cell* (PC) model (Lynch and Houghton, 2013). Large-scale spiking networks of the cerebellum were created using IF models and simplified synapses, to reproduce the neuronal dynamics of the *Granular Cell Layer* (GCL) and of the *Molecular Layer* (ML) (Brette et al., 2007; D'Angelo et al., 2013; Garrido et al., 2013a; Kistler and De Zeeuw, 2003; Lennon et al., 2014; Medina and Mauk, 2000; Medina et al., 2000) and to study the interaction properties of high-level functions, such as working memory (Del Giudice et al., 2003) or typical cerebellar behaviors such as the delayed eye blink conditioning (Yamazaki and Tanaka, 2009).

The IF mathematical description is used for all the cerebellar network models reproduced with HPC techniques, on GPUs and with accelerated neuromorphic hardware systems (Bruederle et al., 2009). Thanks to these emergent techniques, developed recently in the computational neuroscience field, it is possible to do network simulations that run in real-time (Casellato et al., 2014; Garrido et al., 2013b; Indiveri et al., 2011; Li et al., 2013; Luque et al., 2011; Pfeil et al., 2013; Yamazaki and Igarashi, 2013).

Many studies about the cerebellar neuronal activity have been performed in the last 20 years using HH model descriptions. This approach was used preferably for the construction of a highly detailed single neuron models and less for network models, as their computational impact is demanding. The detailed mathematical description of each ionic current permits the clear definition of each

channel and permits the understanding of the ionic mechanisms underlying the neuronal activity, which, depending on the neuronal type, can have a different arrangement of ionic channels.

In the past 20 years, many detailed models of cerebellar single neurons, have been created beginning with one of the most well known, the PC (Bower, 2015; De Schutter and Bower, 1994a, 1994b; Masoli et al., 2015; Masoli and D'Angelo, 2017). The GrC received a lot of attention at the end of the '90s and in subsequent years, with a series of experimental studies used for the reconstruction of several models (D'Angelo et al., 2001; Diwakar et al., 2009; Nieus et al., 2006). The same principle was applied to the *Golgi cell* (GoC) models (Solinas et al., 2007a, 2007b; Szoboszlay et al., 2016; Vervaeke et al., 2010), to the *Unipolar Brush Cell* (UBC) model (Subramaniyam et al., 2014), to the *Inferior Olive* (IO) models (De Gruijl et al., 2012; Torben-Nielsen et al., 2012) and to the *Deep Cerebellar Nuclei* (DCN) models (Luthman et al., 2011; Steuber et al., 2011). All these models reproduced the most important electro-responsive properties of the neurons.

One of the first examples of GCL network reconstruction was with biophysical detailed mono-compartmental neurons built in 1998 to test the inhibitory activity of the GoCs with respect to GrC, mf and pf excitatory input (Maex and De Schutter, 1998). A large-scale network based on HH models, distributed in a 3D environment, was built in 2010 (Solinas et al., 2010), where mono and multi compartmental models of GrC and GoC, with equivalent morphologies were distributed in a 3D volume and connected with synapses based on statistical information.

1.4 The Cerebellum

The cerebellum is part of the *Central Nervous System* (CNS), it is located behind the brain stem and occupies nearly all the space of the posterior cranial fossa. For a century, the cerebellum was acknowledged to be involved only in the motor and coordination control (Ito, 2008) but, in recent years, it has been proved that it is involved in higher cognitive functions like attention, language skills and motion perception (Leroi et al., 2002). The involvement of this organ in specific disease, such as Alzheimer and Parkinson and other neurodegenerative pathologies has only recently been proved experimentally (Larner, 1997; Lefaivre et al., 2016; Mirdamadi, 2016; Sjöbeck and Englund, 2001; Wu and Hallett, 2013).

The main part of the cerebellum is the cortex, which resembles the highly folded hemispheres of the brain cortex and it shares a similar subdivision into layers composed of specific cellular types. From an operative point of view, the brain can be divided into functional columns whereas the cerebellum can be divided into functional modules (Sotelo, 2004). The cerebellum contains a dozen neuronal types divided in two categories, the excitatory (*Glutamatergic*) and inhibitory (*GABAergic and Glycinergic*) neurons (Altman and Bayer, 1997). The excitatory neurons release glutamate neurotransmitter, which binds to its specific *α-amino-3-hydroxy-5-methyl-4-isoxazolepropionic acid* (AMPA) and *N-methyl-D-aspartate* (NMDA) receptors, while the inhibitory neurons release *Gamma-Aminobutyric Acid* (GABA) neurotransmitter. The most abundant excitatory neurons are the GrCs that account for over 60% of the total neurons of the CNS (Herculano-Houzel, 2010) and the UBCs, which are sparsely distributed throughout the lobuli from I to VIII and in a major number in the lobuli IX and X. The main inhibitory neuron is the PC, whereas the inhibitory interneurons are the

GoCs and *Lugaro Cells* (LC), located in the GCL, and the SC, *Basket Cells* (BC) are located in the ML (**Fig. 2**). The cerebellum constitutes only 10% of the total volume of the CNS but contains over half of all the neurons in the central nervous system.

The neuronal information theory concerns the relation between the electrical activity of neurons, in response to specific stimuli, and the quantity of information that can be processed together into the neuronal network (Bialek and Rieke, 1992; Quiroga and Panzeri, 2009; Yarrow et al., 2012) This phenomenon is sustained by the transmission of very fast electrical signals over large distances, through action potentials, and their transformation in chemical signal in the synapses, which connect each neuron. The flow of the elaboration, made by the network, starts with the GCL, which receives the *Mossy Fibers* (mf), originating from the *Pre-Cerebellar Nuclei* (PCN), (e.g., the vestibular and pontine nuclei). Each mf makes a multitude of synapses with GrC dendrites and Goc axons inside the *Glomeruli* (Rossi et al., 2003). The information is elaborated and transmitted to the ML where it is distributed to the extensive PC dendritic tree. These neurons, which form the *Purkinje Cell Layer* (PCL), are the only exit pathway from the network and are responsible for the integration of all the input into a single output. Their intrinsic properties, such as spontaneous firing, is modulated by the information coming from the GCL, the *Molecular Layer Inhibitory Interneurons* (MLI), SC and BC cells and from the IO. This latter nucleus generates the second excitatory pathway, which conveyed by the *Climbing Fibers* (cf), controls the error signal degree. The responses of many synchronous PCs are transmitted to the DCN, where the inhibitory activity, in conjunction with excitatory collaterals from IO and PCN, are integrated into a single outputs sent to the red nucleus, the thalamus and the motor cortex (**Fig. 3**).

Even though some of the cerebellar cells have already been discovered (PC, GoC, LC), the actual structure of the network was firstly described in the early 1900s by Cajal, with an accurate description of cerebellar development, providing the fundamentals for successive studies of cell migration, neuronal differentiation, and synaptogenesis. The analyses of cerebellar development have increased the knowledge of cellular and molecular mechanisms that regulate the assembly of synaptic circuits, but detailed quantitative information is still not available for the whole cerebellum, and the definition of the spatiotemporal dynamics of synaptic development is still fragmentary (Sassoè-Pognetto and Patrizi, 2013).

Cerebellum Functional Subdivisions

The cerebellum can be divided into three main computational areas based on the origin of the afferent fibers (Kandel et al., 2013):

- The largest subdivision that occupies most of the lateral hemisphere in humans and primate is the cerebrocerebellum. It receives input from many areas of the cerebral cortex and is concerned with the regulation of highly skilled movements, especially the planning and execution of complex spatial and temporal sequences of movement (including oral communication).

- The oldest part is the vestibulocerebellum. The caudal lobes, the flocculus and the nodulus are parts of this section and they receive input from the vestibular nuclei in the brainstem. Its primary goal is the regulation of movements underlying posture and equilibrium.
- The last of the major subdivisions is the spinocerebellum. It occupies the median and paramedian zone of the cerebellar hemispheres and is the only part that receives input directly from the spinal cord. The lateral part controls the movements of distal muscles similar to the limb movement while walking. The central part, called the vermis, controls the movements of proximal muscles and regulates eye movements in response to vestibular inputs.

The cerebellar peduncles connect the CNS and the *Peripheral Nervous System* (PNS) with the cerebellum and from the cerebellum to the cerebral cortex:

- The inferior cerebellar peduncle (or restiform body) is the smallest but most complex of the cerebellar peduncles, containing multiple afferent and efferent pathways. The afferent pathways include axons from the vestibular nuclei, the spinal cord, and several regions of the brainstem tegmentum. The main tracts include the olivocerebellar, paraolivocerebellar, vestibulocerebellar, reticulocerebellar, posterior spinocerebellar, cuneocerebellar, and trigeminocerebellar. The efferent pathways in this peduncle project to the vestibular nuclei and the reticular formation and include the cerebelloolivary, cerebellovestibular, and cerebelloreticular tracts.
- The middle cerebellar peduncle (or brachium pontis) is mainly an afferent pathway; most of the cell bodies are in the base of the pons, where they form the pontine nuclei, which receive input from a wide variety of sources, including almost the entire cerebral cortex and the superior colliculus. The axons of the pontine nuclei, called transverse pontine fibers, cross the midline and enter the cerebellum as the pontocerebellar tract. The two middle cerebellar peduncles contain over 20 million axons each and are thus among the largest pathways in the brain. In comparison, the optic and pyramidal tracts contain only about a million axons.
- The superior cerebellar peduncle (or brachium conjunctivum) is almost entirely an efferent pathway. The neurons that give rise to this pathway are in the DCN and their axons project to upper motor neurons in the red nucleus, the deep layers of the superior colliculus, and after, a relay in the dorsal thalamus, the primary motor and premotor areas of the cortex. The afferences to the cerebellum are the anterior spinocerebellar tract, which works in parallel with the posterior spinocerebellar tract, to convey the subconscious proprioceptive information from the body to the cerebellum and the Tectocerebellum. The efferent path *comprises of the Cerebellorubral, Dentatothalamic and the Fastigioreticular fibers.*

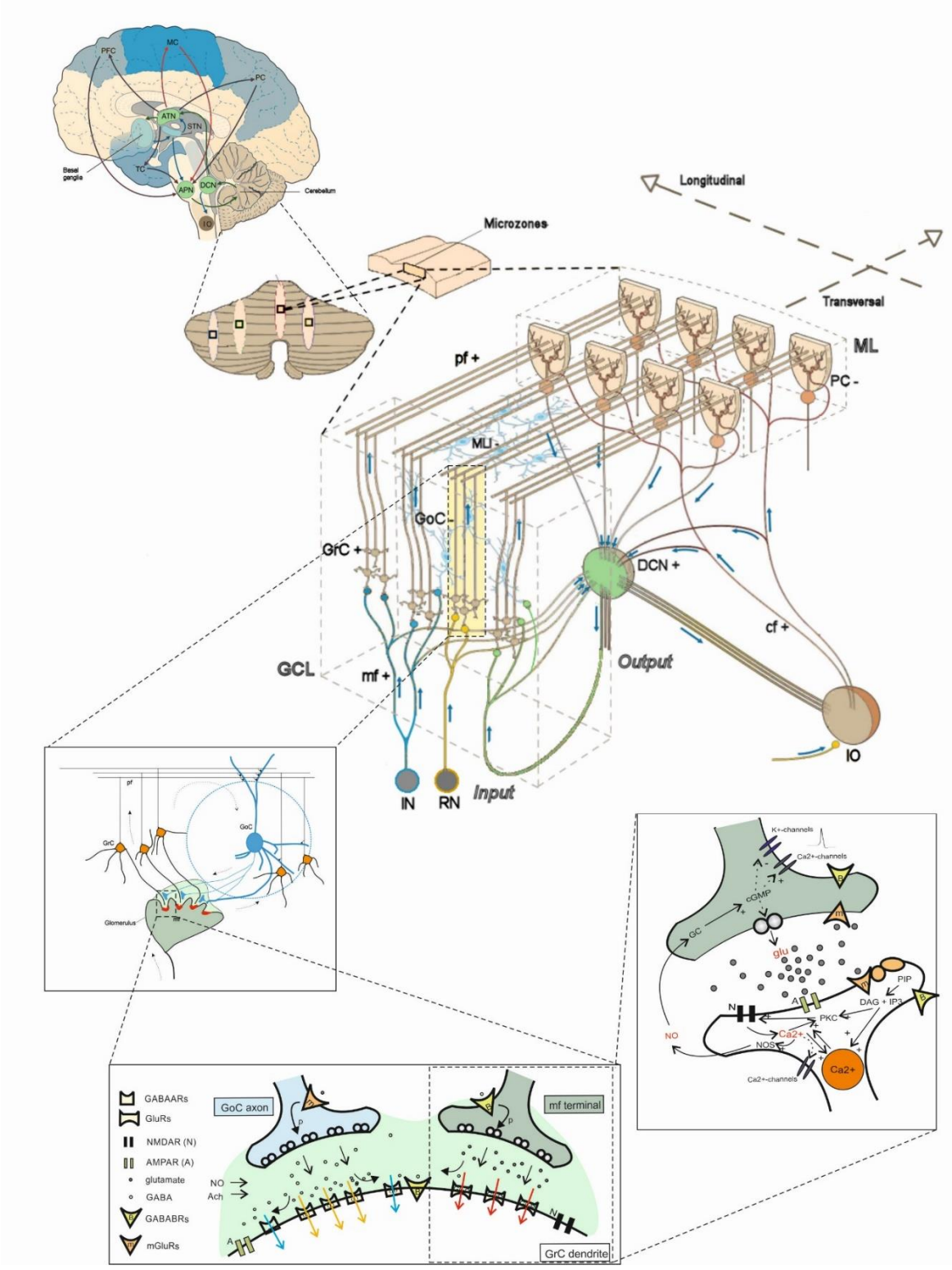

Fig. 2. Cerebellar complex organization (D'Angelo et al., 2016a).

The figure shows the multi-level organization of the cerebellum. The first illustration above shows the circuits that connect the cerebellum with the cerebral cortex (PFC, prefrontal cortex; MC, motor cortex; PC, parietal cortex; TC, temporal cortex) through the DCN, the anterior thalamic nuclei (ATN) and the anterior pontine nuclei (APN). The connections with the basal ganglia (BG) and subthalamic nucleus (STN) are also indicated.

The central part of the figure outlines the subdivision of the cerebellum in functional micro-zones. Three layers compose each micro-zone. The GCL is composed of the GrCs, GoCs and LCs. The ML consists of SCs, BCs and PC dendritic tree and the PCL consists of the PC soma. The close-up below the figure displays in detail the connectivity of the GCL, the formation of the glomeruli, their neurotransmission and synaptic transduction mechanisms.

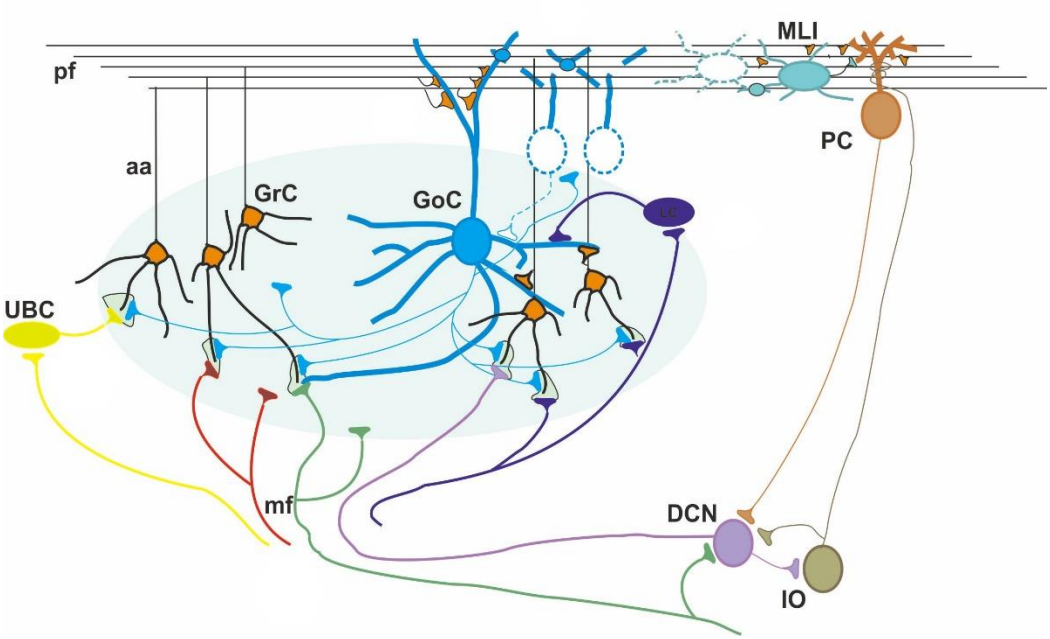

Fig. 3. Cerebellar circuit (D'Angelo et al., 2016a).

The cerebellum contains numerous modules, each of which is made up of uniformly structured neuronal circuits. This schematic view shows the main architecture of the cerebellar circuit. The input from the mf arrives in the GCL, exciting the GrCs in the glomeruli. The glomeruli receive inhibition by the GoCs, which are inhibitory interneurons. The pfs originating from GrCs make synaptic in the GCL, exciting the GoCs, and in the ML, exciting the PCs and the MLIs (SCs). The MLIs (SCs), which are the inhibitory interneurons of the ML, inhibit the PC. The cfs connect the IO with the PCs, providing an excitatory input to the cerebellar circuit. While the PCs provides the only inhibitory output of the entire cerebellar cortex, connecting to the DCN.

1.5 Review: "Modeling the Cerebellar Microcircuit: New Strategies for a Long-Standing Issue"

For further details about the different types of model approaches, see the review: "Modeling the cerebellar microcircuit: new strategies for a long-standing issue" (Egidio D'Angelo, Alberto Antonietti, Stefano Casali, Claudia Casellato, Jesus A. Garrido, Niceto Rafael Luque, Lisa Mapelli, Stefano Masoli, Alessandra Pedrocchi, Francesca Prestori, **Martina Francesca Rizza**,

and Eduardo Ros. Frontiers in Cellular Neuroscience, 2016), (see **Appendix 1.,** D'Angelo et al., 2016a).

1.6 Book chapter: "Single-Neuron and Network Computation in Realistic Models of the Cerebellar Cortex"

For additional clarifications about the cerebellar models, see the chapter: "Single-neuron and network computation in realistic models of the cerebellar cortex" from the book: " The neuronal codes of the cerebellum" (Egidio D'Angelo, Stefano Masoli, **Martina Francesca Rizza**, Stefano Casali. Elsevier, 2016), (see **Appendix 2.,** (D'Angelo et al., 2016b)).

Chapter 2

2. A Biophysically Detailed Cerebellar Stellate Neuron Model

SCs were observed initially by Ramon y Cajal, using the Golgi stain method, which act as inhibitory interneurons in the ML of the cerebellum. Their morphology consists of a stellate body with numerous dendrites and a large plexus of axon collaterals. The neuroscientist observed also the GoCs in the GCL, defining GoCs, SCs and BCs inhibitory interneurons short-axoned neurons. Ramon y Cajal, during his experimental observations, distinguished between smaller SCs, that are concentrated in the deepest part of the ML, and larger SCs located in the more superficial part of the ML (Palay and Chan-Palay, 1974).

Based on his work, the MLIs were divided into two types of GABAergic interneurons, the BCs and SCs. Even though SCs have the same progenitor as the BCs, they show distinct activity and different ionic channels distribution. The progenitors of both cells originate in the *Ventricular Zone* (VZ) and during their migration, from the birthplace, the MLIs are morphologically indistinguishable. From VZ they migrate radially toward the *Internal Granular Layer* (IGL) and the *Purkinje Cell Layer* (PCL) to reach the ML, their final destination. MLIs achieve their definitive location, between P7 and P21, with the stabilization of reciprocal gap junction contacts and reciprocal inhibitory connectivity (Pouzat and Hestrin, 1997). The VZ is also the birthplace for the GoC inhibitory interneurons that will be reach their final location in the GCL (Leto et al., 2006, 2016).

The ML is composed of GrC axons - *Ascending Axons* (aa) and pfs - that make synaptic contacts, at the same time, with PC, GoC, BC and SC dendrites. As the SCs are located in the more superficial region of the ML, they receive excitatory inputs from pfs and their branched unmyelinated axon makes synapses with the spiny part of PC dendrites and with other local SCs. The BCs, instead, are located in the deepest ML and make synapses with the PC soma and AIS.

Several studies showed that the MLIs are influenced by the strong excitatory activity of the cf (Szapiro and Barbour, 2007). It was observed that the excitation was exclusively performed via spillover from neighboring cf-PC synapses (Szapiro and Barbour, 2007). The underlying synaptic mechanisms between cfs and SCs were not well characterized, but the absence of vesicles of neurotransmitter suggests that does not occur in the classical synaptic plasticity. This mechanism allows the glutamatergic transmission and it is involved in the synaptic plasticity control. It is known that the cfs direct the pfs synaptic plasticity and the spillover of glutamate from cfs amplify this form of synaptic plasticity. To further increase the control on PCs, it was observed that multiple cfs contact a single interneuron, activating AMPA and NMDA receptors on interneurons only via spillover. The cf input to SCs is excitatory and the result of SCs activation is the inhibition of the ML and the PC.

Studies showed that the axons of the MLIs contact also GoC dendrites with a more profound impact of SCs than BCs, in the generation of GoC firing pauses (Holtzman et al., 2006). However, other

discoveries showed that the SC axons very rarely contact GoCs (Eyre and Nusser, 2016) and that the SC activity does not modulate the GoC activity at all (Hull and Regehr, 2012).

The SC inhibitory activity, in the cerebellar network, plays a critical role in the modulation of the spontaneous activity of PCs. It was suggested that these neurons control the timing and spatial patterning of neighboring PCs with the generation of a synchronization mechanism to increase the overall activity on the DCN.

SCs with their inhibitory activity play an important role to understand learning and functions of the synaptic activity that connect the ML microcircuits (Jorntell et al., 2010). The description of SC behavior includes overall the analysis of different electrophysiological mechanisms such as the excitatory synaptic responses in SCs, the reciprocal inhibition between SCs, the cellular firing patterns, the plasticity of pf synapses on SCs and the plasticity of SC to PC synapses.

2.1 Stellate Neuron Model

A biophysical reconstruction of SC, based on realistic morphology, was constructed using a multi-compartmental conductance-based model approach, to reproduce the SC critical electro-physiological properties observed in experimental recordings *in vivo* and *in vitro*, such as the auto-rhythmic activity, the linear *input-output* (I/O) relationship obtained with increasing current injections, the inward rectification mechanism as a result of negative current injections, the gap junction modulation and the synaptic integration in the ML.

Starting from a broad range of published experimental observations, I have constructed a biophysically realistic SC model using Python-NEURON. The human morphology, taken from NeuroMorpho.Org DB, consists of a branched dendritic tree, a soma, an *Axon Initial Segment* (AIS), and a branched axon with collaterals. The ionic channels were taken from a published PC model (Masoli et al., 2015) and distributed, on the morphology, based on the available literature (**Para 2.2.1.2 and Tab. 2**). They are Na^+ channels (Nav1.1 and Nav1.6), K^+ channels (Kv1.1, Kv7, Kv3.4, Kv4.3, Kir2.3), Ca^{2+} dependent K^+ channels (KCa1.1, KCa2.2), *High Voltage-Activated* (HVA) Ca^{2+} channels (P-type) (Cav2.1), *Low Voltage-Activated* (LVA) Ca^{2+} channels (Cav3.1, Cav3.2, Cav3.3), *Hyperpolarization*-A*ctivated Cyclic Nucleotide-Gated* (HCN) channels and the background leakage current (Leak).

The Na^+ channels in the soma expressed the *Transient* (Na_t) and *Persistent* (Na_p) components but not the *Resurgent* (Na_r) component (Nav1.1), which was however present in the AIS and axon (Nav1.6). The main potassium channels were Kv3.4, Kv4.3 and contributed to spike repolarization and firing pattern regulation. The Ca^{2+} and Ca^{2+}-dependent K^+ channels, including KCa1.1 and KCa2.2, as well as intracellular Ca^{2+} dynamics played a major role in spike repolarization. The model showed spontaneous firing with an average frequency of 14 Hz. The gap junctions (**Para. 2.2.1**) were able to synchronize coupled SCs and the firing behavior was modulated through GABAergic synapses coming from a network of SCs. I investigated the activity of the glutamatergic synaptic inputs from pfs and the GABAergic synapses between SCs as well as their activity on PCs. The AMPA and NMDA

synapses were modeled using a deterministic scheme whereas GABA synapses were described with a stochastic scheme.

The biophysical mechanisms of SC electro-responsiveness are described in detail in the model, providing a valuable tool to further investigate the SC function in cerebellar network models.

SC postsynaptic responses are generated both through direct release, from active zones onto corresponding postsynaptic receptors, and through spillover of glutamate from neighboring releasing sites. For AMPA receptors, glutamate concentration is obtained combining a synaptic pulse with a diffusion wave. In addition, NMDA receptors are activated by glutamate concentration and diffusion. The glutamate diffusion is modeled following the equation described in the paper of (Barbour, 2001)(Barbour, 2001)(Barbour, 2001)(Barbour, 2001)(Barbour, 2001).
The kinetic schemes used to model the AMPA receptor and the NMDA receptor are described in detail in the work of Nieus et al., 2006, specifically in the figure 5 of the paper (Nieus et al., 2006).

The AMPA receptor is a simple 3-state AMPA receptor kinetic scheme using a parameterization reported in the paper of (Saftenku, 2005).

Most of the NMDA current is determined by NMDA receptors with low open probability (Rossi et al., 2002), I adopted a corresponding kinetic scheme (Rosenmund et al., 1995), for cortical neuronal cultures, with two identical closed states and the desensitized state is entered from the second closed state.

GABA released from SC presynaptic terminal can act directly on receptors facing the postsynaptic site (fast direct component) or indirectly on extra synaptic receptors through spillover from neighboring sites (slow indirect component). Direct release from the presynaptic terminal activates α1 GABA-A receptors. Fast kinetics of the direct component are explained by rapid gating of α1-containing GABA-A receptors.

GABA release was implemented through a phenomenological 3-state model that reproduces well the synaptic dynamics. The scheme was governed by recovery rates and release probability from the reserve pool and its output was GABA release. The neurotransmitter concentration, [GABA], was modeled by summing a pulse to a diffusive term:

$$[GABA] = [GABA]_P + [GABA]_D \quad (4)$$

$[GABA]_P$ activates the receptors facing the releasing site, while $[GABA]_D$ accounts for GABA spillover (T. R. Nieus et al., 2014).

The α1 GABA-A receptor responses were reproduced using the kinetic scheme described in the Fig.2 of the paper of Nieus et al. 2014 (Nieus et al., 2014). The GABA-A receptor models are characterized by two desensitized, three closed and two open states. The kinetic rate constants used to simulate α1 GABA-A receptor are shown in the Table 3 of the paper of Nieus et al. 2014.

The voltage dependence of AMPA and NMDA receptors is modeled following the equation:

$$i = g * \Delta V = gmax * O(T) + (V - Vrev) \quad (5)$$

Glutamate binding to postsynaptic receptors, activates kinetic schemes governed by microscopic first-order transitions (see Fig. 6 and 7 - T. Nieus et al., 2006), leading to the open state, *O(T)*. *Vrev* is the ionic reversal potential, and *gmax* is the maximum synaptic conductance for either NMDA or AMPA channels.

The presynaptic dynamics is modeled following the Tsodyks and Markram (1997) three-state scheme (Tsodyks et al., 2000; Tsodyks and Markram, 1997).

The NMDA current of the SC model is modeled following the curve shown in the **Fig. 4**. The result of the equation 5, that reflects the curve shape, is multiplied for the Mg^{2+} block parameter (Kampa et al., 2004; Ruppersberg et al., 1994).

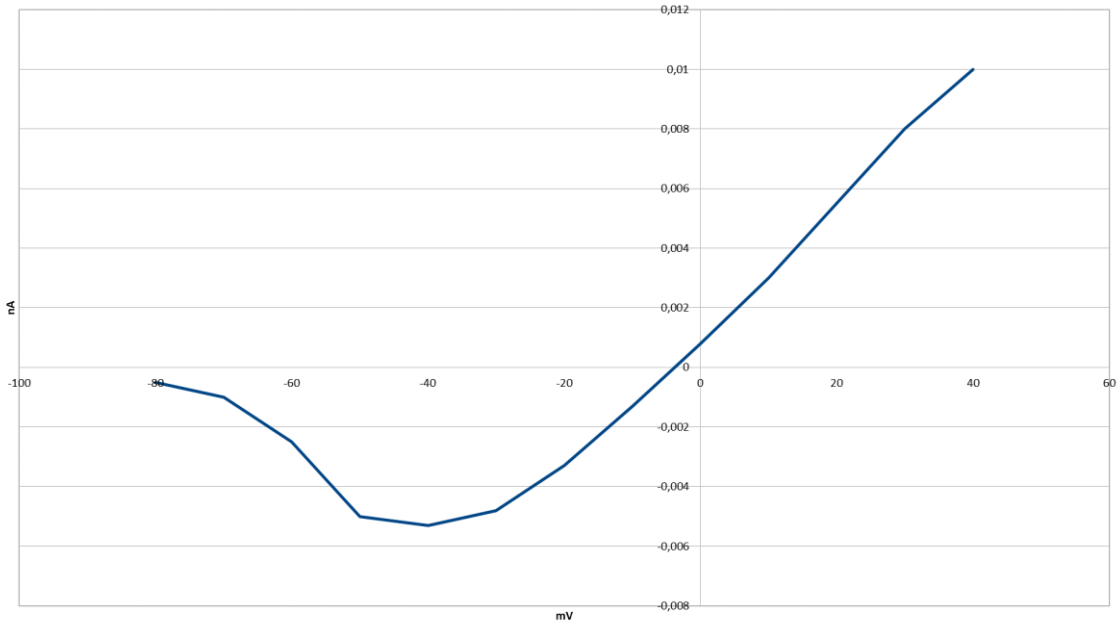

Fig. 4. NMDA current/voltage relation.

Firing Patterns

It was observed that the SC firing patterns recorded *in vivo* are irregular. This irregularity could be due to the irregularities in the firing of the afferent fibers. It was recently found the role of the cf in the SC firing pattern, increasing the spike firing of the interneurons and synchronizing their activity. Furthermore, this synchronization is enhanced by the reciprocal SC inhibition and the gap junction modulation.

Synchronized SC activity produces PC firing pauses during their inhibition.

It was observed that the pf excitatory quanta influenced the SC firing (Carter and Regher, 2002). Single synaptic inputs to MLIs consist of numerous quanta of neurotransmitter arising from multiple release sites that produce changes in the membrane potential and have a critical effect on the neuronal activity. It is important to investigate the mechanisms underlying the SC firing, given the complete activity of these interneurons have important effect for the entire cerebellar function. SCs direct the Ca^{2+} signals into PC dendrites, having a key role in the *Long-Term Potentiation* (LTP) and L*ong-Term Depression* (LTD) phenomena and guiding the PC electrical responses.

In the study of (Carter and Regher, 2002), it was observed that single inhibitory and excitatory quantal events influence the SC firing during the synaptic activity. Moreover, a few coincident excitatory quanta of neurotransmitter released are necessary to induce the SC firing and that the quanta of inhibitory neurotransmitters can modulate the results of the excitatory inputs on the neuronal activity.

Synaptic Plasticity

SCs have Ca^{2+}- permeable AMPA receptors activated by pf synaptic activity, but it was observed that these postsynaptic AMPA receptors could be reduced by repetitive pf stimuli, causing the LTD phenomenon. It was also demonstrated, in several studies, that the combination of cf and pf synaptic activity on interneurons induces LTP in these cells.

LTP depends on intracellular Ca^{2+} concentration and NMDA receptors, but LTD requires Ca^{2+} entry through the Ca^{2+}-permeable AMPA receptors. The NMDA receptors in interneurons are normally activated by the cf activity, for this reason, the combination of cf and pf activity could induce LTP and only activation of pfs could evoke LTD. The Ca^{2+} concentration assumes a key role for the synaptic plasticity and, as in the case of the PC, high intracellular Ca^{2+} levels induce LTD and low levels leads to LTP (Jorntell and Hansel, 2006).

Another form of plasticity exists at SC-PC synapses; this synaptic activity is potentiated in combination with the cf activity on PCs.

2.2 Methods

The multi-compartmental SC model was implemented using Python-NEURON (Python 2.7; NEURON 7.3; (Hines et al., 2007, 2009).

NEURON is a simulation environment for the creation of electrical signaling models of neurons and networks (Carnevale and Hines, 2006). The simulator uses algorithms that are highly efficient to solve the equations describing the neuronal properties. The main integration methods implemented are the implicit Euler, the Crank-Nicolson and CVODE for the variable time step integration. NEURON is capable of computing biophysical properties comprising: the spatial representation of neurons, with complex morphologies composed of thousands of sections; the fundamental membrane properties like *Axial Resistance* (Ra) and *Membrane Capacitance* (Cm); the ions channels

interactions. The complexity arising from this approach allows computing specific behaviors in a small time frame lasting usually for only seconds or minutes.

Simulations were performed on a 4 cores AMD FX 7500 CPU (8 GB ram) and on a single blade of a cluster, composed of 12 cores/24 threads (two Intel Xeon X5650 with 24 Gigabyte of DDR3 ram). The simulations were all performed with the fixed time step method of 0.025 ms and the multi-split was used to distribute computation of different cell compartments over all the CPU cores (Hines et al., 2007). Each simulation lasted between 1 second and 5 seconds depending on the protocol.

2.2.1 Model Construction

The $G_{i\text{-}max}$ values were distributed over the somatic, dendritic and axonal compartments based on published immunochemistry data (**Table 2**).

The ionic channel gating kinetics were normalized at 37°C and modeled following the HH formulation or Markov-chains for multi-state transitions using mathematical methods reported previously (Anwar et al., 2012; D'Angelo et al., 2001; Nieus et al., 2006; Solinas et al., 2007a; Solinas et al., 2007b) (**Tables 3 and 4**).

The kinetic constants reported in different papers, were corrected from T_{exp} (experimental temperature) to T_{sim} (model temperature) using the equation $Q_{10}^{(Tsim - Texp)/10}$ and $Q_{10} = 3$ (Gutfreund and Segev, 1995). The Nernst equilibrium potentials were pre-calculated from $G_{i\text{-}max}$ values used in current-clamp recordings and maintained fixed, except for the Ca^{2+} equilibrium potential, which was updated during simulations according to the Goldman-Hodgkin-Katz equation. The $G_{i\text{-}max}$ values were regulated to match the SC responses to various stimulations.

In each compartment, membrane voltage was obtained as the time integral of the equation (Yamada, 1989):

$$\frac{dV}{dt} = -\frac{1}{C_m} * \{\sum[g_i * (V - V_i)] + i_{inj}\} \quad (6)$$

Where V is the membrane potential, C_m is the membrane capacitance, g_i are the $G_{i\text{-}max}$ values, V_i indicates the E_{rev} (the subscript i indicates different channels), and i_{inj} is the injected current. Adjacent compartments communicated through an internal coupling resistance (Diwakar et al., 2009).

The gap junctions were modeled following the example presented in the NEURON book (Carnevale and Hines, 2006a) and the synapses based on the Tsodyks - Markram scheme (Tsodyks et al., 1998).

2.2.1.1 Model Morphology

The SC 3D human morphology was taken from Neuromorpho.org DB (Ascoli et al., 2007; Halavi et al., 2008; Jacobs et al., 2014) and it consisted of a branched dendritic tree, subdivided in proximal

and distal dendrites, a soma, an AIS and a branched axon with collaterals. 55 sections were used to reproduce the distal dendrites, with the section diameter between 0.47 and 0.93 µm and the section length between 4.3 and 259 µm; 16 sections were used to reconstruct the proximal dendrites, with the section diameter between 0.98 and 5.32 µm and the section length between 5.2 and 63.3 µm; 1 section was used to represent the soma with the section diameter of 9 µm and the section length of 9 µm; 1 section was used for the AIS with the section diameter of 0.49 µm and the section length of 46 µm and 31 sections were used to reproduce the axon, with the section diameter between 0.18 and 0.49 µm and the section length between 0.92 and 119 µm (**Fig. 5 and Table 1**).

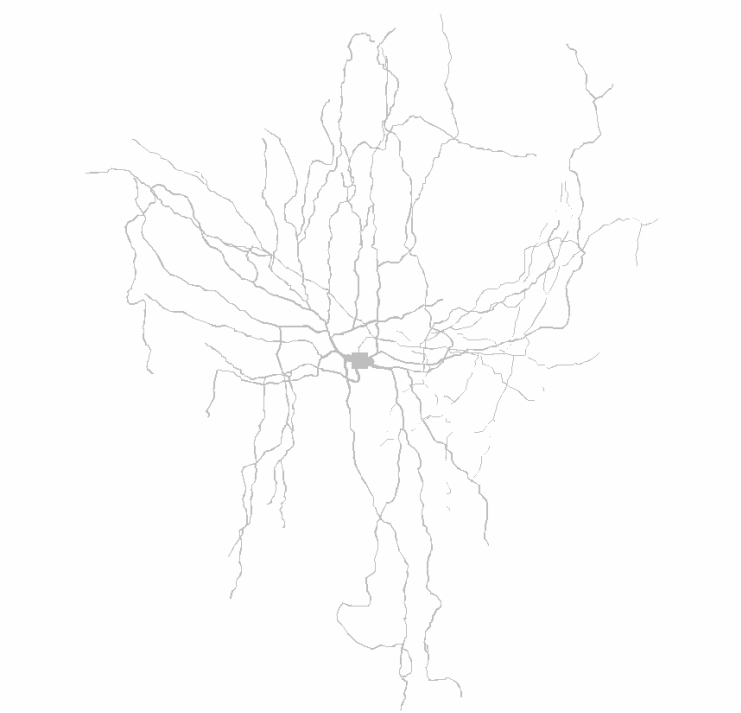

Fig. 5. The branched morphology of the human SC with the axon arborisation.

2.2.1.2 Passive and Active Properties

The passive properties of the SC model include the Ra which was set to 100 Ωcm for all the sections (distal and proximal dendrites, soma, AIS and axon), Cm which was defined as 1µF/cm^2 for all the sections and E_{rev} of the different ionic species defined with the following values: E_{Na} = 60 mV; E_k = -75 mV; E_{Ca} = 137 mV E_h = -43 mV; E_{leak} = -59 mV.

The leakage $G_{i\text{-}max}$ was set to 0.0003 S/cm^2 for all the sections.

Table 1. Passive properties.

	Diameter (μm)	Length (μm)	N° sections	Ra (Ωcm)	Cm (μF/cm^2)
Distal dendrites	0.47-0.93	4.3-259	55	100	1
Proximal dendrites	0.98-5.32	5.2-63.3	16	100	1
Soma	9	9	1	100	1
AIS	0.49	46	1	100	1
Axon	0.18-0.49	0.92-119	31	100	1

Table 1. Dimensions, number of sections and their basic biophysical properties.

The channel locations and types were chosen in accordance with immunohistochemical discoveries (Lorincz and Nusser, 2008; Molineux et al., 2005; Rowan et al., 2014; Schaller and Caldwell, 2003). All the membrane mechanisms were previously constrained and validated during the construction of the PC model and used in accordance with it (Masoli et al., 2015) (**Table 2**).

The kinetics have been maintained unaltered, the model runs at the physiological temperature of 37° and only the $G_{i\text{-}max}$ parameters have been adapted to obtain the ensemble of behaviors.

The mathematical description of each ionic mechanism is shown in **Tables 3 and 4**. The $G_{i\text{-}max}$ values were pre-adapted to experimental values and then used for the model hand-tuning. Each value was modified repeatedly to find the right parameter configuration and was able to reproduce the main electrophysiological properties of the neuron. Each channel needed a precise value of $G_{i\text{-}max}$ as it has to interact, in an optimal way, with all the others values to achieve the exact balance between all the ionic dynamics. All the membrane mechanisms used in the model have been named according to NC-IUPHAR (International Union of Basic and Clinical Pharmacology Committee on Receptor Nomenclature and Drug Classification) (Yu et al., 2005).

<u>The ionic channels used in this model are the following:</u>

- *Nav1.6* – Voltage-dependent Na^+ channel (Na_t, Na_p and Na_r components)
- *Nav1.1* – Voltage-dependent Na^+ channel (Na_t, Na_p components only)
- *Kv1.1, Kv3.4, Kv4.3* – Voltage-dependent K^+ channels (delayed rectifier, A-type, M-type)
- *KCa1.1, KCa2.2 and KCa3.1* - Big, small and middle conductance Ca^{2+}- dependent K^+ channel

- *Kir2.x* - Inward Rectifier K^+ channel
- *HCN1* - Hyperpolarization activated cyclic nucleotide-gated cationic channel
- *Cav3.1, Cav3.2, Cav3.3* – Low voltage-activated (LVA) Ca^{2+} channels (T-type)
- *Cav2.1* – High voltage-activated (HVA) Ca^{2+} channel (P -type)
- *Ileak* - Background leakage channel

Na^+ channels (subfamilies Nav1.6, Nav1.1)

The Na^{2+} channels of these neurons are voltage-gated tetrodotoxin (TTX) - sensitive channels of the Nav 1.6 subtype. These channels generate both Na_t and Na_r currents elicited by repolarisation steps from positive potentials (Raman and Bean, 1999) as well as the Na_p current. These properties, associated with a rapid recovery from inactivation of the Na_t current, were supposed to facilitate high frequency firing of action potentials (Raman and Bean, 1999, 2001; Khaliq et al., 2003).

The Nav1.6 channel, recorded in PCs, was built as Markovian 13 states channel (Khaliq et al., 2003), later improved with better Q10 parameters to be used at physiological temperature (Akemann and Knopfel, 2006). This channel was placed in the AIS and axon to support the generation of the spikes and their transmission in the axonal plexus (Lorincz and Nusser, 2008; Schaller and Caldwell, 2003).

Immunohistochemical studies have shown that SCs can also express Nav1.1 (Lorincz and Nusser, 2008). This channel consists of the Na_t and Na_p currents but not the Na_r component and it was used only in the soma (Lorincz and Nusser, 2008; Schaller and Caldwell, 2003).

K^+ channels (subfamilies Kv1.1, Kv3.4, Kv4.3, Kv7)

In SCs, the regulation of neuronal excitability and action potential shape depends on several K^+ channels, mostly those of the Kv1, Kv3, Kv4, and Kv7 subfamilies (Rowan et al., 2014).

Kv1.1 is commonly expressed in cerebellar neurons as heteromultimeric tetramers in arrangement with other Kv1.x proteines. Immunoprecipitation experiments suggest that in the cerebellum over 80% of channels that contain a Kv1.1 subunit also contain more than one Kv1.2 subunits (Koch et al., 1998; Khavandgar et al., 2005). The importance of this channel is to prevent dendritic hyper excitability which is generated by the influx of Ca^{2+} through the LVA Ca^{2+} channels when the Ca^{2+} concentration or the voltage is too low to activate the Ca^{2+} dependent K^+ (KCa) channels. The channel is expressed in all the SC model sections (Lorincz and Nusser, 2008).

Kv3 is a K^+ family abundant in the CNS, with each Kv3 gene (Kv3.1–Kv3.4) exhibiting a unique pattern of expression. It was observed that Kv3 channels are expressed at high level in GABAergic neurons (Perney et al., 1992). Strangely, the mRNA for the four members of the Kv3 subfamily was not found (Weiser et al., 1994), but the presence was proved of the Kv3.4 channel proteins using an antibody for a specific amminoacid sequence (Brooke et al., 2006). The channel was distributed on the soma, AIS and axon to repolarize the Na^{2+} spikes as it counterbalances the I_{Nar} optimally.

Another K^+ channel, Kv4.3, was seen expressed and concentrated on the soma, proximal and distal dendrites (Molineux et al., 2005; Anderson et al., 2013). These channels, important molecular components of transient K^+ currents (A-Type current) in the brain, exhibit a rapid activation and inactivation in response to subthreshold membrane depolarization. The closed state inactivation of the channel was seen to be PKC dependent (Xie et al., 2009). This current is involved in setting the frequency of neuronal firing and heart pacing (Serodio and Rudy, 1998). The use of a wide range of blockers for Kv1 and Kv4 subunits to determine the nature of the A-current, revealed a relevant contribution of Kv4. Inhibition with hongotoxin of Kv1.1, Kv1.2, Kv1.3, and Kv1.6 reduced the A-type current by only 10%, indicating that the main part of the current is generated by Kv4 subfamily members (Hourez et al., 2011).
A recent paper demonstrated that Kv4 K^+ channel interacts with the LVA Ca^{2+} (T-type) channels to create a complex where the current A-Type and T-type lead to the first-spike latency mechanism in the SCs (Molineux et al., 2005). The co-expression of these two channels allows membrane hyperpolarizations that reduce or extend the latency to the first spike in SCs. The latency SC modulation controls the SC discharge in response to excitatory synaptic depolarizations and influences the PC output. This mechanism is involved in the synaptic integration process (Molineux et al., 2005; Turner and Zamponi, 2014). The Cav3-Kv4 complex has also another important function in SC firing control, it acts as a Ca^{2+} sensor that responds to a decrease of concentration of extracellular Ca^{2+}, controlling the SC inhibitory output to maintain the transmission of the inhibitory firing to PCs, regulating the PC excitability during the repetitive afferent activity (Anderson et al., 2013). It is known, in fact, that the extracellular Ca^{2+} concentration decreases, when the neurons were exposed to repetitive synaptic input.

Kv7 channels form a family that includes five K^+ channels subunits (Kv7.1 - Kv7.5), four of these (Kv7.2 – Kv7.5) are expressed in the nervous system. Kv7.2 and Kv7.3 contribute to form a functional low-threshold voltage-gated K^+ channel, with an important role in neuronal excitability control. These channels are characterized by a slow activation and the absence of inactivation, important gating properties that permit the stabilization of the membrane potentials in presence of depolarizing currents, contributing to the resting potentials. Kv7 is expressed in the SC AIS (Brown and Passmore, 2009; Pan et al., 2006; Miceli et al., 2012).

Inward rectifier K^+ channels (Kir2.x)

Kir2.3 - The Kir channels ensure the stabilization of membrane potential regulating neuronal excitability and neurotransmitter release. The Kir subunit expressed in the SC soma and dendrites is the PKC-dependent isoform Kir2.3 (Stonehouse et al., 1999).

Ca^{2+} - dependent K^+ channels (Kca1.1, Kca2.2)

The KCa channels are gated by changes in intracellular Ca^{2+} concentration and by changes in membrane voltage (Liu et al., 2011). The members of this subfamily are divided into three categories: large conductance or BK (Kca1.1), medium conductance or SK4 (Kca3.1) and small conductance or SK2 (Kca2.2). Kca1.1 channels control spontaneous firing and intracellular Ca^{2+}

concentration (Womack et al, 2010) and are present on the SC dendritic tree and on the soma, where they form clusters with HVA (Cav2.1) Ca^{2+} channels (Kaufmann et al., 2009) and LVA (Cav3) Ca^{2+} channels (Rehak et al., 2013; Stocker and Pedarzani, 2000; Turner and Zamponi, 2014).

The critical role of KCa1.1 in the cell hyperpolarization is noted looking at the spike shape. When the channel is blocked, the spontaneous action potential duration is prolonged in SCs, increasing the influx of Ca^{2+} inside the cell, influencing the AMPA receptor and the synaptic transmission (Liu et al., 2011).

HVA and LVA Ca channels (Cav2.1, Cav3.x)

The main HVA Ca^{2+} channels, Cav2.1, was placed on the dendrites and on the soma (Choi et al., 2010) to act as the major Ca^{2+} source for Kca1.1 and Kca2.2, which are also located on the dendrites and soma (Lang et al., 2000; De Gruijl et al., 2012; Gymnopoulos et al., 2014). The LVA channels Cav3.1, Cav3.2, Cav3.3 were placed on the soma and on the entire dendritic tree (Park et al., 2010). There are only small kinetic differences between Cav3.1 and Cav3.2, instead Cav3.3 has seven times longer activation phase and a ten times longer deactivation phase (Cain and Snutch, 2010; Turner and Zamponi, 2014).

The Cav3.1, Cav3.2, Cav3.3 channels (T-type channels) interact with Kv4 channel (A-type current) to create a complex mechanism that influences the SC firing pattern and the subsequent PC output, as described previously in the Kv4 description (Turner and Zamponi, 2014; Molineux et al., 2005; Anderson et al., 2013).

Hyperpolarization-activated cyclic nucleotide-gated (HCN1)

To complete the channel arrangement, it was used HCN1 placed on the soma, AIS, axon and all the dendrites (Angelo et al., 2007; Lujàn et al., 2005; Milligan et al., 2006;). HCN1 activates at hyperpolarized potential and is cyclic nucleotide-gated. The mixed Na^+ and K^+ current generated by this channel is smaller than the currents generated by Ca^{2+}, Na^+ and K^+ channels, (10pA vs 1nA) but is critical for tuning post-synaptic activity. The voltage dependent activation curve of HCN1 is only slightly modulated by cyclic adenosine monophosphate (cAMP) second messenger (2-4mV) (He et al., 2014). The Ih (HCN1-channel) is fundamental to obtain the inward rectification behavior in the SCs one of the main electrophysiological properties reproduced by the SC model (**Fig. 13**).

Calcium intracellular dynamics: pumps and buffers

SCs are characterized by multiple Ca^{2+} regulation systems including a set of diffusible passive and active Ca^{2+} buffers (Bastianelli, 2003), Na^+ - Ca^{2+} exchangers and ATP dependent Ca^{2+} pumps. The intracellular Ca^{2+} stores are connected with ionic channels and enzymes with a wide network of biochemical interaction (Kitamura and Kano, 2012). Many of the previous cited channels are central to the trafficking of Ca^{2+} ions, are activated by the Ca^{2+} and are modulated by Ca^{2+} - dependent enzymes.

The published data about the Ca^{2+} buffer dynamic of the SC offered an incomplete picture about which Ca^{2+} binding protein was present. The expression of the passive diffusible Ca^{2+}buffer *Parvalbumin* (PV) was already acknowledged, since SC neurons do not have *Calbindin* (CB) expression (Anwar et al., 2012; Alcami and Marty, 2013). It was observed that, among the MLIs, the PV is expressed at earlier stages of development (P10-P12 rats age) in the BCs, whereas at P19-P21 is also expressed in SCs (Collin et al., 2005).

Table 2. Active properties.

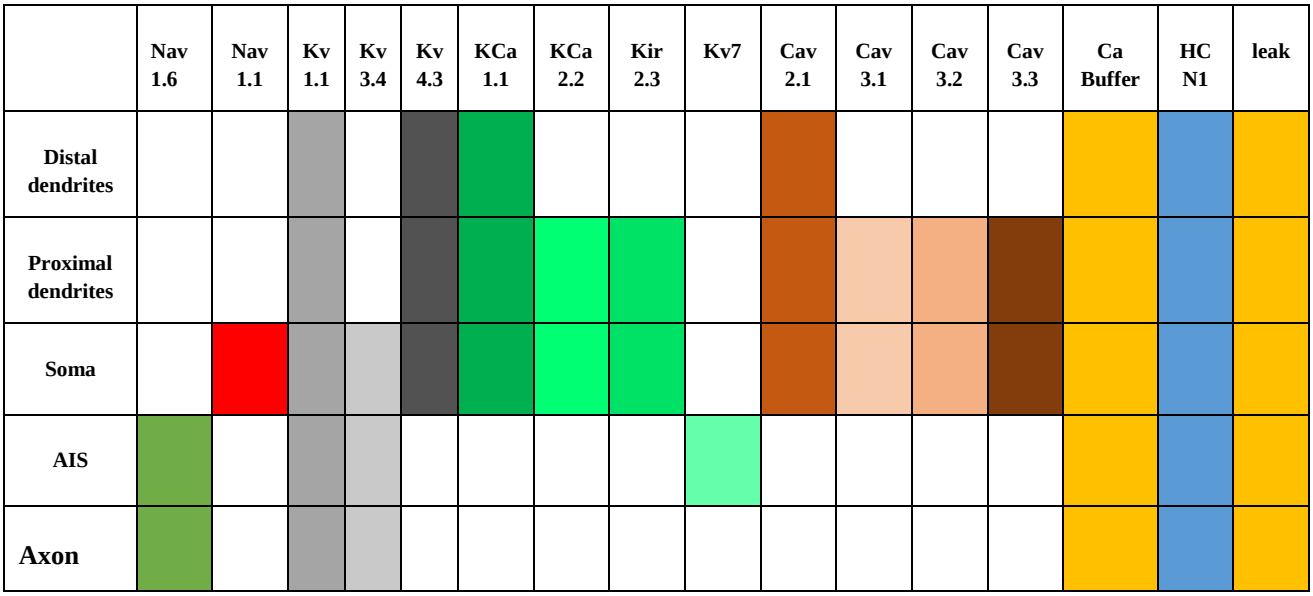

Table 2. Distribution of 13 ionic channels along the morphology. Ionic channels include Na^+, K^+ and Ca^{2+} channels (Nav1.6, Nav1.1, Cav2.1, Cav3.1, Cav3.2, Cav3.3, Kv3.4, Kv1.1, Kv4.3, Kv7, KCa1.1, KCa2.2, Kir2.x, HCN1) and Ca^{2+} buffering system.

Table 3. Ionic mechanisms in SC model: I.

$G_{i\text{-}max}$/Location		$G_{i\text{-}max}$ (S/cm^2)	E_{rev} (mV)	Description of channel (HH or Markovian)	Reference
Na^+ channel					
Nav1.6	AIS	0.6	60	Markovian 13 states	(Raman and Bean, 2001)
	Axon	0.04			
K^+ channels					
Kv1.1	Distal Dendrites	0.007	-75	HH	(Akemann and Knopfel, 2006)
	Proximal dendrites	1e-4			
	Soma	0.05			
	AIS	0.01			
	Axon	0.004			
Kv3.4	Soma	0.1	-75	HH	(Raman and Bean, 2001; Khaliq et al., 2003)

	AIS	0.05			
	Axon	0.04			
Kv4.3	Distal Dendrites	0.005	-75	HH	(Diwakar et al., 2009)
	Proximal dendrites	5e-4			
Kir2.x	Proximal dendrites	0.007	-75	HH	(Diwakar et al., 2009)
	Soma	1e-4			
Ca^{2+} dependent K^+ channels					
Kca1.1	Distal dendrites	0.001	-75	Markovian	(Anwar et al., 2012)
	Proximal dendrites	0.005			
	Soma	0.004			
Kca2.2	Proximal dendrites	0.001	-75	Markovian	(Solinas et al., 2007a, 2007b)
	Soma	0.001			
Ca^{2+} channels					
Cav2.1	Distal dendrites	1e-5	137	HH	(Swensen and Bean, 2005; Anwar et al., 2010)
	Proximal dendrites	1e-6			
	Soma	0.005			
Cav3.1	Proximal dendrites	1e-4	137	HH	(Anwar et al., 2012)
	Soma	1e-3			
Cav3.2	Proximal dendrites	1e-6	137	HH	(Huguenard and McCormick, 1992)
	Soma	1e-5			
Cav3.3	Proximal dendrites	1e-6	137	HH	(Xu and Clancy, 2008)
	Soma	1e-5			
Mixed cationic channel					
HCN1	Distal dendrites	1e-4	-43	HH	(Angelo et al., 2007; Larkum et al., 2009)
	Proximal dendrites	0.005			
	Soma	0.01			
	AIS	1e-4			
	Axon	1e-4			
Ca^{2+} buffer - pumps density					
Ca Buffer	Distal dendrites	2e-8		Markovian	(Anwar et al., 2012)
	Proximal dendrites	2e-8			
	Soma	5e-8			
	AIS	5e-8			
	Axon	5e-8			

Table 3. The table shows ionic channel localization, $G_{i\text{-}max}$ and E_{rev} values. Gating equations were written either in HH style or in Markovian style according to indicated references.

Table 4. Ionic mechanisms in SC model: II.

$G_{i\text{-}max}$ State Variables	n	$\alpha(s^{-1})$	$\beta(s^{-1})$

Nav1.6	Open		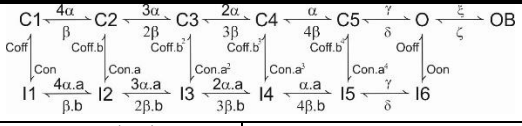	
	Blocked			
	Closed			
	Inactivated			
Kv1.1	Activation	4	$\text{Alphan} = 0.12889 * \exp^{\frac{-(v+45)}{-33.90877}}$ $\text{Ninf} = \frac{0.12889 * \exp^{\frac{-(v+45)}{-33.90877}}}{0.12889 * \exp^{\frac{-(v+45)}{-33.90877}} + 0.12889 * \exp^{\frac{-(v+45)}{12.42101}}}$	$\text{Betan} = 0.12889 * \exp^{\frac{-(v+45)}{12.42101}}$ $\text{Taun} = \frac{1}{(qt*(0.12889 * \exp^{\frac{-(v+45)}{-33.90877}} + 0.12889 * \exp^{\frac{-(v+45)}{12.42101}})}$
Kv3.4	Activation	3	$Minf = \frac{1}{1+exp^{\frac{-v+24}{15.4}}}$ $Mtau = 1000 * \frac{mtau\_func(v)}{qt}$ *If Vm < -35* $Mtau = (3.4225e^{-5} + 0.00498exp^{\frac{-v}{-28.29}}) * 3$ *else* $Mtau = 0.00012851 + \frac{1}{exp^{\frac{v+100.7}{12.9}} + exp^{\frac{v+-56.0}{-23.1}}}$	$Hinf = 0.31 + \frac{0.69}{1+exp^{\frac{v-(-5.802)}{11.2}}}$ $Htau = \frac{1000 * htau\_func(v)}{qt}$ *If Vm > 0* $Htau = 0.0012 + 0.0023 * exp^{-0.141*Vm}$ *else* $Htau = 1.2202e^{-05} + 0.012 * exp^{\frac{-(Vm-(-56.3))}{49.6^2}}$
	Inactivation	1		
Kv4.3	Activation	2	$Alp\_a = Q10 * 0.8147 * sigm(v-(-9.17203,-23.32708))$ $Alp\_b = Q10 * 0.0368 * sigm(v-(-111.33209, 12.8433))$ $Tau\_a = \frac{1}{q10*0.8147*sigm(v-(-9.17203,-23.32708))+ Q10*\frac{0.1655}{exp^{\frac{v-(-18.27914}{19.47175}}}}$	$Bet\_a = \frac{Q10*0.1655}{exp^{\frac{v-(-18.27914)}{19.47175}}}$ $Bet\_b = Q10 * 0.0345 * sigm(v-(-49.9537, -8.90123))$ $Tau\_b = \frac{1}{(Q10*0.0368*sigm(v-(-111.33209,12.8433))+ Q10*0.0345*sigm(v-(-49.9537,-8.90123))}$
	Inactivation	1		
Kir2.x	Activation	1	$Alp\_d = Q10 * 0.13289 * exp^{\frac{v-(-83.94)}{-24.3902}}$	$Bet\_d = Q10 * 0.16994 * exp^{\frac{v-(-83.94)}{35.714}}$ $Tau\_d = \frac{1}{Q10*0.13289*exp^{\frac{v-(-83.94)}{-24.3902}} + Q10*0.16994*exp^{\frac{v-(-83.94)}{35.714}}}$
Kca1.1	Open/closed		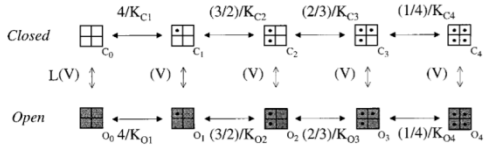	
Kca2.2	Open/closed		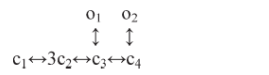	
Kca3.1			*Cai < 0.01* $Yconcdep = 500\left(\frac{1}{ms}\right) * \frac{0.015-cai*\left(\frac{1}{mM}\right)}{exp^{\frac{0.015-cai*1\left(\frac{1}{mM}\right)}{0.0013}}-1}$ $Yconcdep = 500\left(\frac{1}{ms}\right) * \frac{0.005}{exp^{\frac{0.005}{0.0013}}-1}$ $TauY = \frac{1}{Yalpha + Ybeta}$	
Cav2.1	Activation	3	*If x>=-40* $Taumfkt = 0.2702 + 1.1622 * exp^{\frac{(-(v+26.798)*(v+26.798)}{164.19}}$ $Taumfkt = 0.6923 * exp^{\frac{v}{1089.372}}$	
Cav3.1	Activation	2	$Minf = 1/(1+exp((v+52)/-5))$ $\tau_m = (1 + \frac{1}{\frac{exp(v+40)}{9}} + exp((v+102)/-18)$	$Hinf = 1/(1+exp((v+72)/7))$ $\tau_h = (15 + 1/exp((v+32)/7))$
	Inactivation	1		
Cav3.2	Activation	2	$M\_inf = \frac{1.0}{1+exp^{\frac{-(v+shift+54.8)}{7.4}}}$ $Tau\_m = 1.9 + \frac{1.0}{exp^{\frac{v+shift+37.0}{11.9}} + \frac{exp^{\frac{-(v+shift+131.6)}{21}}}{5^{\frac{12}{10}}}}$	$H\_inf = \frac{1.0}{1+exp^{\frac{v+shift+85.5}{7.18}}}$ $Tau\_h = 13.7 + \frac{1942 + exp^{\frac{v+shift+164}{9.2}}}{\frac{1+exp^{\frac{v+shift+89.3}{3.7}}}{3^{\frac{12}{10}}}}$
	Inactivation	1		
Cav3.3	Activation	2		*If v > -60*

	Inactivation	1	$N\_inf = \frac{1}{(1+exp^{\frac{-(v-vhalfn)}{kn}}}$ $L\_inf = \frac{1}{1+exp^{\frac{-(v-vhalfl}{kl}}}$	$Tau\_n = \frac{7.2+0.02*exp^{\frac{-v}{14.7}}}{qt}$ $Tau\_l = \frac{79.5+2.0*exp^{\frac{-v}{9.3}}}{qt}$ $Tau\_n = \frac{0.875*exp^{\frac{v+120}{41}}}{qt}$ $Tau\_l = \frac{260}{qt}$
HCN1	Activation	1	$h = \frac{1}{(0.0018*(exp^{v-(-58,7)/-22})+exp^{\frac{v-(-58,7)}{7.14}}/qt}$	

Table 4. The table reports the equations used to calculate membrane $G_{i\text{-}max}$ values used in the model.

In most cases, α_x, β_x, α_y, and β_y were used to calculate x_∞, y_∞, τ_x and τ_y according to the HH scheme (Hodgkin and Huxley, 1952):

$$g_i = G_{i-max} * x_i^{zi} * y_i$$

Where, $G_{i\text{-}max}$ is the maximum ionic conductance value, x_i and y_i are state variables (probabilities ranging from 0 to 1) for a gating particle, and z_i is the number of such gating particles in ionic channel *i*. *x* and *y* (the suffix *i* omitted) were related to the first order rate constants α and β by the equations:

$$x_\infty = \frac{\alpha_x}{\alpha_x+\beta_x}, y_\infty = \frac{\alpha_y}{\alpha_y+\beta_y}\ ; \qquad \tau_x = \frac{1}{(\alpha_x+\beta_x)}, \tau_y = \frac{1}{(\alpha_x+\beta_x)}$$

Where α and β are functions of voltage. The state variable kinetics were:

$$\frac{dx}{dt} = \frac{(x_\infty - x)}{\tau_x}, \frac{dy}{dt} = \frac{(y_\infty - y)}{\tau_y}$$

In some cases, the equations for x_∞, y_∞, τ_x or τ_y are reported directly. Exceptions to this general scheme were Markovian channel models for Nav1.6 and KCa1.1. Eventually, the probability of channel opening was transformed into G_{imax} values and used to calculate the model currents.

2.2.1.3 Synapses

The neuronal communication is mediated largely by chemical synapses and SCs receive extensive connections from excitatory and inhibitory pathways, both as local feedback as well as input pre elaborated by GrCs.

The AMPA and NMDA receptors where used to simulate the excitatory synaptic activity from the pfs to SC dendrites and the GABA receptor was used to reproduce the efferent SC inhibitory activity to PC dendrites and to other SCs. Since the literature about the parameters of these synapses is not as extensive as with other neurons, the AMPA and NMDA membrane mechanisms from GrCs were used. The GABA-A receptors were known to be composed of alpha 2 and 3 subunits (Devor et al., 2001) but in the absence of an ad hoc membrane mechanism, a modified GABA-A receptor recorded from alpha1 subunits was used (Nieus et al., 2014).The synaptic activity in the SC model is described with the following synaptic mechanisms:

The AMPA pf -SC synapses: the receptor (Nieus et al., 2006) was built with the Tsodyks and Markram formalism (Tsodyks et al., 1998). The synaptic properties were as follows: release probability = 0.42, τREC = 35.1 ms, τ facil = 54 ms, τ_1 = 6 ms, $G_{i\text{-}max}$ = 2800 pS, E_{rev} = 0 mV.

The NMDA pf - SC synapses: The NMDA receptor (Nieus, 2005), impermeable to Ca^{2+} ions, was based on the same properties: release probability = 0.42, τREC = 8ms, τ facil = 5 ms, τ_1 = 1 ms, $G_{i\text{-}max}$ = 40000 pS, E_{rev} = -3.7 mV.

The GABA SC-SC synapses: i) The synaptic mechanism GABA-A was built with the Tsodyks and Markram formalism (Nieus et al., 2014). The mechanism was built with a stochastic approach with only two free parameters: the reversal potential set at -60mV and a Gmax of 8000 pS.

The GABA, AMPA and NMDA synapses were located on the whole dendritic tree, one for each dendrite, for a total of 147 GABA synapses and 147 AMPA/NMDA synapses. The synapses were located, exactly, at the half of each section (**Fig. 6 and Fig. 7**).

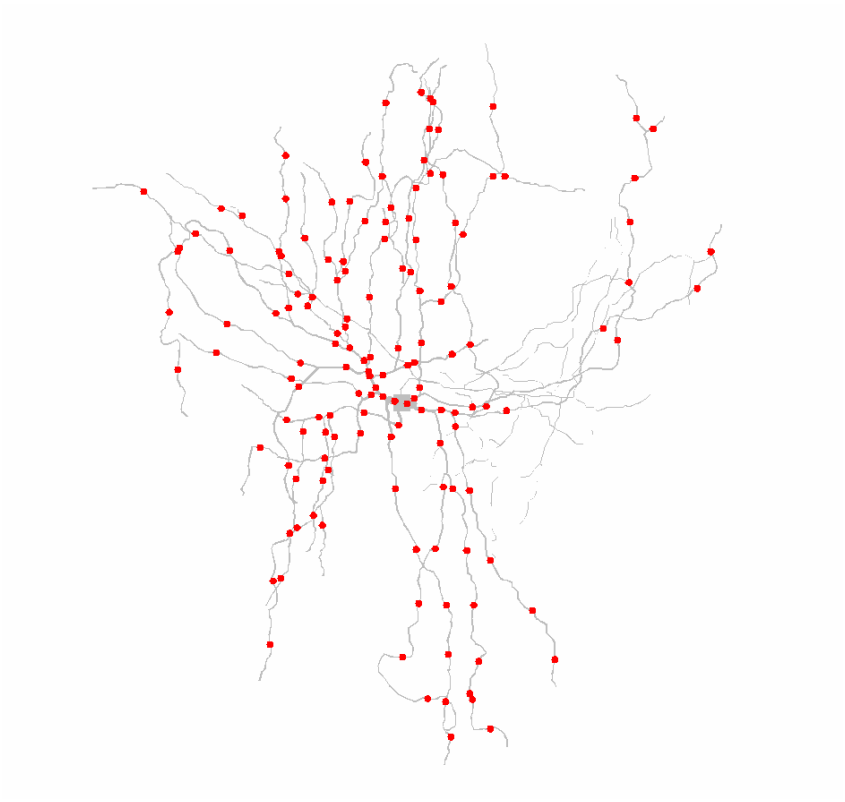

Fig. 6. Synapses AMPA and NMDA location on the dendrites.

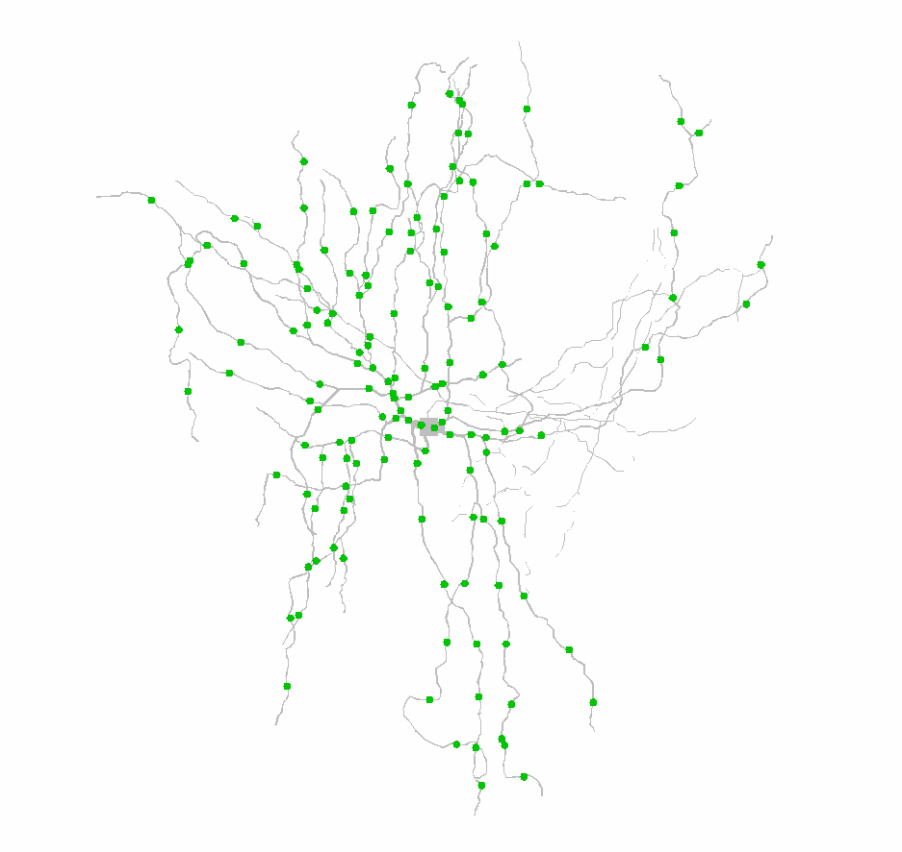

Fig. 7. Synapses GABA location on the dendrites.

2.2.1.4 Gap Junctions

The inhibitory interneurons in the cerebellum and in other parts of the brain e.g. the cerebral cortex, thalamus, hippocampus and striatum, are interconnected by electrical synapses. The discovery of the presence of gap junctions between inhibitory interneurons demonstrated that the electrical coupling characterized all the inhibitory microcircuits. The first scientists to discover the presence of gap junction structures between the dendrites of the inhibitory interneurons in the ML were Sotelo and Llinàs who published their experimental observations in 1972 (Sotelo and Llinàs, 1972).

Cerebellar GABAergic interneurons BC, SC and GoC families show the reciprocal gap junction modulation, electrical synaptic activity, forming functional networks. The electrical synapses between interneurons induce the synchronization in the network firing (Mann-Metzer and Yarom, 1999). A current passes across the gap junctions, which equalizes the voltage between cells and provides the synchronization of membrane potential of the coupled cells (Vervaeke et al., 2010).

In the nervous system, a gap junction channel is formed by two Connexons located in the plasma membrane of two coupled cells. Each Connexon is composed of six Connexins (Cx) which are proteins coded by a multigene family. The most known proteins are Cx32, Cx36, Cx43, Cx45, Cx47 or Cx57, depending on the type of neuron or glial cell and on the state of brain development.

Cx 36 and Cx 45 were found in the SCs which are electrically coupled through dendrodendritic gap junctions along the sagittal plane of the ML (Alcami and Marty, 2013; Galarreta and Hestrin, 2001 Maxeiner et al., 2003). Cx36 is expressed in GABA interneurons that express parvalbumin (a Ca^{2+}-binding protein that can act in SCs as an endogenous Ca^{2+} buffer) and the presence of this type of protein is a fundamental feature for the electrical synapses between cerebellar inhibitory interneurons (Galarreta and Hestrin, 2001). Cx45 is largely expressed during embryogenesis and for approximately two post-natal weeks, after which, its' expression is present in the cerebellar MLIs. Cx36 is expressed, instead, at the end of embryogenesis and for two post-natal weeks. This latter observation suggests that Cx36 and Cx45 could be involved together in the gap junction formation (Maxeiner et al., 2003; Van Der Giessen, 2006). The presence of Cx36 in MLIs and the lack of electrical activity between cells that does not express Cx36, suggests that the Cx36 is the fundamental protein to allow the gap junction formation and the electrical activity in the MLIs network (Alcami and Marty, 2013).

To model the functional role of gap junctions , this membrane mechanism was based on an example available in the NEURON book (Carnevale and Hines, 2001) and set with an unitary conductance of 100pS (Fortier, 2010). Each dendrite was provided with a total current of 1000pS, equivalent to 10 gap junctions and the gap junctions were located at 50µm distances from the soma (Devor and Yarom, 2002). The gap junctions in the SC model are located on the 16 proximal dendrite sections, exactly in the center of the section.

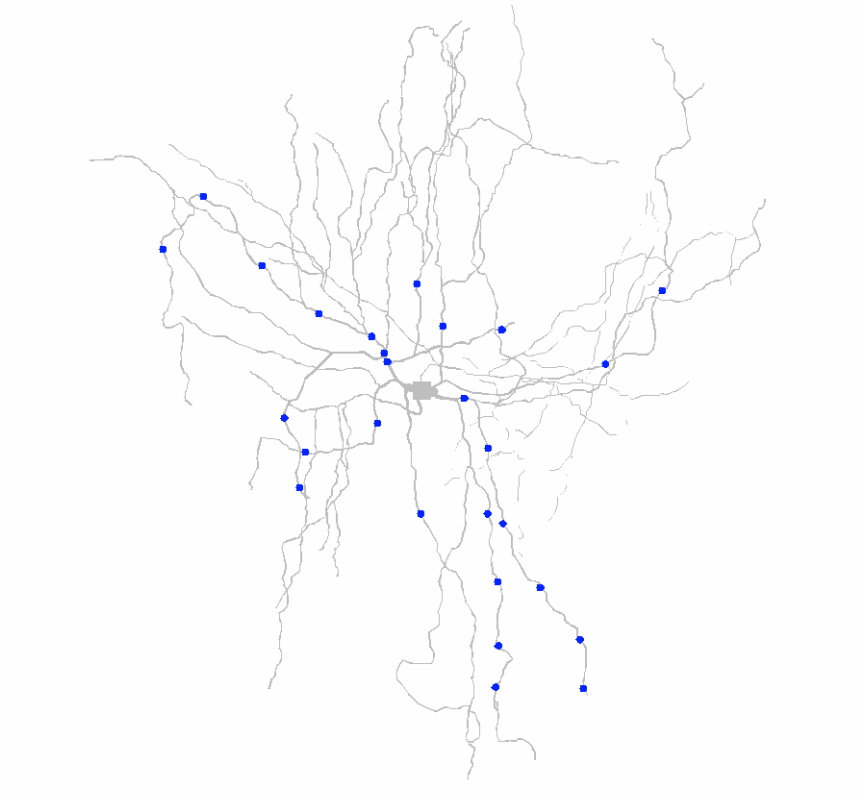

Fig. 8. Gap junction location on the dendrites.

2.2.2 Model Tuning, Testing and Validation

The model construction follows these steps: a morphology is taken from actual neurons, appropriate passive properties and ionic channels type and location. With a manual fitting to find the correct values for the $G_{i\text{-}max}$, during the process, the model for basic behaviours can be validated. It then precedes the final validation phase where it is tested for protocols not used during its construction.

The $G_{i\text{-}max}$ parameters, located in each section of the model, are the unknown parameters in the parameter space that need to be searched with a hand-tuning process. The parameters were initially set to the basic experimental data provided by the author of the MOD files and the fine-tuning required a trial-and-error approach. The following procedure was followed to perform the hand-tuning parameters of the model. The calibration of each $G_{i\text{-}max}$ parameter was tuned following experimental indications and validated using specific tests, which permit to determine the best model parameterization able to reproduce three fundamental functional properties: spontaneous firing, I/O relationship, inward rectification. Parameter tuning was performed varying the $G_{i\text{-}max}$ values to achieve the best model results that match the experimental results in a biologically acceptable way.

After setting the morphological and passive properties, the model hand-tuning started with the definition of the ionic channel location and the respective $G_{i\text{-}max}$ value for that section following these steps: i) The first ionic channels added were the Na^{2+} channels located in the soma and AIS sections followed by the different types of K^{+} channels over the whole morphology, to permit the basic Na^{2+} spike generation mechanism of the SC model. ii) The HCN ionic channel was then added to the model to reproduce the hyperpolarizing responses to current negative injections. iii) The different types of Ca^{2+} channels, the Ca^{2+} buffering system and the KCa channels were added (Anwar et al., 2010). iv) The fine-tuning process was executed comparing the main electro responsive properties of the model with the appropriate experimental voltage traces. To validate the neuronal model behavior, during the construction, a series of protocols was defined, based on experimental procedure. The protocols were run after each parameter change to test the direction taken by the model at each change of conductance configuration.

Protocol one – It was defined to test the presence and speed of the SC spontaneous firing and to evaluate the SC model discharge, in the absence of current injection, so as to obtain a complete picture of the ionic channels (Ca^{2+}, K^{+}, KCa) involved in the duration of spontaneous firing and in the achievement of the right spike shape and amplitude. **Protocol two** – It consisted of a series of positive current injections to test the SC model I/O relationship curve. **Protocol three** – It was used to test the voltage responses to negative current injections, to evaluate the impact of the I_h and K_{ir} currents, fundamental in the inward rectification mechanism. **Protocol four** – It was defined to test the behaviours obtainable with two cells coupled with gap junctions. **Protocol five -** A highly

tuneable protocol was devised to investigate the inhibitory SC synaptic activities and the response of SC to pf excitatory synaptic inputs.

A relevant issue, in complex neuron models, is to perform a faster and more precise calibration of large numbers of $G_{i\text{-}max}$ parameters and the PE can be used to solve the complex optimization problem of the SC model. This interesting application will be described in the next chapter (**Ch. 3**). Different computational techniques can be applied to solve the parameter optimizations for these type of problems. The most known approaches are the GA (Druckmann et al., 2007, 2008, 2011; Van Geit et al., 2007) and the recent BluePyOpt framework (Van Geit et al., 2016). I wanted to explore the application of SI algorithms, proposing the implementation of PSO for the $G_{i\text{-}max}$ estimation of SC model, which will be described in detail in **Ch. 3**. For the first time this technique was applied to a complex conductance-based model, able to reproduce SC behaviors.

2.3 Results

The detailed SC conductance-based model was reconstructed and tested following the procedure described in **Methods** (**Para. 2.1**). The model output reproduced the main electrophysiological properties of the neuron e.g. the section of the model the spike shape was generated, the spontaneous firing, the I/O relationship and the inward rectification, the gap junction activity modulation and the SC synaptic activity.

2.3.1 Electrophysiological Properties

The first neuronal feature investigated was the spike shape during spontaneous firing. This fundamental property was observed in the soma and was similar to that measured during experimental recordings (**Fig. 9**) (Liu et al., 2011). The model was able to reproduce the spike shape only in the presence of Kca1.1 in the soma and proximal dendrites. This was proved further when there was no evidence of the KCa1.1 ionic channel (knock out (KO) of KCa1.1 ionic channel) in the soma section and in the proximal and distal dendrite sections, demonstrating the critical role of KCa1.1 in the cell hyperpolarization (**Fig. 10**) (Liu et al., 2011).

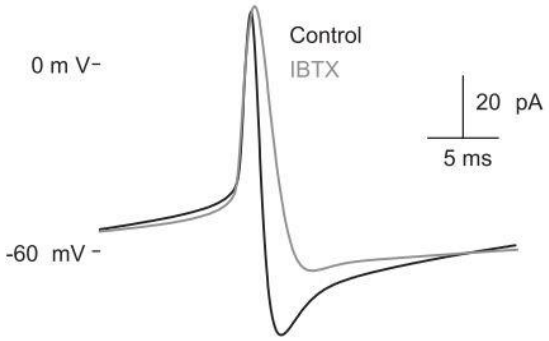

Fig. 9. Experimental results: the black line represents the spike shape in control conditions; the grey line is the experimental result in KO KCa1.1 conditions. The experimental traces are taken from the work of (Liu et al., 2011).

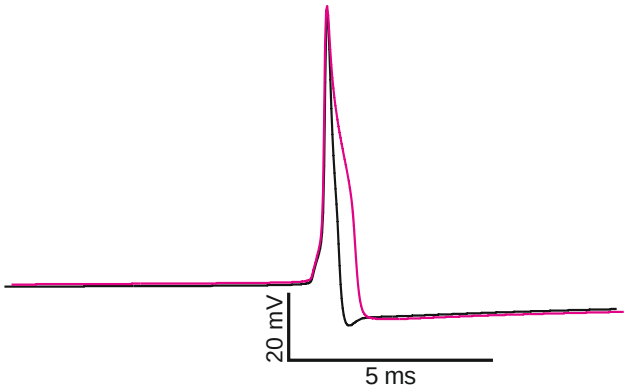

Fig. 10. Model traces: the normal spike shape (black) compared with the shape obtained during the KO of KCa1.1 (purple).

I investigated which section the spike was generated and how the spike propagation occurs during the simulation time. The SC model showed that the spike was generated initially in the AIS (red)(Bender and Trussell, 2009), then it back propagated in the soma (blue), the dendrites (green) and only at the conclusion of the simulation, forward propagated in the axon (black). The axonal

traces were recorded in a terminal axonal and showed a 2ms delay. The AIS was the site of spike generation and it was thought to be responsible for the SC auto-rhythmic activity (**Fig. 11**).

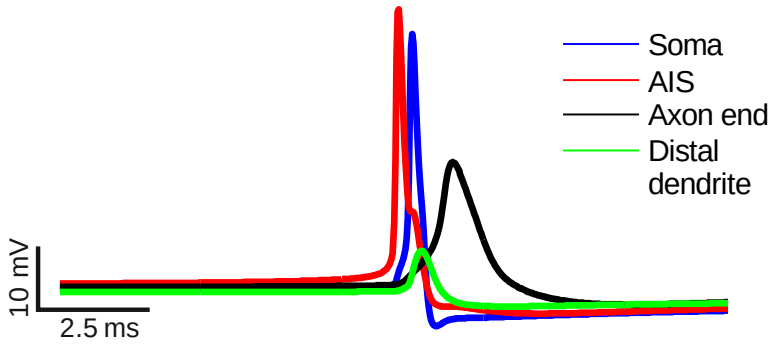

Fig. 11. Spike generation.

As observed in experimental recordings, SCs show a regular and synchronized spontaneous activity (Carter and Regher, 2002). The model showed an average spontaneous firing of 14 Hz (**Fig. 12**) which is in the range of 0-30 Hz (Beierlein and Regehr, 2006) recorded from experiments. This typical behavior was due to the exact balance and localization over the morphology of the all $G_{i\text{-}max}$ parameters that characterize the cellular responses. The mechanisms of depolarization and repolarization based on Na^{2+} and K^{+} channels activation and deactivation are reproduced by the model, generating the spontaneous cellular activity. Several intrinsic cellular currents contribute to the pacemaker firing pattern, the most important are the I_{Nap}, the I_{Ca} and the I_h (Llinàas, 1988; Jaeger et al., 1997).

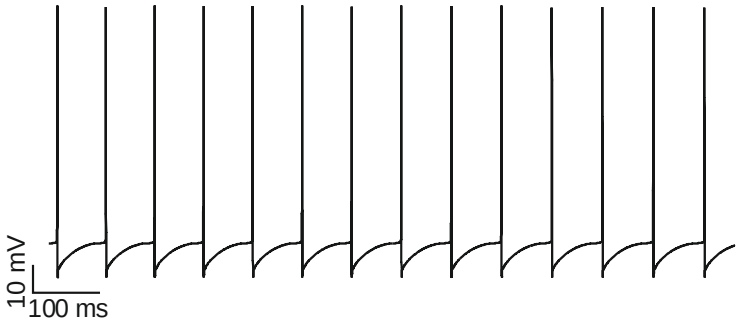

Fig. 12. The model shows an average spontaneous firing of 14 Hz.

Experimental recordings *in vivo* and *in vitro* showed, in addition to the auto-rhythmic activity, an almost linear I/O relationship with increasing current injections. The model I/O relationship matched the experimental data during positive somatic current injections applied in steps from 0.04

nA to 0.32 nA. In response to these increasing step current injections, the spike frequency increased from about 14 Hz to a maximum of 70 Hz (**Fig. 13**).

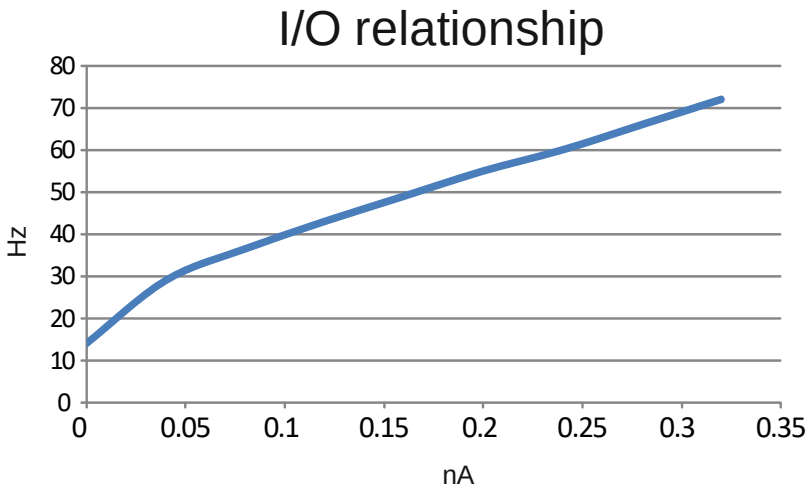

Fig. 13. I/O relation.

Upon hyperpolarizing current injection, the model reproduces the SAG generated by the inward rectification mechanism, followed by rebound excitation (**Fig. 14**). The HCN1-channel activation and deactivation mechanism were fundamental to obtain this typical behavior.

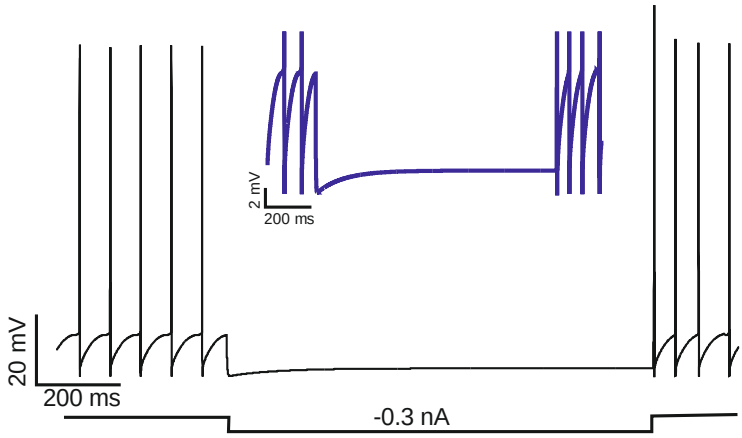

Fig. 14. SCs present the sag as the result of a negative current (- 0.3 nA) injection in the soma. The inset (blue trace) is a zoom of the sag.

2.3.2 Gap Junctions Modulation

The SCs electro-responsive properties were the basis to explain gap junction modulation and synaptic integration. The investigation of these processes is fundamental to analyze the connectivity rules of electrically connected interneurons to form complex networks. The electrical activity in

addition to the inhibitory synaptic activity between interneurons allows the growth of local microcircuit with a synchrony and rhythmic behavior.

The model reproduces the correct responses when two cells (Cell 1 and 2 in the **Fig. 15**) are connected through gap junctions located on the proximal dendrites. The Cell 1 (black) received two positive current injections in the soma (0.1 nA and 0.2 nA) and Cell 2 responded with an increase of 10 Hz in its frequency and with a clear synchronized firing activity.

The simulation demonstrated a direct current flow between coupled neurons that led to synchronize activity. This result occured in absence of inhibitory and excitatory synaptic activity, demonstrating that only the electrical activity triggered a regular and synchronized activity between coupled SCs. As the experimental results reported (Mann-Metzer and Yarom, 1999), the model reproduced the synchronized electrical activity in the Cell 2 connected with the Cell 1 that received current injection steps (**Fig. 15**).

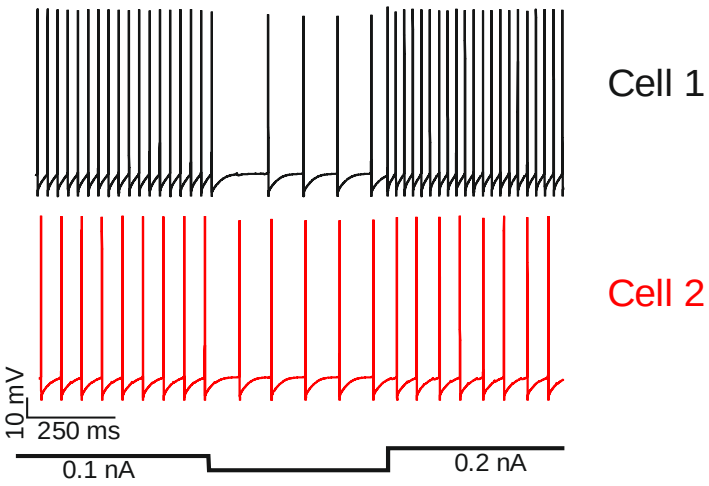

Fig. 15. Synchronized reciprocal cellular activity modulated by gap junctions.

2.3.3 Synaptic Activity

SCs receive synaptic excitation input from the pf and synaptic inhibition from other SCs in the ML. The SCs transmit inhibitory synaptic input to other SC dendrites, which causes them to have a reciprocal inhibition, to form a horizontal inhibitory network able to influence many adjacent PCs and finally to transmit the inhibitory activity to each PC, the only output of the cerebellar circuit.

The SC synaptic activity was simulated with membrane mechanism reproducing the behavior of AMPA/NMDA and GABA receptors applied to the dendritic sections.

Inhibitory Synaptic Activity

The model reproduced the SC inhibitory synaptic activity, showing the responses of interconnected SC receiving reciprocal inhibition. The inhibitory synaptic activity was configured as a background of random activity received by other cells in the vicinity.

The model responded to a background synaptic activity of 40Hz, to simulate the random activation of synapses coming from four other SCs. This activity was applied to 146 inhibitory synapses spread over the entire dendritic tree. The background activity was able to generate a complex and synchronized response in the second cell (Cell 2) connected with the first (Cell 1) through gap junctions (**Fig. 16**) (Carter and Regehr, 2002).

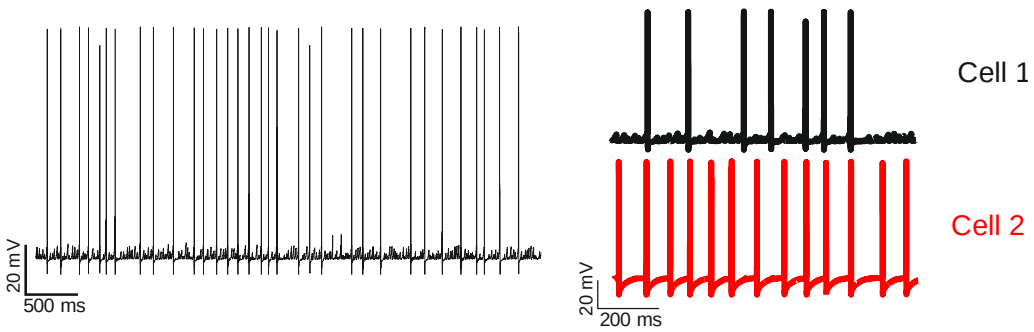

Fig. 16. The model responds to a background inhibitory synaptic activity. The background activity is able to generate a complex response in the second cell (Cell 2) connected with the first (Cell 1) through gap junctions (on the right).

SCs receive synaptic inhibitory inputs from other SCs in the neighborhood and it was found that this reciprocal inhibition occurs in the same microzone, observing that the ML inhibition is organized parasagittally following the microzone orientation, and also the inhibition evoked by the pf in the ML is compartmentalized into the same parasagittal zones (Gao et al., 2006).

Inhibitory and Excitatory Synaptic Activity

The model responded to excitatory bursts (500 Hz every 600 ms), delivered during the background, by excitatory synaptic inputs (red arrows in the Fig.) located on the entire dendritic tree.

The background activity and the excitatory inputs were able to generate a complex and synchronized response in the second cell (Cell 2) connected with the first (Cell 1) through gap junctions (**Fig. 17**).

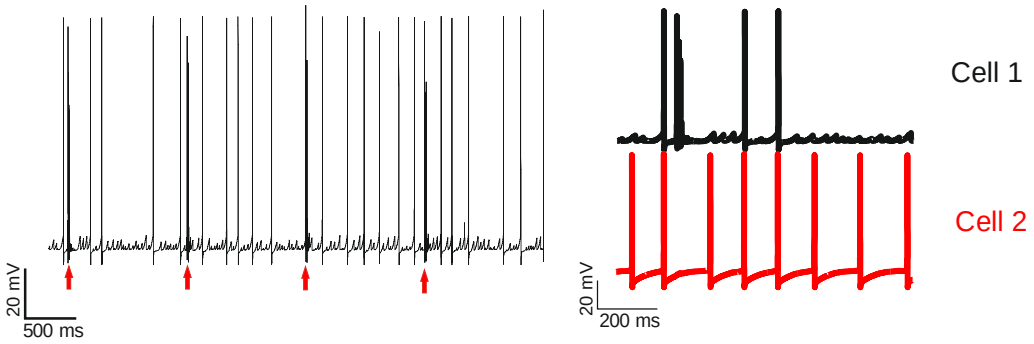

Fig. 17. The model responds to bursts (500 Hz every 600 ms), delivered during the background, by excitatory synaptic inputs (red arrows). The background activity and the excitatory inputs are able to generate a complex response in the second cell (SC 2) connected with the first (SC 1) through gap junctions (on the right).

As reproduced in the experimental recordings (Carter and Regeher, 2002), I tested only the activity of the pf on SC dendrites, simulating an excitatory activity background of 50 Hz (**Fig. 18**). The measured AMPA value was 100 pA to compensate for the absence of Ca^{2+} entry through the AMPA receptor. The synaptic input was applied to each dendrite section, for a total of 147 sections.

It was also observed, during experiments *in vitro* and *in vivo*, the presence of single pf excitatory synaptic inputs that can have a major influence on the excitability of SCs, but this property cannot be reproduced directly by this model as the absence of clear experimental data on the location and activation of that single pf is not available (Carter and Regeher, 2002).

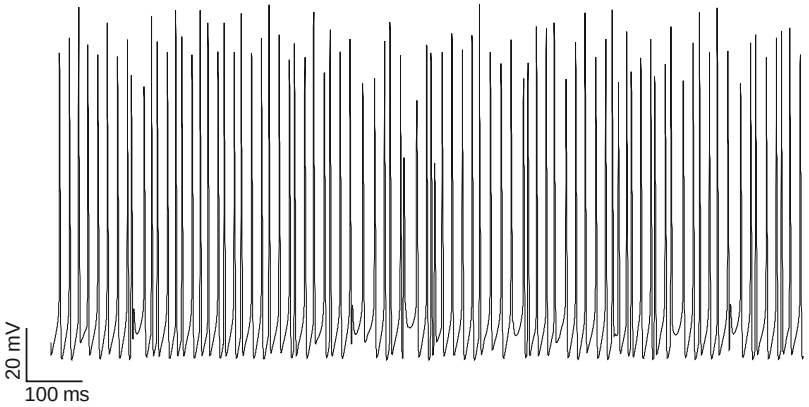

Fig. 18. The model trace reproduces the cellular activity in response to 50 Hz of pf excitatory activity.

Neuronal Transmission

SCs innervate each other, releasing GABA neurotransmitter, to form inhibitory synchronized interneurons networks, providing the inhibitory transmission to PCs.

The background inhibitory activity and the excitatory inputs of the SC 1 are transmitted to SC 2 through GABA synapses and gap junctions. The model reproduced the reciprocal physical connection between two cells. The excitatory and inhibitory synaptic activity received from the first cell (**SC 1 in the Fig. 19**) is transmitted to the second cell (**SC 2 in the Fig. 19**). During the simulation, the gap junctions are active, leading to a synchronized and regular activity in SC 2, as it is shown in the **Fig. 19**. The inhibitory synaptic activity and the electrical activity between cells contribute together which results in a synchronized cellular activity in the second cell. All this activity occurs in the entire SC network in the ML.

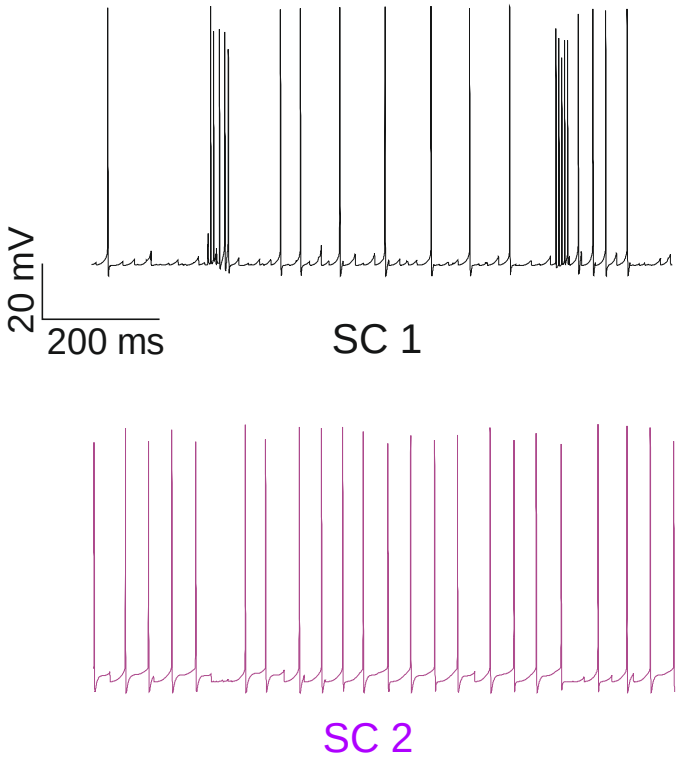

Fig. 19. The background activity and the excitatory inputs of the SC 1 are transmitted to SC 2 through GABA synapses and gap junctions.

Stellate Neuron Synaptic Activity on Purkinje Neuron

A relevant role is the SC inhibitory output transmitted to PC, to regulate the PC firing patterns, which based on recent experiments, influences directly the GrCs (Guo et al., 2016).

A recent study showed, with Ca^{2+} imaging experiments, the fundamental role of SCs in the organization of PC activity, which in turn will influence the final DCN activity. The transmission of inhibitory activity from SCs, as a result of pf excitatory synaptic activity and inhibitory SC synaptic activity integration in the SCs, gives rise to simultaneous pauses in the PC simple spike (SS) activity and also in the neighboring PCs (Ramirez and Stell, 2016). Pauses in the SS of PCs, generated by the SC activity transmitted to the PCs, were investigated in many others experiments, as it is reported

in these works (Häusser and Clark, 1997; Loewenstein et al., 2005; Oldfield et al., 2010; Schonewille et al., 2006; Yartsev et al., 2009). Several studies demonstrated the role of PC pauses in memory formation and information storage (Grasselli et al., 2016; Maiz et al., 2012). It was also observed that the excitation transmits to the PCs by the pf, together with the SC activity on PC, causes in PCs bursts of action potentials, which terminate with a brief pause in PC firing, showing the typical Burst/Pause behavior (Steuber, et al. 2007; Womack et al., 2004).

To reproduce the PC behaviors that depend on the SC activity they receive, the SC model was connected directly with a PC model (Masoli et al., 2015). In this way, the SC inhibitory background activity, at 40 Hz, was transmitted to then PC model through pre validated GABA synapses. The trace showed the impact of the activity on the PC model with the pauses in the *simple spike* (SS) firing (**Fig. 20**).

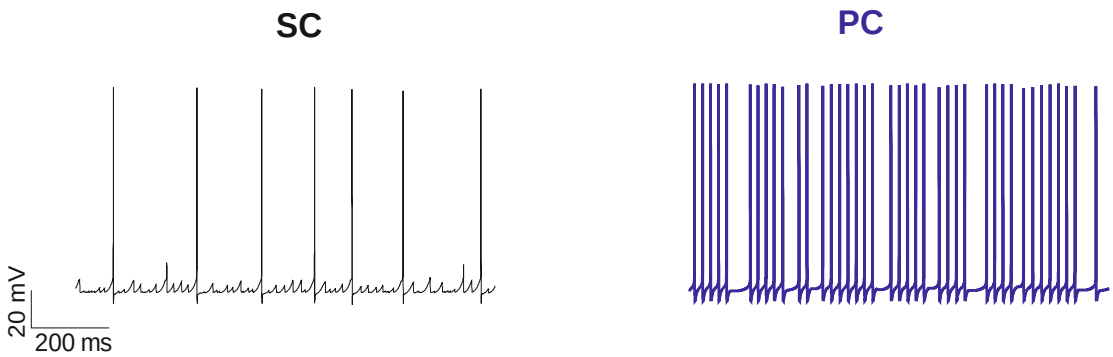

Fig. 20. The SC inhibitory background activity, at 40 Hz (on the left) is transmitted to the PC model through GABA synapses. The trace (on the right) shows the PC model modulation of the SS firing.

Another simulation shows how the PC responds when it receives a SC activity obtained with an inhibitory background interrupted by several pf bursts, with 5 spikes at 250 Hz every 400 ms. The PC responds to the SC activity, showing longer pauses in the SS firing (**Fig. 21**).

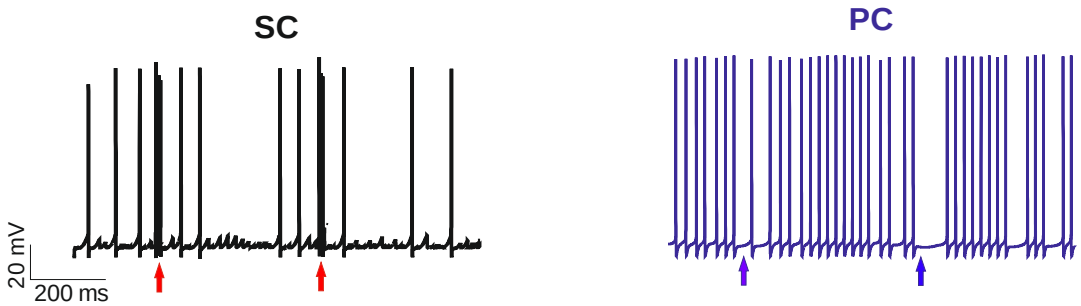

Fig. 21. The SC activity, obtained with the inhibitory background, is interrupted by several pf bursts, with 5 spikes at 250 Hz every 400 ms (on the left). The PC responds to the SC activity, showing longer pauses in the SS firing (on the right).

The last simulation showed a critical PC behavior, largely investigated in experimental conditions. The PC trace showed the modulation of the SS by pf bursts transmitted through AMPA receptors and the inhibition received from the SCs. Both pf bursts, in SCs and PCs, composed by at 250 Hz, were delivered at the same time every 400ms, in both type of cells. This configured the typical PC Burst/Pause behavior (**Fig. 22**).

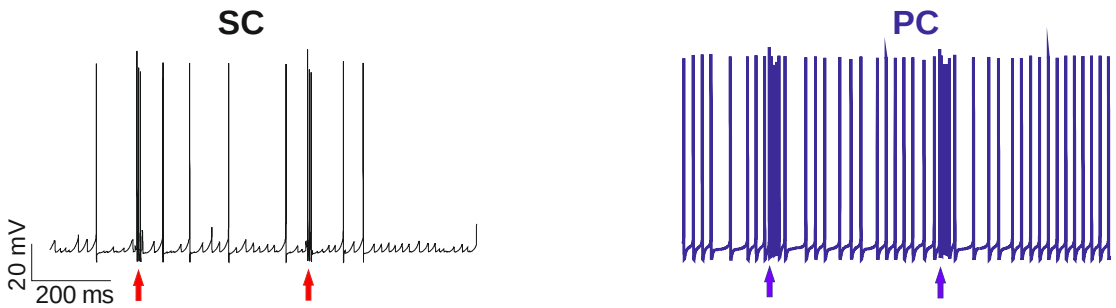

Fig. 22. The PC trace (on the left) shows the modulation of the SS by pf bursts transmitted through AMPA receptors and the inhibition received from the SCs. Both pf bursts, were at 250 Hz, delivered at the same time at 400ms.

2.4 Discussion

The SC model is the first detailed conductance-based SC model tuned with a hand process that simulates the typical electrophysiological properties of the SC, reproducing the cellular experimental behaviors. The biophysical reconstruction of SC functions is based on intrinsic ionic mechanisms, able to reproduce the electroresponsive properties and the capability to respond to different types of synaptic activity that characterize this type of neuron.

Model morphology is based on a human morphology (Jacobs et al.,) and was reconstructed adding fifteen voltage-dependent ionic channel subtypes, located in the different sections of the morphology, following pharmacological and physiological experimental data. The channels include Na^{2+} channels (Nav1.6 and Nav1.1), many members of different K^{+} channels subfamilies (Kv3.4/4.3/1.1/7), several Ca^{2+} (Cav2.1/3.1/3.2/3.3), Ca^{2+}-dependent K^{+} channels (KCa1.1/2.2) and some additional channels like the K^{+} inward rectifying (Kir2.x) and the K^{+}/Na^{2+} hyperpolarization-activated cyclic nucleotide-gated channel 1 (HCN1).

The results obtained with the simulations described several critical properties of the SCs. It was observed that the cellular auto-rhythmic activity, at 14 Hz, was generated by Na^{2+} channels in the AIS and that the ionic channels mechanisms led together to generate the spike in the AIS section. The model responded to a series of positive somatic current injections, from 0.04 nA to 0.32 nA, with a linear I/O relationship, showing the increase in frequency. The role of KCa1.1 channel was investigated, which is critical for the spikes' hyperpolarization, and the role of I_h during the SAG inward rectification mechanism, in response to a negative current injection.

Simulations that are relevant are the ones that reproduce the gap junction modulation, peculiar for these types of inhibitory interneuron, and the synaptic activity, showing how SCs are connected with the others cerebellar neurons to form complicated microcircuits and to regulate the entire cerebellar network activity.

The model showed that the responses of SCs linked by gap junctions, located on proximal dendrites and that their effect was, to synchronize the activity of couples of neurons, giving rise to a synchronized and regular activity that characterized the entire ML.

The SC model responded to inhibitory SC synapses and to excitatory pf synapses with a complex interaction, showing the activity of the SC connected with another SC through gap junctions and GABA synapses.

Finally, the model reproduced the interaction of the SC with the PC and the resulting modulation of PC firing. The PC is a complex neuron and it is the only output of the cerebellar network and as such, plays the critical role of encoding all the output signals transmitted by GrCs and IO. The control of PC firing is the most important feature of SCs, because of their influence on PCs which has an impact on the entire cerebellar network control.

Chapter 3

3. Parameter Estimation of Single Neuron Models

The PE problem is a complex one, trying to solve the problem of estimating unknown information of a (biological) system (e.g., molecular concentrations, kinetic constants, $G_{i\text{-}max}$ values), by means of different algorithms applied to problems of systems biology. Algorithms that solve the optimization problem exploit different techniques, such as, in the context of this work, mostly stochastic and probabilistic methods like *Simulated Annealing* (SA), *Evolutionary Algorithms* (EA), GA and SI.

Detailed mathematical models of neurons are a valuable tool for the investigation of these complex and fundamental cells. The most advanced models based on the HH theory require the fine-tuning of a large number of parameters, which are the $G_{i\text{-}max}$ values. This activity is generally performed by hand, in a time-consuming and error-prone process. Due to the complexity and non-linearity of neuronal dynamics, the identification of proper *parameterization* (θ) of $G_{i\text{-}max}$ values, to stabilize their interaction and dynamics to lead the physiologically plausible neuronal behaviors, it is a difficult task, leading to the PE problem, which is generally solved by global optimization techniques.

In the last decade, the interest of the neuroscientists for automated procedures for tuning of computational neuron models increased and many techniques were progressively improved to reach optimal results. In addition, the computational resources, available to study this complex PE problem, are constantly increasing and allow scientists to take advantage of the automated parameter tuning software.

A detailed review of automated techniques for the neuron model optimization can be found in (Van Geit et al., 2008). This work explains the importance of the optimization algorithm procedure of fitness functions and of the search process of algorithms. The fitness functions compare the output of models with a different candidate set of parameters (model θ) with experimental data. After determining the fitness functions, it is fundamental to choose the algorithms in order to find the optimal solution to the problem, the best model θ, in less computational time.

The algorithms for the optimization problem can be classified as *stochastic* or *deterministic*, *local* or *global*, *single* or *multi-objective*. The goal of an optimization algorithm is to find the global minimum to reach the optimal solution in the search space. However, in the case of neuron model θ, because of the complexity of the problem, it is impossible to reach a unique global minimum, finding a set of parameters that replicate perfectly the experimental data. However, it is possible to define optimal models, whose solutions show negligible differences compared with the experimental traces.

The GA, for example, were exploited in the works of (Druckmann et al., 2007; 2011) and in the paper of (Hay et al., 2011). Following the principles of GA, which include the creation of an initial population of random individuals, their fitness evaluation, reproduction, mutation and selection to form a new population, neuronal models with different electrophysiological properties were optimized, achieving good results.

PSO is inspired by the collective movement of bird flocks and fish schools (Kennedy and Eberhart, 1995). PSO formulation is based on a swarm of N individuals (particles) that moves inside a bounded search space, collecting and sharing information about the best position found, with respect to a user-defined fitness function, and cooperating to identify the optimal solution for a complex problem (**Para 3.2.1**).

GA implemented in the recent BluePyOpt framework, an extensible Python-based framework for data-driven model parameter optimization (Van Geit et al., 2016), and PSO methods are compared to test the computational effectiveness (quality of results) and efficiency (convergence rates and runtimes) of both algorithms for PE of neuronal models (**Para 3.2.5**). The techniques are applied on the SC model, using the same model parameters: morphology, channel locations in the different sections, $G_{i\text{-}max}$ boundaries values. The optimization tests provided for the same number of individuals and generations. To compare the convergence rates and the runtimes, the algorithms are implemented for parallel architectures and tested on a dual processor equipped with a total of 12-cores, using the fixed time step of 0.025ms and simulations of 2000ms.

3.1 Application of High Performing Computing to Computational Neuroscience

In the computational neuroscience field it is increasingly necessary to apply HPC techniques, because the computational neuronal models represent an indispensable approach to test hypotheses and theories on the brain functioning and the achievement of high quality results in a feasible amount of time depends on the computational resources. The models able to reproduce the realistic behaviors become increasingly complex every time new biological details are added, and even a single simulation can be unaffordable in conventional architectures.

Computers based on single CPUs are constantly improving, offering high performance, exploitable only using specific parallelism techniques, such as multi-threading.

To improve the performance even further, the best solution is to write programs capable of scaling on more than one CPU. Furthermore, GPUs are now used to accelerate simulations due to their ability to perform extensive quantities of computations in parallel, showing significant improvement in execution time compared to CPUs.

In order to study the parameters of the mathematical neuron models, by using automatic PE methods, it is mandatory to employ parallel computing techniques, as will be shown in section (**Para. 3.2.3**).

In this way, it is possible to build networks comprising neurons that are not all identical, thus providing more dynamics, which can be used to understand the mechanisms that underlie fundamental neuronal functions and processes, such as learning, memory consolidation and neuronal development.

Most neural simulators are built to exploit the multithread approach or an MPI approach (explained in **Para. 3.2.3**) to run on more than one CPU, running on a cluster of multiple machines, or specific HPC devices (Xeon Phi), or a single-multiple GPU. All of these approaches still show limitations in execution time when biological details are complex and numerous (Richert et al., 2011; Hoang et al., 2013). Many simulators can simulate more than one million neurons and 100 million synapses in real-time but usually using simplified models, IF above all. The implementation of a network model of 10^8 neurons was investigated in 2012, using the NEST simulator, to exploit supercomputers, (Eppler et al., 2008; Helias et al., 2012) and the works of (Djurfeldt et al., 2008) described the distributed simulations of spiking networks on parallel computers with the SPLIT simulator. Instead, for the construction of HH models, the most popular simulator is NEURON (Hines and Carnevale, 2001), which was built with the support for parallel network simulation using MPI. A model with a network consisting of 40000 realistic neurons was simulated using 100 processors in parallel (Migliore et al., 2006; Hines and Carnevale, 2008). Various other models were performed to investigate parallel neuronal network simulations with NEURON simulator, exploiting the power of modern supercomputing architectures (Helias et al., 2012; Hines et al., 2008, 2011).

Several studies performed on GPU were performed to simulate cerebellar models that run in real-time. They consist of reproducing large-scale spiking network models of the cerebellum, used to study the role of the cerebellum as a learning machine. The models could be used as a real-time adaptive neural controller for humanoid robots, which are instructed to learn a complete activity (Yamazaki and Igarashi, 2013). The model of the IO-networks, which is responsible with the cerebellum for crucial sensorimotor integration functions in humans, was simulated on 4 different GPU platforms. A model of a large-scale spiking network of the cerebellum, composed of more than 1 million neurons, was implemented to be executed on 4 GPUs simultaneously, achieving simulations in real-time, in order to study the neural mechanisms of memory consolidation in the brain (Gosui and Yamazaki, 2016).

More recently, accelerated neuromorphic hardware systems have been utilized for the implementations of neuronal models. In a silicon form, neuromorphic devices mimic the structure and emulate the function of biological neural networks. The neuromorphic approach is relevant in neuroscience for its high parallelism (Bruderle et al., 2011; Pfeil et al., 2013).

3.2 Parameter Estimation of Cerebellar Stellate Neuron Model

In this work, an approach based on an automatic PE method which exploited the SI technique known as PSO was investigated. PSO is applied to the SC conductance-based neuronal model and the results show that the methodology is promising. The multi-compartmental SC model was implemented in Python-NEURON and followed the construction and the description analyzed in detail in **Ch.2**, the

only difference with the SC optimized model concerns the type of cellular morphology (**Para. 3.2.2**). To reduce the computational costs, HPC techniques are necessary. In this work, the methodology was implemented with MPI to build a concurrent parallel approach, accelerating the fitness evaluations by mean of a cluster.

3.2.1 Particle Swarm Optimization

An optimization problem, to be solved, requires finding the optimal solution in an *N*-dimensional search space of possible solutions by mean of mathematical and computational methodologies. Optimization problems can be problems of minimization, as in our study, or maximization. The goal is to identify the solution $x \in R^N$ that minimizes or maximizes a given objective function $F: R^N \rightarrow R$.

In this research, the SI technique was exploited, known as PSO, to solve the optimization problem for single neuron models. SI is based on the observation and on the successive simulation of the collective behavior of groups of living organisms. According to sociobiological principles, social insects e.g. ants and bees, animals, fishes and birds, demonstrate a collective intelligence, which allows groups to self-organize, share information and perform complex tasks together (Hölldobler and Wilson, 2008; Seeley, 1989).
PSO is a bio-inspired stochastic meta-heuristic algorithm feasible for the global optimization of complex problems whose solutions can be encoded as real-valued vectors. Introduced by Kennedy et al. (Kennedy and Eberhart, 1995), this SI technique mimics the collective movement of groups of animals (flocks of birds, schools of fish) to explore a bounded D-dimensional search space. In PSO, a population (swarm) of N candidate solutions (in this work 100 and 50 particles, depending on the tests performed) moves inside a D-dimensional search space to reach the best solution and it repeats the search until a fixed number of iterations is performed (this work is equal to 100 or 50 iterations, depending on the tests performed), exchanging information about the most promising solutions found and cooperating to identify the optimal solution.

At the initialization of the algorithm, all the particles of the swarm are distributed randomly in the search space and have a random velocity. The procedure is iterative and, for each iteration, a number of points in the parameter space, that are the parameter sets, are found. The fitness function is evaluated for all the particles and a new set of parameters, which depends also on the results of the previous iteration, is ready to start the next iteration and so on.

The *n*-th particle, $n = 1, ..., N$, is characterized by two vectors: the position $x_n \in R^D$ and the velocity $v_n \in R^D$, that is used to update the particle position. During each iteration of the algorithm, velocities are used to update particles' positions. In particular, each velocity is updated according to two attractions: the best solution found by the swarm $g \in R^D$ (G_{best}) and the best solution found by the *n*-th particle $b_n \in R^D$ (P_{best}).

Specifically, the velocity is updated according to the following equation:

$$v_n = w * v_n + C_s * r_1 * (x_n - g) + C_c * r_2 * (x_n - b_n) \quad (7)$$

Then, the position of the particle is updated by calculating:

$$x_i = x_i + v_i \quad (8)$$

For all $i = 1, \ldots, n$

Where C_s and $C_c \in R^+$ are two scalar factors, which balance the attraction towards g and b_n, respectively. C_s is the social attraction and C_c is the cognitive attraction, which control the global exploration and the local exploitation of the search space. Two common settings for C_s and C_c are 1.9; they are used as a default in this work. The change of velocity, with respect to the previous iteration, is weighted by an inertia factor $w \in R^+$, to avoid chaotic behaviors of the swarm. In this work, I used an inertia value linearly decreasing from 0.9 down to 0.4. Finally, the two attractions, C_s and C_c, are perturbed by means of two vectors $r_1, r_2 \in R^D$ of random numbers with uniform distribution in (0, 1), to prevent particles from prematurely converging to local minima.

I defined a feasible region for each parameter under optimization. In order to prevent particles from reaching non-feasible regions, the search space is bounded and “damping" boundary conditions (Xu and Rahmat-Samii, 2007) are applied: whenever a particle leaves the search space along one of its dimensions, it is relocated on the boundary along that dimension; moreover, its velocity is reversed and multiplied by a random value sampled from [0, 1) with uniform distribution.

Each particle in the swarm is characterized by a specific position, which corresponds to a candidate θ. The quality of the particles, which drives the movement of the swarm, is determined by means of a fitness function f: $R^D \rightarrow R^D$.

The PSO algorithm halts when a termination criterion is met (for example 100 or 50 iterations) and returns g as the result of the optimization. At the end of the iterative process, the swarm converges to an optimal solution, with θ able to minimize the fitness function.

PSO satisfies the principles of exploration and exploitation, underlying the convergence of the global search algorithms. The exploration provides checking many regions of the parameter space, while the exploitation allows obtaining as much information as possible from the parameter space and from the space visited during the past iteration of the search, in order to find the new sets of parameters.

PSO is a stochastic algorithm, the advantage of the randomness is to increase the exploration of the parameter space.

3.2.1.1 *Particle Swarm Optimization Applied to the Parameter Estimation Problem of the Cerebellar Stellate Neuron Model*

PSO estimates the most fitting $G_{i\text{-}max}$ parameters, exploring the extensive parameter space of single-neuron models. The goal of the procedure is to determine a combination of solutions (particles with a set of $G_{i\text{-}max}$ values) that minimize the distance between the mean value of the experimental responses and that of the model response.

The particles are models with a set of parameters that generates a neuronal simulation. PSO was performed with 100 and 50 particles and 100 or 50 iterations, depending on the tests performed (**Para. 3.2.4**).

The parameters that were estimated with this methodology are 17 $G_{i\text{-}max}$ parameters distributed over the model morphology. Each parameter has a minimum boundary and a maximum boundary, in these constraints the $G_{i\text{-}max}$ values for the first PSO iteration are chosen.

Each particle in the swarm is characterized by a specific position, which corresponds to candidate Θ.

The fitness function assesses the "goodness" of the particles and drives the movement of the swarm. The fitness functions based on experimental measures (e.g. membrane potential (mV) at time *t*, frequency (n° action potentials/second, (Hz)), are the features that characterized the neuron. This work investigated the study of two fitness functions applied to the specific PE problem, the first is based on the neuronal output dynamics and the second is based on the mean frequency value of the voltage traces. The first approach, known as point-to-point comparison, compares the target electrophysiological traces, that derives from the SC model used as benchmark (**Ch. 2**) in a direct manner but it is highly sensitive to time shifts between the traces. The second approach uses features of the target data as points of comparison with the optimized models' data.

Both the fitness functions show fundamental properties which the model is able to reproduce and are quick to calculate, so they can perform many fitness evaluations during the optimization run, allowing a speedy convergence of the algorithm to optimal solutions.

The choice of the fitness functions is fundamental to quantify how well the optimized model voltage traces compare with the target model voltage traces.

The fitness function based on the output dynamics of the neuron is described as follows:

$$f(\theta) = \sum_{t=1}^{T} |S(t,\theta) - E(t)| \tag{9}$$

Where *S (t, θ)* is the simulated potential at time *t* using *θ* and *E (t)* is the experimental potential at time *t*. I assume a set of *T* discrete-time samples and the NEURON simulator performs the simulation of the dynamics.

To assess the fitness function based on the mean frequency value of the voltage traces, I compared the target mean frequency value (σ_t) with the estimated mean frequency value using θ (σ_θ).

The fitness function is calculated as follows:

$$f(\theta) = |\sigma_t - \sigma_\theta| \tag{10}$$

The NEURON simulator was used to calculate the fitness value (**Eq. 9/10**). Specifically, a novel model was created using the putative parametrization of each particle. The model was then simulated with NEURON for 2000ms. Then the features of the output (the dynamics of the output potential or the mean frequency) were compared against the target features to assess the fitness value. The dynamics of the output potential was saved to file every 0.025 milliseconds (ms) for a total of T = 80000 samples. The mean frequency value was obtained with the Electrophys Feature Extraction Library (eFEL) (Van Geit, 2015), which permits to extract values from voltage traces.

3.2.2 Model Construction

The SC neuron model used for the PE problem, exploiting PSO methods, was a simplified version of the model described in **Ch. 2**.

I implemented a multi-compartmental SC model in Python-NEURON (Python 2.7, NEURON 7.4). The SC model was a biophysically detailed conductance-based model containing a morphology reconstructed from statistical information obtained from a real cell, passive properties and 15 ionic channels, with their kinetic mechanism descriptions, distributed in the different sections, for a total of 42 parameters.

The fundamental difference with the model described previously concerns the model morphology. The morphology is composed of 36 sections forming distal dendrites, proximal dendrites, soma, AIS and axon (**Fig. 23**).

Fig. 23. SC model morphology.

The passive properties of the SC model include the Ra which was set to 100 Ωcm for all the sections (distal and proximal dendrites, soma, AIS and axon), the Cm was defined as 1µF/cm^2 for all the

sections and the E_{rev} of the different ionic species were defined at the following values: E_{Na} = 60 mV; E_k = -75 mV; E_{Ca} = 137 mV E_h = -43 mV; E_{leak} = -59 mV.

The total of parameters estimates in our optimization tests are 17 distributed in the different sections of the SC morphology: the Na^{2+} channels (Nav1.6 and Nav1.1) in the soma, AIS and axon sections, the K^+ channels (Kv3.4) in the soma, AIS and axon sections, the Ca^{2+} channels (Cav2.1) in the soma, proximal and distal dendrite sections, Ca^{2+}-dependent K^+ channels (KCa1.1) in the proximal and distal dendrite sections, the K^+/Na^{2+} hyperpolarization-activated cyclic nucleotide-gated channel 1 (HCN1) in the soma, proximal dendrite, distal dendrite and axon sections and the Leakage (leak) located in the soma section.

The $G_{i\text{-}max}$ parameters with their value boundaries are clearly described in **Table 5**.

Table 5. $G_{i\text{-}max}$ values in the multi-compartment SC model.

Conductance/ Location	Range $G_{i\text{-}max}$ (S/cm2)
leak_soma	0.00015- 0.00045
Nav1.1_soma	0.045-0.135
Kv3.4_soma	0.01-0.035
HCN1_soma	0.00005-0.0002
Cav2.1_soma	0.0002-0.001
Cav2.1_proximal dendrites	0.00011-0.0008
Kca1.1_ proximal dendrites	0.01-0.03
HCN1_ proximal dendrites	0.00005-0.0003
Cav2.1_distal dendrites	0.00011-0.0008
Kca1.1_ distal dendrites	0.005-0.03
HCN1_ distal dendrites	0.00005-0.0008
Nav1.6_ais	0.2-0.7
Kv3.4_ais	0.02-0.08
HCN1_ais	0.00005-0.00015
Nav1.6_axon	0.02-0.06
Kv3.4_axon	0.005-0.015
HCN1_axon	0.00005-0.00015

Table 5. The table defines the parameter types, their location in the different morphology sections and the range for each $G_{i\text{-}max}$ parameter.

The parameter boundaries, the experimental trace to evaluate the output voltage potential during the simulation time and the mean spike frequency value, 14 Hz ± 6,77 (*mean* and *standard deviation* (SD)), to assess the fitness functions are provided to start the optimization process. The mean and SD of the spike frequency of the spontaneous firing are extracted from multiple runs of the target traces of the SC model, descripted in **Ch. 2**, and used as benchmark.

For the fitness evaluations, I used NEURON's implicit Euler integration method with fixed time step.

Ionic channel gating was modeled following the HH formulation or Markov-chains for multi-state transitions. The membrane voltage for each compartment is calculated using the time integral of the equation:

$$\frac{dV_m}{dt} = -\frac{\sum_{h=1}^{H}(g_h\,(V_m - V_h) + i_{inj})}{C_m} \tag{11}$$

Where V_m is the membrane potential; C_m is the membrane capacitance; g_h and V_h denote respectively the $G_{i\text{-}max}$ values and the E_{rev} with the subscript h representing the different channels (h = 1, …, H and H = 15 in this model). Finally, i_{inj} is the injected current.

The SC is an inhibitory interneuron located in the ML of the cerebellar cortex, involved in the local microcircuit providing inhibition to the PC, as we saw in detail in **Ch. 2**. SCs are characterized by an auto-rhythmic behavior, the cellular intrinsic spontaneous firing of about 14 Hz, which is the specific neuron target of this automatic procedure. The optimal solution, at which the optimization process converges, reproduces this critical and fundamental SC behavior.

3.2.3 Parallel Computing

To reduce the computational costs, I extended the methodology with MPI, in order to leverage a distributed architecture for the fitness evaluations required by PSO. The fitness evaluations were accelerated with a cluster. I tested the methodology on a dual processor equipped with a total of 12-cores, using the fixed time step of 0.025ms and simulations of 2000ms. With this distributed architecture, a parameter estimation was performed in about 3 hours, using 50 particles and 100 iterations.

3.2.3.1 Message Passing Interface

MPI is a standardized message-passing system designed to function on a wide variety of parallel computers. The standard defines the syntax and semantics of library routines and allows users to write programs in the main scientific programming languages (Fortran, C, or C++). The MPI is a language-independent communications protocol used to pass information between CPUs. It can be used from a multi-core CPUs to cluster composed by hundred thousand nodes.

The fundamental commands for an MPI program are *MPI_Init* (initializes the MPI environment), *MPI_Comm_size* (returns the number of processes), *MPI_Comm_rank* (returns this process's number (rank)) needed for the initial communications; *MPI_Send* (sends a message), *MPI_Recv* (receives a message) to communicate data to each rank; *MPI_Finalize* for exit from the message-passing system.

Most MPI programs are written on C using standard libraries provided for all the major computing platforms. In order to run parallel programs in python, was used a module called MPI4py which means "MPI for Python". This module provides standard functions to do tasks such as get the rank of processors, send and receive messages/data from various nodes in the clusters. It allows the program to be parallel executed with messages being passed between nodes.

3.2.3.2 Integration between Python Particle Swarm Optimization and NEURON Simulator

Since the simulation of each particle in the iteration does not require communicating with the other particles, each simulation runs in parallel and, depending on the number of particles and the core/CPU availability, it can be readily decided how many simulations per core/CPU can be done. The **Fig. 24** explains how the PSO algorithm, written in Python programming language, is used with the NEURON simulator for the PE of the unknown $G_{i\text{-}max}$ values. NEURON is used to run simulations for each particle with a different θ and to evaluate the fitness function for each particle, at the end of the simulation. For each particle, a new set of $G_{i\text{-}max}$ particles is estimated and, interacting with the prefixed morphologies and passive properties of the neuron, is simulated with NEURON for 2000 ms. Each particle of each iteration is a model that gives an output. The features of the output (the output dynamics (time/voltage traces) or the mean frequency) are compared against the target features to assess the fitness value. The mean frequency value is obtained with a python library, eFEL, which permits to extract values from voltage traces.

eFEL allows to automatically extract features (spike frequency, spike amplitude, spike width, inter spike interval, etc.) from time series data recorded from neurons with experiments or with simulations. The user has to provide the traces and the features to be calculated. In the feature library the voltage trace is represented by two vectors, the voltage vector *v* and the corresponding time vector *t*. The library will then extract the requested features and return the values to the user, that are represented as vectors as well (Van Geit et al., 2016).

The entire optimization process can be divided in different phases. The process is iterative and the number of iterations and the number (N) of particles for each iteration are decided for each optimization run. The process starts with the *PSO Generation Phase*, in this phase, the generation of the swarm composed of N particles occurs and each particle of the first iteration receives a set of parameters ($G_{i\text{-}max}$ values). This set of parameters is a vector of real numbers, which characterized the specific position of the particle in the search space. The position corresponds to a specific θ of

that particle, which is a candidate solution. Then, the N particles are sent to the ranks available on the distributed architecture used, where NEURON provides to run the simulation for each particle to achieve the model output (the generation of the time/voltage traces or the extraction of the mean frequency value from each simulated trace, depending on the fitness value we want to evaluate). In this way, the data necessary for the fitness calculation are available to be used in the next *PSO Updating Phase*. In this latter phase, the features of the output (the output dynamics or the mean frequency value) are compared against the target features to assess the fitness function. The fitness value is calculated for each particle in the swarm, defining the b_n (P_{best}), the best position of each particle. Then, it is possible to calculate the g (G_{best}) of the swarm, the best particle among the whole swarm. The P_{best} and G_{best} values are necessary to update the velocity and the position of each particle, to start with a new set of particles for the next iteration. The velocities are iteratively updated until some termination criterion is met. In this work, the optimization process is stopped when a maximum number of iterations is reached. At the end of the process, the G_{best} of the last iteration is returned as the optimal solution. The swarm converges to a common solution, characterized by a specific parametrization, able to minimize the fitness function.

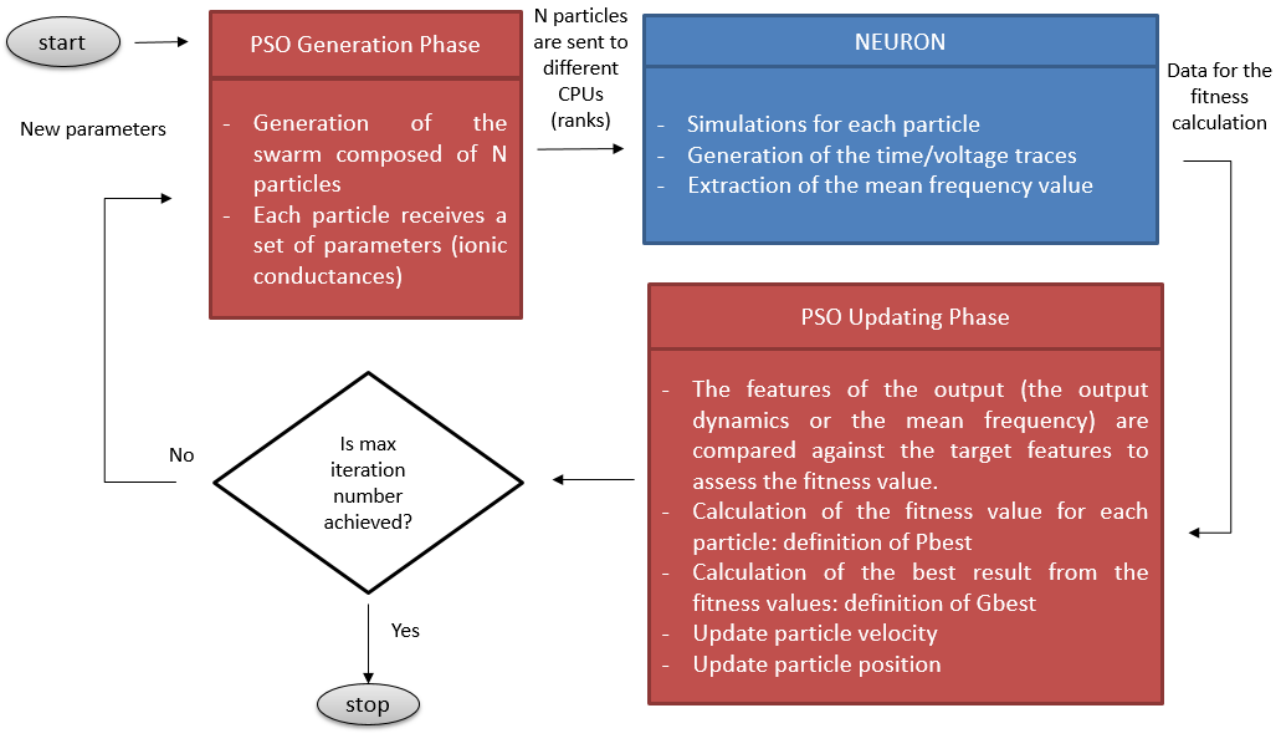

Fig. 24. PSO method integrated with NEURON.

The implementation on multi-core is explained in **Fig. 25**, which clearly describes the division of the optimization process on the different ranks (CPUs) available of the distributed architecture. In the rank 0 the generation of N particle occurs, then the particles are sent to all the other rank (1, …, M) where each candidate solution is simulated and the fitness function is evaluated for each particles. The fitness values are, then, transmitted again to rank 0, where the procedure continues to calculate the best particle in the swarm, which is the candidate solution with the best fitness value that minimizes the distance between the mean value of the experimental responses and that of the model simulated in the process response. For each iteration, this scheme of operations is repeated, until the optimal solution is achieved.

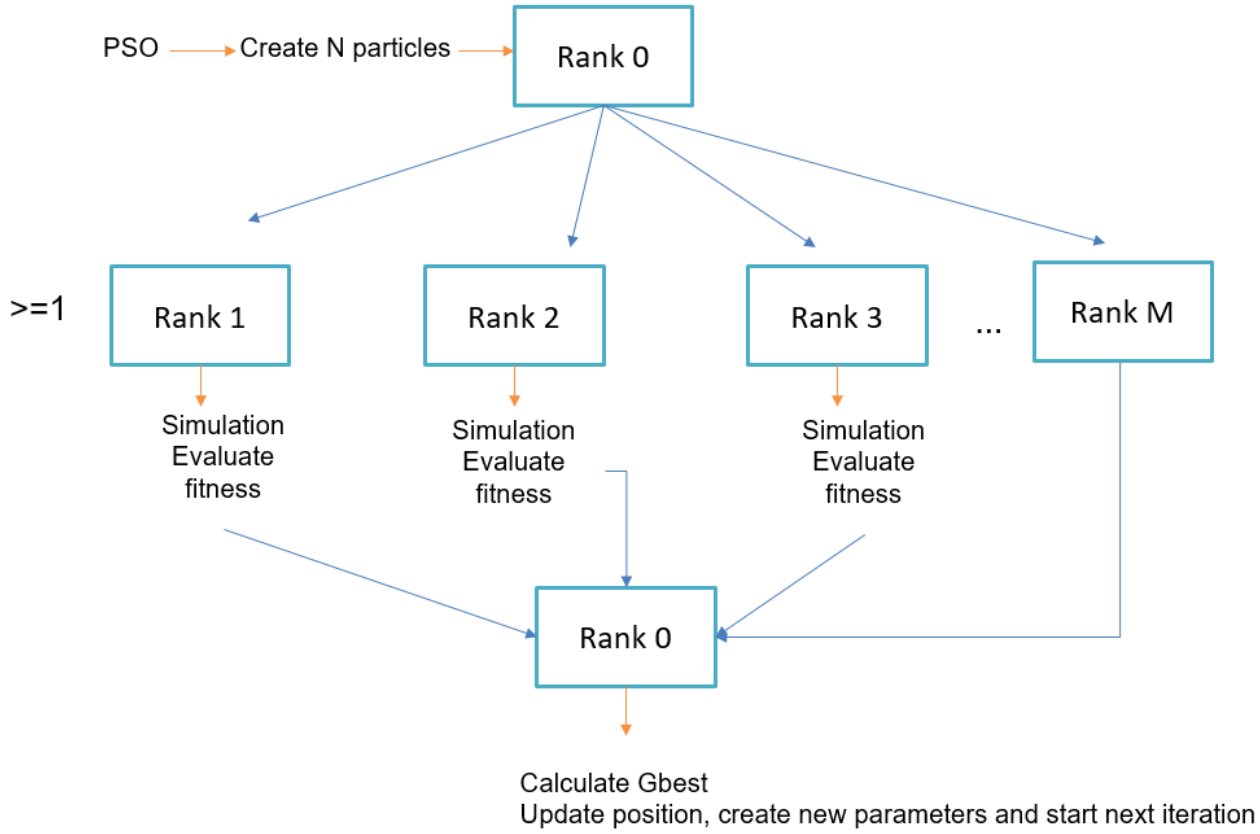

Fig. 25. PSO process implementation on multi-core.

3.2.4 Results

I investigated the feasibility and the computational costs of the methodology by performing tests of increasing complexity. I run the estimation of all 17 parameters and the tests that follow were performed using the SC model defined with NEURON; the model was also used to create the target time-series (the red trace showed in the following figures of the Results).

The fitness function used in the following analysis is based on the mean frequency value of the voltage traces. To assess the fitness value, I compared the target mean frequency value (σ_t) with the estimated mean frequency value using θ (σ_θ). The best θ of the PSO process will minimize the distance between the two values. In this way, the simulated model will reproduce the experimental behavior and the results will show an overlap between the experimental voltage trace and the model voltage trace, showing that the simulated traces have a mean frequency value of 14 Hz ± 3,35 (mean and SD). The mean and SD of the feature is extracted from multiple optimal solution results.

Thanks to this distributed architecture, parameter estimations were performed in about 6 hours and 30 minutes, using 100 particles and 100 iterations. The speed up of the parallel architecture compared with the tests running on single-core is massive. The optimizations with 100 particles

and 100 iterations on single-core need to 72 hours for a single run. The voltage traces in **Fig. 26** (on the left) show the output dynamics of the target (green line) and the output dynamics of a simulation using the best θ of the tests with 100 particles and 100 iterations (red line). The output dynamics of the simulation estimated reproduces the spontaneous firing of the target. **Fig. 26** (on the right) shows the convergence speed (the average best fitness of 20 tests) of the methodology. On average, the methodology converges toward an optimal solution in less than 20 iterations.

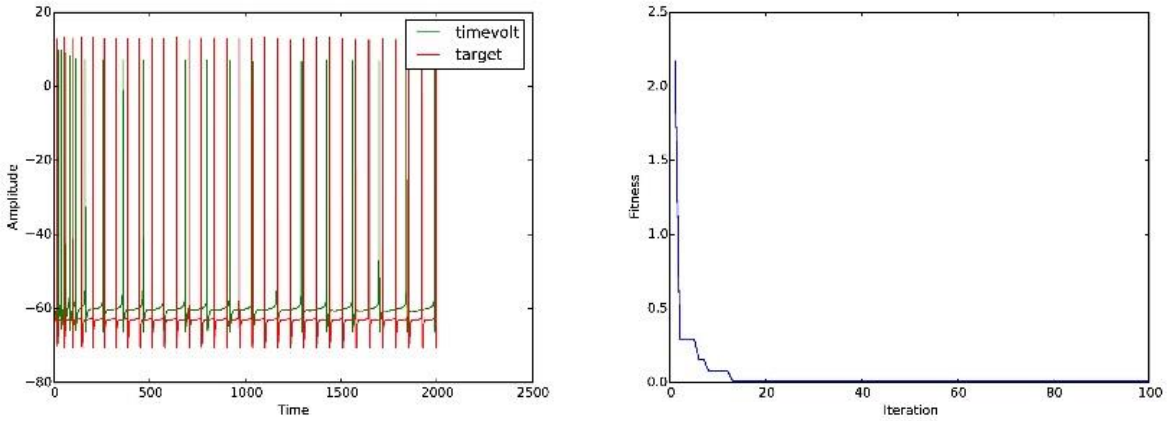

Fig. 26. Optimization tests using 100 particles and 100 iterations.

Parameter estimations were performed in about 3 hours and 20 minutes, using 100 particles and 50 iterations. The speed up is huge since the tests running on single-core needed 42 hours. The voltage traces in **Fig. 27** (on the left) show the output dynamics of the target (green line) and the output dynamics of a simulation using the best θ of the tests with 100 particles and 50 iterations (red line). The output dynamics of the simulation estimated reproduces the spontaneous firing of the target. **Fig. 27** (on the right) shows the convergence speed (the average best fitness of 20 tests) of the methodology. On average, the methodology converges toward an optimal solution in less than 20 iterations.

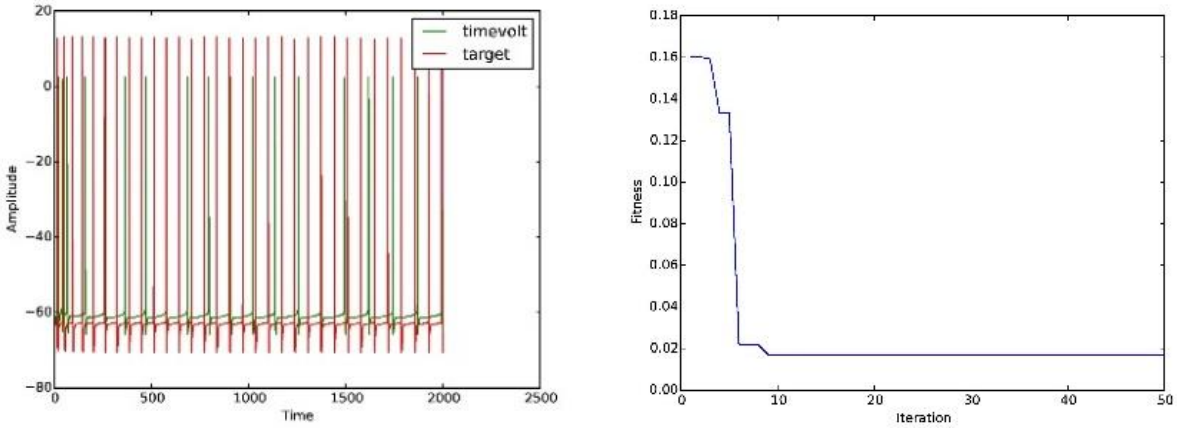

Fig. 27. Optimization tests using 100 particles and 50 iterations.

Parameter estimations were performed in about 1 hour and 20 minutes, using 100 particles and 20 iterations. In addition, in this case, the speed up is huge, since the tests running on single-core needed 18 hours. The voltage traces in **Fig. 28** (on the left) show the output dynamics of the target (green line) and the output dynamics of a simulation using the best θ of the tests with 100 particles and 20 iterations (red line). The output dynamics of the simulation estimated reproduces the spontaneous firing of the target. **Fig. 28** (on the right) shows the convergence speed (the average best fitness of 20 tests) of the methodology. On average, the methodology converges toward an optimal solution in less than 20 iterations.

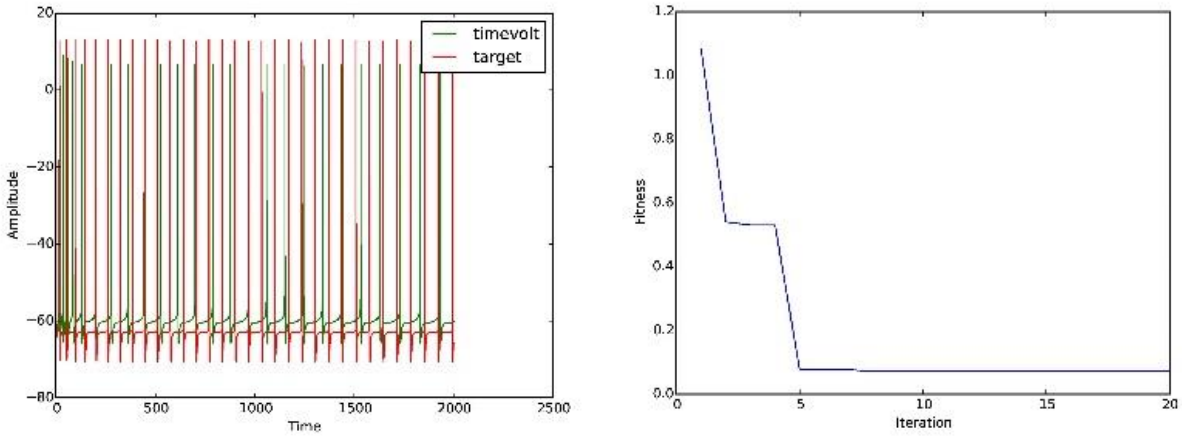

Fig. 28. Optimization tests using 100 particles and 20 iterations.

Parameter estimation was performed in about 3 hours and 38 minutes, against the 44 hours of the single core, using 50 particles and 100 iterations. The voltage traces in **Fig. 29** (on the left) show the output dynamics of the target (green line) and the output dynamics of a simulation using the best θ of the tests with 50 particles and 100 iterations (red line). The output dynamics of the simulation estimated reproduces the spontaneous firing of the target. **Fig. 29** (on the right) shows the convergence speed (the average best fitness of 20 tests) of the methodology. On average, the methodology converges toward an optimal solution in less than 20 iterations.

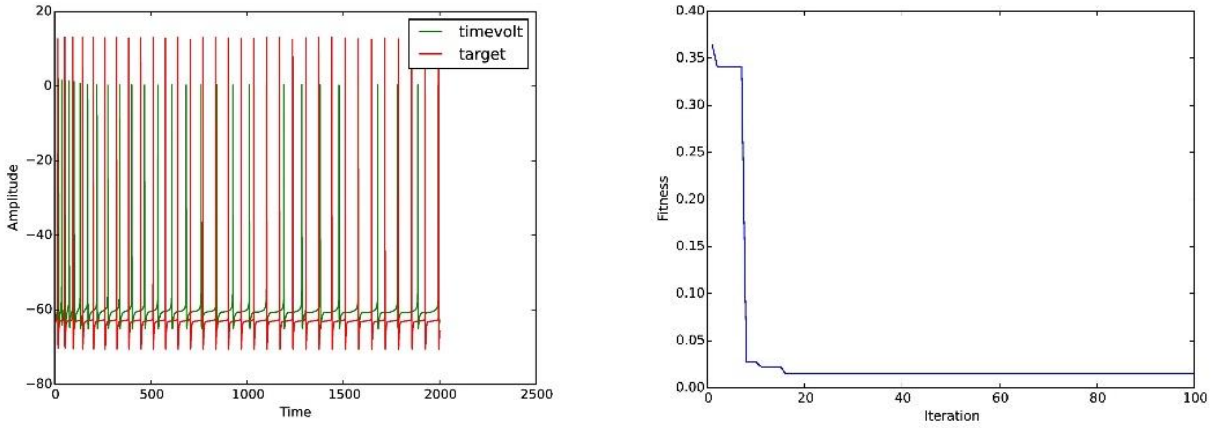

Fig. 29. Optimization tests using 50 particles and 100 iterations.

Parameter estimation was performed in about 1 hour and 50 minutes, against 24hours of the single core approach, using 50 particles and 50 iterations. The voltage traces in **Fig. 30**(on the left) show the output dynamics of the target (green line) and the output dynamics of a simulation using the best θ of the tests with 50 particles and 50 iterations (red line). The output dynamics of the simulation estimated reproduces the spontaneous firing of the target. **Fig. 30** (on the right) shows the convergence speed (the average best fitness of 20 tests) of the methodology. On average, the methodology converges toward an optimal solution in less than 20 iterations.

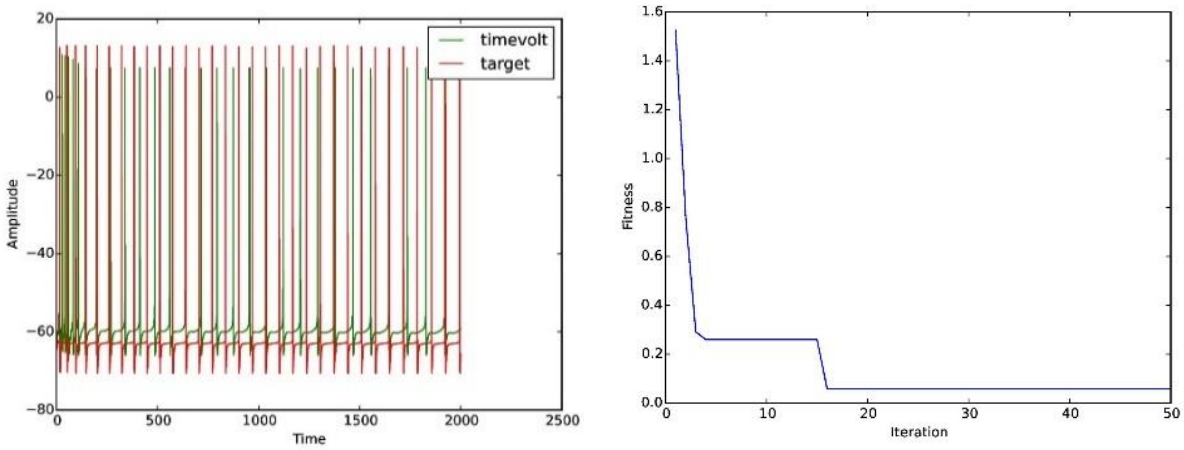

Fig. 30. Optimization tests using 50 particles and 50 iterations.

Parameter estimation was performed in about 43 minutes, instead of 9 hours with a single core, using 50 particles and 20 iterations. The voltage traces in **Fig. 31** (on the left) show the output dynamics of the target (green line) and the output dynamics of a simulation using the best θ of the tests with 50 particles and 20 iterations (red line). The output dynamics of the simulation estimated reproduces the spontaneous firing of the target. **Fig. 31** (on the right) shows the convergence speed (the average best fitness of 20 tests) of the methodology. On average, the methodology converges toward an optimal solution in less than 20 iterations.

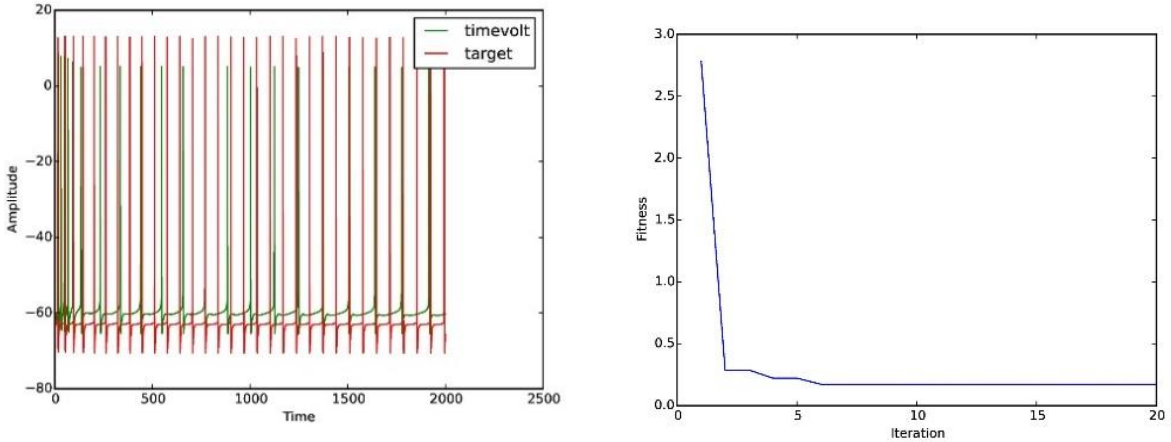

Fig. 31. Optimization tests using 50 particles and 20 iterations.

Between all the results, it is important to notice that the best tests performance is reached with optimizations with 100 particles and 100 iterations. In this case, the methodology converges toward an optimal solution, reaching exactly the value 0 (**Fig. 26** (on the right)). The PE problem studied for higher dimensional search space requires a large number of particles. A higher number of particles increases the probability of creating solutions in optimal positions.
In all the tests, the methodology converges toward an optimal solution in less than 20 iterations.

3.2.5 Comparison of the Particle Swarm Optimization and the BluePyOpt framework

To test the efficiency of the PSO to solve the complex PE problem of neuronal parameters, the algorithm was compared with the BluePyOpt framework based on GA algorithm.

In the GA, the first step is the creation of an initial population of random individuals and for each individual the fitness value is assessed. According to the fitness value, some individuals are selected to reproduce themselves and to be mutated. The newly generated individuals are evaluated and selected to form a new population that evolves generation after generation (Deb et al., 2002; Panda and Padhy, 2008).

At the start of PSO, the particles of the swarm are distributed randomly in the search space and have a random velocity. Their position and velocity are updated iteration after iteration, leading to an optimal solution (**Para 3.2.1**).

The information sharing mechanism in PSO is significantly different from GA. In the GA the individuals update themselves through reproduction and mutation phases, whereas, in the PSO, particles update themselves with the internal velocity and they maintain memory of the best position reached so far.

Both GA and PSO are population-based search methods and they search for the optimal solution by updating generations. As the two techniques are supposed to find a solution to a given objective function but employ different strategies, it is appropriate to compare their performance.

The application, performance and results comparison, of PSO and GA optimization techniques, was achieved through the following workflow:

i) the PSO framework requires:

- Model construction with NEURON – Python (**Para 3.2.2**).
- Definition of the neuron model morphology (**Fig. 23**).

Fig. 23. SC model morphology (see above).

- PSO algorithm (**Para. 3.2.1**).
- Setting the parameters located in the different sections and for each parameter set boundaries (**Table 5**).

$G_{i\text{-}max}$ / Section location	**Range $G_{i\text{-}max}$ (S/cm2)**
leak_soma	0.00015- 0.00045
Nav1.1_soma	0.045-0.135
Kv3.4_soma	0.01-0.035
HCN1_soma	0.00005-0.0002
Cav2.1_soma	0.0002-0.001
Cav2.1_proximal dendrites	0.00011-0.0008
Kca1.1_ proximal dendrites	0.01-0.03
HCN1_ proximal dendrites	0.00005-0.0003
Cav2.1_distal dendrites	0.00011-0.0008
Kca1.1_ distal dendrites	0.005-0.03
HCN1_ distal dendrites	0.00005-0.0008
Nav1.6_ais	0.2-0.7
Kv3.4_ais	0.02-0.08
HCN1_ais	0.00005-0.00015
Nav1.6_axon	0.02-0.06
Kv3.4_axon	0.005-0.015
HCN1_axon	0.00005-0.00015

Table 5. $G_{i\text{-}max}$ values in the multi-compartment SC model (see above).

- Decide and implement the fitness function. The fitness function is based on experimental frequency measures (n° action potentials/second, (Hz)).
- NEURON simulator was used to calculate the fitness value. Specifically, a novel model was created using the putative parametrization of each particle. The model was then simulated with NEURON for 2000ms. Afterwards, the features of the output (the mean frequency) were compared against the target features to assess the fitness value.
- The values of the feature are extracted for each particles in the iterations, with eFEL (Van Geit, 2015). The target value was set to an average frequency of 14 Hz.
- The best individual was chosen based on the best parameterization able to minimize the fitness function.
- It is possible to analyze different individuals with good parameterizations and voltage traces as output that overlap the voltage trace of the benchmark model.
- To reduce the computational costs, the methodology was extended with MPI, in order to leverage a distributed architecture for the fitness evaluations required by PSO. The fitness evaluations were accelerated with a computer cluster. The methodology was tested on a dual processor equipped with 12-cores, using fixed time step of 0.025ms and simulations of 2000ms.
- Parameter estimations were performed in 3 hours and 20 minutes, using 100 particles and 50 iterations. The increase in speed was around 13 times as the tests running on a single-core needed 42 hours to be completed. The voltage traces in the **Fig. 27** (on the left) show the output dynamics of the target (green line) and the output dynamics of a simulation using the best θ of the tests with 100 particles and 50 iterations (red line). The output dynamics of the simulation estimated reproduces the spontaneous firing of the target. The **Fig. 27** (on the right) shows the convergence speed (the average best fitness of 20 tests) of the methodology. On average, the methodology converges toward an optimal solution in less than 20 iterations.
- The mean value of the frequency of the optimized models is 15 Hz. The value of each model trace was extracted with eFEL.

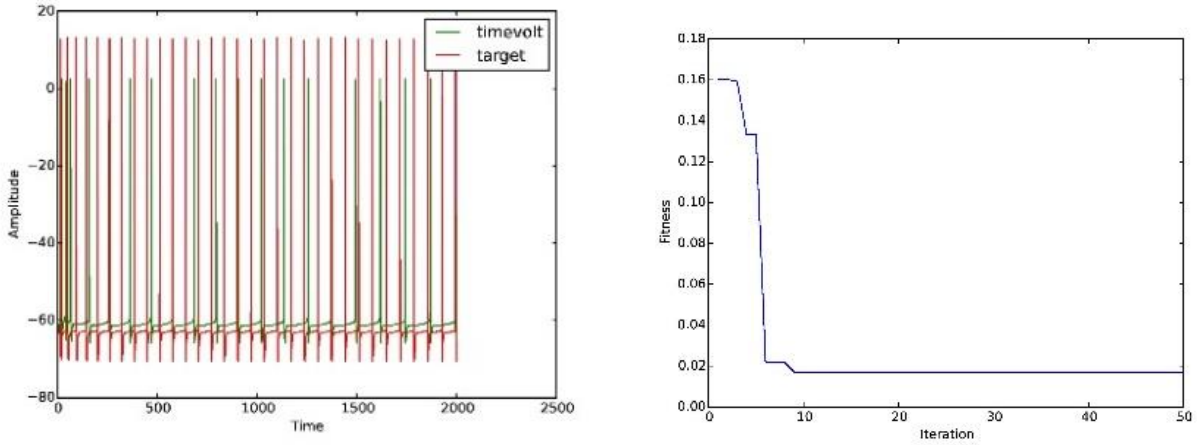

Fig. 27. Optimization tests using 100 particles and 50 iterations.

ii) the BluePyOpt framework , based on GA algorithm, provides:

- Model construction following the BluePyOpt framework scheme (Van Geit et al., 2016).
- Specification of the neuron model morphology as SWC, shown in the **Fig. 23.**

Fig. 23. SC model morphology (see above).

- Parameters localization, in the different sections, with specific boundaries (**Table 5**).

$G_{i\text{-}max}$ / Section location	**Range $G_{i\text{-}max}$ (S/cm2)**
leak_soma	0.00015- 0.00045
Nav1.1_soma	0.045-0.135
Kv3.4_soma	0.01-0.035
HCN1_soma	0.00005-0.0002
Cav2.1_soma	0.0002-0.001

Cav2.1_proximal dendrites	0.00011-0.0008
Kca1.1_ proximal dendrites	0.01-0.03
HCN1_ proximal dendrites	0.00005-0.0003
Cav2.1_distal dendrites	0.00011-0.0008
Kca1.1_ distal dendrites	0.005-0.03
HCN1_ distal dendrites	0.00005-0.0008
Nav1.6_ais	0.2-0.7
Kv3.4_ais	0.02-0.08
HCN1_ais	0.00005-0.00015
Nav1.6_axon	0.02-0.06
Kv3.4_axon	0.005-0.015
HCN1_axon	0.00005-0.00015

Table 5. $G_{i\text{-}max}$ values in the multi-compartment SC model (see above).

- Genetic Algorithm. IBEA

The technique that allows rapid and automatic PE is based on multi-objective evolutionary algorithms (MOEA), called "Indicator-Based Evolutionary Algorithm" (IBEA) (Zitzler and Künzli, 2004). This is based on a genetic approach, in which the unknown parameters are treated like the genes forming a chromosome (Deb et al., 2002; Druckmann, 2007; Druckmann et al., 2008, 2011; Zitzler and Künzli, 2004). The multi-objective algorithm calculates different feature values shown in **Table 6.** For each feature, the target value, concerning the spontaneous firing behavior, is extracted from the experimental data, using eFEL and compared with the one obtained from each optimized model. The methodology was implemented for parallel architectures and was tested on a dual processor equipped with 12-cores, using fixed time step of 0.025ms and simulations of 2000ms. The optimizations involved 100 individuals for 50 iterations, running with the same computational time required by PSO (3 hours).

Table 6. Features.

Features	Experimental value
spike count	36
mean frequency	14 Hz
AP amplitude	71.8 mV
AP width	0.25 mV
AP height	10.78 mV
ISI values	55.9 ms
spike half width	0.23 mV

Table 6. The table shows the mean values of features, obtained from experimental traces using eFEL.

- Results.

The methodology provided satisfactory results in reproducing the cellular spontaneous firing behavior. The **Fig. 32** shows the spontaneous firing of one of the optimized models. The mean value of the frequency of 20 optimization tests is 16 Hz. The **Fig. 33** shows the mean values of the fitness evaluating 20 optimization tests.

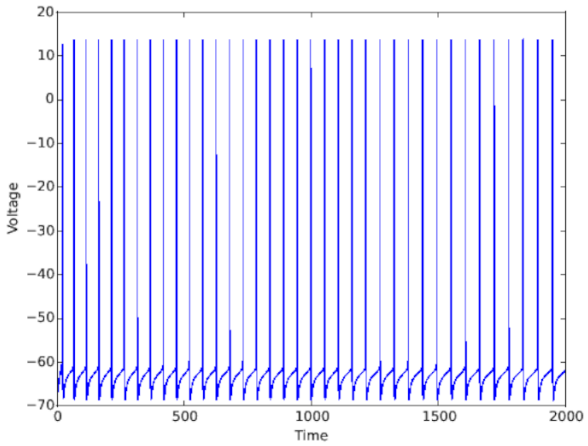

Fig. 32. Electrophysiological behavior of one individual obtained with optimization tests using 100 particles and 50 iterations.

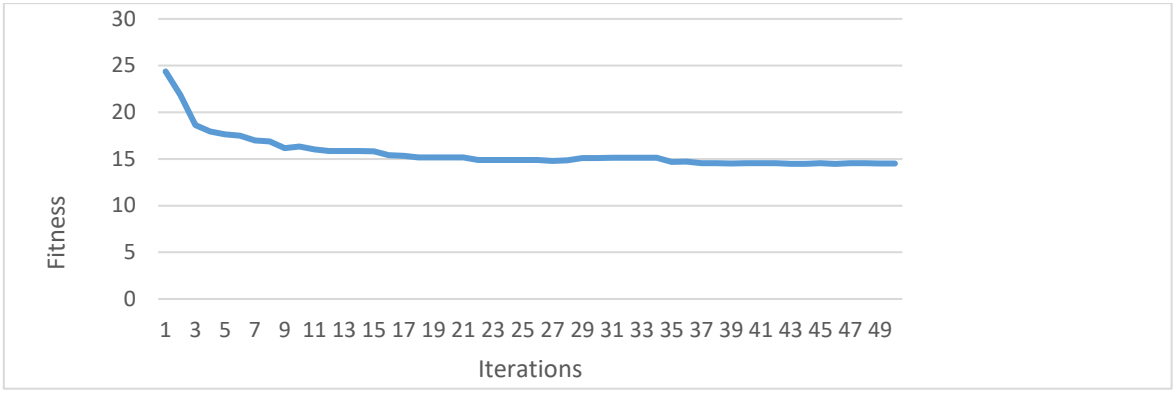

Fig. 33 Mean values of the fitness running optimization tests using 100 particles and 50 iterations.

The PSO Framework and the BluePyOpt framework were used with the same SC model components: morphology and ionic channel with the same $G_{i\text{-}max}$ boundaries values. Both the algorithms were implemented to be used on parallel architectures, providing a tangible decrease in simulation time. It is not possible to do a complete comparison, since the GA used in the BluePyOpt framework is a multi-objective, able to evaluate different neuronal features, while the current PSO algorithm, evaluates only a single objective. When I'll extend the methodology to implement a MOPSO (Kumar and Minz, 2014; Reyes-Sierra and Coello, 2006), then it will be able to analyze different feature values. PSO is characterized by a higher speed of convergence, however, both the fitness curves described a good fitness minimization.

The performance of both optimization techniques, in terms of computational time and convergence rate was compared. In conclusion, both algorithms achieve overall good optimization performances and biological satisfactory results, with the same computational efficiency. The PSO method has the advantage of achieving optimal results with a single objective, even though the technique will be extended to explore more varied objectives. The aim of my PhD project was to realize a framework for the PE problem, for the single neuron model and I tried to employ the PSO methodology.

3.2.6 Conclusions

The results showed that the methodology is promising, to obtain models with 17 $G_{i\text{-}max}$ parameters estimated with the PSO, capable of reproducing the most important behavior of SCs, such as the spontaneous activity.

To reach more suitable optimized model solutions, the mean frequency was used, based on fitness function. With the point-to-point based feature I observed a relevant time shift between voltage

traces, a premature convergence of the methodology to a local optimum of the parameter space, which resulted in very high fitness values.

I have demonstrated that the methodology reached an optimal solution with the best θ that reproduces the characteristic auto-rhythmic behavior of the neuron.

PSO was successfully applied to PE the free $G_{i\text{-}max}$ parameters of SC neuron model, integrating NEURON simulator for the fitness evaluations. This study is the first example of application of PSO method for PE of HH complex neuron models. Its implementation simplicity and impressive optimization performances make it an attractive and popular methodology to solve complex problems.

The implementation of multi-core makes the algorithm more efficient, fast and less time consuming. The fitness evaluations were accelerated using a distributed architecture, extending the methodology with MPI to strongly reduce the running time. Effectively, since the computational complexity of PSO is small, the running time is mainly due to the fitness evaluations and to the simulations of the models by means of NEURON.

The use of parallel architectures is helpful in performing multiple independent estimations, in order to increase the probability of determining an optimal θ. However, all fitness evaluations are mutually independent, they can accelerate using a parallel architecture, strongly reducing the running time. With parallel simulations, it is possible to run multiple optimizations. In this way, it is feasible to increase the number of particles, due to the extensive search spaces, and to realize multiple runs of the algorithm, increasing the probability of convergence. In fact, the PSO being a stochastic algorithm could converge to completely different solutions, characterized by very different fitness values.

This methodology can be applied to investigate neurons with other properties and behaviors, the creation of models with an automatic procedure makes the study of neurons more accessible and feasible. A detailed observation of neuronal functioning is increasingly important to explore the functional microcircuits and networks, involved in physiological and pathological levels.

The next step to improve the application of the methodology will be the evaluation of more fitness functions to test different neuronal behaviors, such as the fast responses to positive current injections, the activity generated by the interaction of coupled SC through gap-junctions and their interaction in a large network.

3.3 Paper: “Single Neuron Optimization as a Basis for Accurate Biophysical Modelling: the Case of Cerebellar Granule Cells”

In this paper, I investigated the optimization of important neurons of the cerebellum, the GrCs, which can be considered as a benchmark to explain the optimization process. In this work, the PE

problem is studied exploiting the genetic algorithms approach. (Stefano Masoli, **Martina Francesca Rizza**, Martina Sgritta, Werner Van Geit, Felix Schürmann, Egidio D'Angelo. Frontiers in Cellular Neuroscience, 2016) (**Appendix 3.,** Masoli et al., 2017).

Chapter 4

4. Cerebellum Development

The development of the cerebellum is a complex phenomenon that includes many biological processes: cellular differentiation and migration, axonal and dendritic growth, the establishment of synaptic connectivity requiring synaptic formation, competition, stabilization and pruning. These steps are critical to define the appropriate citoarchitecture and the connectivity forming the cerebellar microcircuits. Many of these properties were extensively studied with techniques belonging to physiology, immunohistochemistry, biochemistry and molecular biology. The physiological discoveries, thanks to the minor difficulties in obtaining and analyzing the data, were more often transformed into computational models. These models were the first and most used to show specific characteristics and behaviors of single neurons and networks, but limited by the available data and computational power. The majority of the tools developed to simulate such models were built to solve the neuronal behaviors in a restrict time frame lasting from thousands of *Milliseconds* (ms) to a few hours. To permit the simulation of an evolving system, frameworks to recreate the natural steps leading to the development of the neural tissue, constrained by biochemical and immunohistochemical data, were built or are still under construction. These tools reproduced, with various degree of detail, a cerebral cortical column, but are not suitable for the creation of the specific three layered structure of the cerebellum (Zubler et al., 2013).

This chapter reviews the state of the art of the tools and techniques used for the modeling and simulation of the neurogenesis, synaptogenesis and development processes in the cerebral cortex and in other portions of the SNC. The expected successive step will be the definition of a new multiscale framework for the simulation of the development in the cerebellum.

4.1 A Review of Conceptual Frameworks and Tools for Reconstructing the Cerebellar Network Based on Developmental Growing Processes

4.1.1 Neurogenesis

This section focus on the cerebellar region development and on the formation of the cerebellar neurons with the differentiation and migration from their birthplace to their final destination.

The cerebellum derives from the region of the neural tube which includes the caudal portion of the mesencephalon and the rostral portion of the metencephalon (Carletti and Rossi, 2008; Ishikawa et al., 2012). The cerebellar region is under control of the isthmic organizer, which acts as a signaling center that secretes the morphogens *Fibroblast Growth Factor* 8 (Fgf8). Instead the Rhombomere1 roof plate guides the differentiation of the neurons through *Bone Morphogenetic Protein* (BMP) and *Proto-Oncogene Protein Wnt1* (Chizhikov, 2013). Furthermore, strong Fgf8 signaling activates the *Ras-ERK* pathway which phosphorylates *Iroquois Related Homeobox 2* (Irx2) and initiates the cerebellar development in the rostral hindbrain (Sato et al., 2004). The *Engrailed-2* (En2) and *paired*

box Pax1 and Pax2 proteins exert their function in the midbrain-hindbrain territory too. Mutants of Wnt1*, Engrailed-1* (En1) and *LIM Homeobox Transcription Factor 1 Beta* (Lmx1b) show patterning defects in the midbrain-hindbrain region (Goldowitz and Hamre, 1998; Wang and Zoghbi, 2001; Wassef, 2013; White and Sillitoe, 2013).

Many studies were conducted on the animal model, such as rats and mice, to address the functional components and behaviors generated by the electrophysiological activity and to define the biochemical processes underlying the cerebellar development. These studies described that the cerebellar primordium arises, between embryonic days (E) 8.5 and 9.5 in the mouse, from dorsal rhombomere 1, adjacent to the fourth ventricle. The progenitors of the different types of cerebellar neurons derived from two distinct germinative zones, the VZ and the *Rhombic Lip* (RL), divided in *Upper Rhombic Lip* (URL) and *Lower Rhombic Lip* (LRL) (Cajal, 1911; Altman and Bayer, 1997; Sotelo, 2004) beginning around E9 and E11.

The VZ was seen as the birthplace of GABAergic neurons, including PCs, GoCs, LCs, nucleo-olivary projection neurons (DCN-IO) and inhibitory interneurons such as BCs and SCs. The progenitors cells in the VZ express the *Pancreas Specific Transcription Factor 1a* (Ptf1a).

The RL was defined as the birthplace of Glutamatergic neurons since the secreted *Atonal Homolog 1* (Atoh1) known as Math1 is required for the development of the glutamatergic DCNs, GrCs, and UBCs.

4.1.2 Biological Processes of the Cerebellar Development

This section focuses on the main processes of the cerebellar development that can be mathematically modeled, to reproduce a large-scale model of the entire cerebellar development. The subsection 4.1.2.1 describes the neuronal differentiation and migration with the specific mechanisms and a timetable schedule that summarizes the events that happen before and after the birth of the experimental animal, in this studies the experimental data are obtained from mice and rats. In the subsection 4.1.2.2 are reported the processes of axon and dendrites growth, in the subsection 4.1.2.3 are presented the events underlying the synapse formation and in the subsection 4.1.2.4 the mechanisms controlling the neuronal electrical activity (**Table 8**).

4.1.2.1 Neuronal Differentiation and Migration

In this subsection are described the principal processes involved in the neuronal differentiation and migration, highlighting peculiar characteristics of the cerebellum. In order to build a model of neuronal is important to consider the different types of migration, radially and/or tangentially, depending on the migration of different neurons and the role of glial cells, critical during the neurogenesis process, guiding the PCs and GrCs migration. Each type of neuron requires a huge amount of data to be precise reconstruct and placed in the development modeling framework.

The following data can be used as a blueprint for the creation of a model of the cerebellar network since it provides the precise time of birth, time of final development, migration trajectory, glial interaction, most important biochemical signals and specific internal/external factors.

The first type of neuron born in the VZ is the GABAergic DCN (E10-E12), followed shortly after by PC (E11 - E13). The generation of GABAergic projection neurons from VZ is completed during the early phases (E13). As development proceeds (E14 - E17), DCNs reache their final position in the center of the cerebellum. The PCs migrate radially, along radial glia cells, toward the cortical surface and complete their migration beneath the newly formed *External Granular Layer* (EGL). EGL signaling, likely mediated by *Reelin* and by other factors, is critical in terminating PC migration and inducing the characteristic monolayer around *Postnatal Days* (P) 4 and 5. Inhibitory interneurons, born from VZ during late embryonic and postnatal development, derive from *Pax2*-positive precursors (Weisheit et al., 2006) that appear in the medial region of the VZ at E13. These progenitors continue to divide while migrating through the white matter toward their final destination in the cerebellar nuclei or cortex (Goldowitz and Hamre, 1998; Carletti and Rossi, 2008; Larouche and Goldowitz, 2013) (**Table 7, Fig. 34/35**).

The RL is located between the IV ventricle and the roof plate (Wingate and Hatten, 1999) and, around E13, the cells in this region start expressing the transcription factor Math1 (Ben-Arie et al., 1997). This expression persists in precursors GrC in the EGL, but the gene is turned off in postmitotic GrCs. Glutamatergic DCNs and UBCs also originate from this germinative layer but at early stages, prior to the generation of GrCs. Math1-expressing precursors that first emigrate form the germinative layer become DCNs, whereas those exiting later become GrCs. The Math1 expression is switched off in DCNs as soon as they leave the RL, whereas GrC progenitors remain Math1-positive in the EGL. RL generates also the ventrally located *Pontine Nucleus* (PN) and the IO nucleus, projecting respectively the mfs and cfs (**Table 7, Fig. 34/35**).

The early phase of the process involves the generation of glial cells, called radial glia, because of two spatially oriented radial processes, from the VZ toward the external layers, emerging on the opposite sides of their cellular body. The radial glia guides PCs toward the EGL and, after completing this task, undergoes a progressive morphological transformation into *Bergmann Glia* (BG). BG is composed of unipolar astrocytes with their soma located in the proximity of PCs and extends their multiple branched processes radially to the pial surface. BG guides the GrCs to lay a straight axon during the migration from EGL to IGL and by SCs/BCs to extend their axons to innervate PCs dendritic tree, soma and axon (Altman and Bayer, 1997). BG is fundamental for neurons survival, to stabilize the synaptic interactions and to control the extracellular K^+ concentration that can modify the overall neuronal activity. Many molecules and signaling pathways are involved both in the radial migration of GrCs along BG and in the development of BG, such as *Sonic Hedgehog* (Shh), Notch, and growth factors including *ErbB* and *FGFR* (Buffo and Rossi, 2013; Xu et al., 2013; Barry et al., 2014).

GrC Migration

Around E15, GrC precursors leave the neuroepithelium to migrate tangentially from RL on the surface of the cerebellar anlage, the EGL, where they proliferate extensively until P14. Postmitotic GrCs leave the EGL and migrate inwards to form the internal granular layer (IGL) where GrCs terminate the differentiation and start interacting with the migrated GoCs. The EGL ceases to exist

by the end of the third postnatal week in the mouse, and in this period, the stabilization of the mfs and cfs occurs. GrCs show two intrinsic characteristics: 1) the axons, pfs and aas, are generated before the soma finds its finally location in the IGL, 2) the length of the aas is not predefined by the connectivity and is guided by the interaction with the PCs. The process starts between P4 and P15, when GrCs differentiate and initiate the process of outgrowth in the inner EGL, expressing the axonal glycoproteins *TAG-l*, *Ll* and the neuron-glial ligand A*strotactin*. Several other proteins play a role in this process, such as *Thrombospondin* and *Tenascin*, which are involved in axon extension, *Neuregulin,* which binds the *ErbB4* protein expressed by glial cell, which control the regularity of the migration. From the inner EGL, GrC precursors migrate into the IGL interacting with the BG, through a specialized process called "interstitial junction". All these interactions are critical for the creation of the pfs stacking. Instead, the definition of the aas length is under control of the intracellular Ca^{2+} signaling, which, in conjunction with external cues, such as neuropeptides, regulates the migration of GrCs. The expression of Ca^{2+} channels in the EGL and the presence of high concentration of Ca^{2+} play a role in controlling the speed of migration, which is reduced by blocking the channels activity with an antagonist. EGL granule neuronal precursors require Shh signaling for proliferation, which at least in mice could be driven first by transient autocrine Shh signaling and then by Shh from PCs. Shh induces also the differentiation of Bergmann glia, consistent with the requirement of PCs for BG differentiation (Dahmane and Ruiz i Altaba, 1999). Another critical property is that the soma can follow only a straight line, and their passage is restricted by the PC somas. This process is controlled by the neuropeptide *Somatostatin* (SST) which inhibits their radial migration in the IGL and the neuropeptide pituitary *Adenylate Cyclase-Activating Polypeptide* (PACAP), expressed by PCs, slows the GrCs migration in the PCL (Hatten et al., 1997; Komuro et al., 2013; Larouche and Goldowitz, 2013). At the end of this process, the soma of each neuron will be located in their final location and the neuron will start to emit from 3 to 5 short dendrites which will interact with the mfs and GoCs into the glomeruli.

UBC Migration

The glutamatergic interneurons UBC are generated from the same progenitors of GrCs and are born in the URL between E15.5 and E17.5. They migrate into the white matter during late embryonic and early postnatal development. The majority of UBCs reaches the adult IGL at P10, where they continue to proliferate until the first postnatal month. They have a particular morphology, a single brush-like dendritic ending which receive excitatory inputs from mfs and inhibitory activity by GoCs (Harris et al., 1993; Mugnaini and Floris, 1994) and their axon project to GrCs.

GoC Migration

GoCs are GABAergic inhibitory interneurons located in the GCL, receiving excitatory synaptic inputs from mfs and pfs and making inhibitory synapses with GrCs and UBCs. GoC precursors are produced in the VZ, migrate to the IGL, express the transcription factor Ptf1a and, after leaving the ventricular neuroepithelium, start to express the gene Pax2. Their development is not completed until P4 (Zhang and Goldman, 1996) and their final location is restricted by the PCs (Sillitoe et al., 2008). The

only known specific characteristic is the presence of an extensive axonal arborization which can contact up to a thousand of different GrCs (Valera et al., 2016).

PC Migration

The PCs are among the oldest neurons in the CNS and show one of the most elaborated dendritic tree of all. These neurons aggregate in a primordial cortical layer, the *Purkinje Cell Plate* (PCP) and, around E14-E15, each neuron starts to extend an axon and to express high levels of cell-surface antigen Thy 1. Their timely arrest (P4-P5) of migration depends on the Reelin gradient (Nakamura et al., 2016), which is a glycoprotein secreted, in the beginning by glutamatergic neurons of the DCNs and later by GrC precursors in the EGL. The PCs were postulated to be homogeneous, but recently was proven the existence of two distinct members with identical morphological properties, but with diverse presence or absence of Aldolase C (Zebrin II). These neurons are generated in two distinct waves (Leto et al., 2015) with the (Z+) reaching the PCP before the other group (Z-) and generating a pattern composed of alternating strips of PCs (Zhou et al., 2014). When a PC settle in the PCP it initiates the development of the dendritic tree which goes on from E16 to P90 (McKay and Turner, 2005). The principal regulators of the orientation and maturation of the dendrites are connected with the generation of the synaptic contact (pf), synaptic activity (cf), trophic factors and hormones. During the development*, Nerve Growth Factor*, *Acetylcholine*, *Neurotrophin 4/5*, *Brain-Derived Neurotrophic Factor (BDNF)*, *ciliary neurotrophic factor* and the gene *Rorα* are important for PCs survival. In the later phases of development, specific proteins, such as *Aldolase-C (Zebrin II)*, *MgluR1*, *PLCB (B3 and B4)* (Cerminara et al., 2015) and other, are produced and involved in the specification of the electrophysiological characteristics of the two members of the PCs family (Hatten et al., 1997; Goldowitz and Hamre, 1998; Wang and Zoghbi, 2001; Komuro et al., 2013; Larouche and Goldowitz, 2013; Sotelo and Rossi, 2013).

MLI Migration

The ML is composed of the aas, pfs, the PC dendrites and the BCs and SCs, which are GABAergic interneurons. These cells receive excitatory inputs from pfs and their branched unmyelinated axon makes inhibitory synapses with PCs. Although these cells are born from the same progenitor and, during their migration, are morphologically indistinguishable, it is still debate if they can be treated as the same neurons with different localization, or if they are distinct even in their intrinsic composition. The progenitors of both cells originate in the VZ, from where they migrate outward to reach the deep white matter of the embryonic cerebellum, then they migrate radially toward the IGL and the PCL to the ML, their final destination, during postnatal development (P1 - P14). These neurons express the transcription factor Ptf1a and, after leaving the VZ, precursors of these express the gene Pax2. They achieve their final location, gap junction and reciprocal inhibitory connectivity between P7 and P21 (Pouzat and Hestrin, 1997).

DCN Migration

The final elaboration of the cerebellar cortex is sent from PCs to the DCNs as a constant inhibitory activity, which is counterbalanced by mf and cf collaterals. Each DCN contains glutamatergic

projection neurons, GABAergic inhibitory interneurons and GABAergic projection neurons that are arranged into local networks. Glutamatergic projections neurons derive from URL progenitors and express the transcription factor Atoh1. These cells migrate from the URL to the *Nuclear Transitory Zone* (NTZ) (Jensen et al., 2004) a transitory cell cluster that will give rise to the DCN. GABAergic interneurons migrate radially from the VZ and continue to proliferate until to settle in the DCN (Zhang and Goldman, 1996).

Table 7. Development time of the cerebellar neurons.

Birtplace	Neurons	Development time	Final place
VZ (Gabaergic neurons)	DCN	E10-E12/P20	DCN
	PC	E11-E13/ P21	PCL
	GoC	E14/P4	GCL
	MLI	E14/P7-P21	ML
RL (Glutamatergic neurons)	DCN	E14/P20	DCN
	GrC	E15/ P14	GCL
	UBC	E17/ P10	GCL

Table 7. The table shows the development time of the different cerebellar neurons, their birthplace and their final place, achieved at the end of the development.

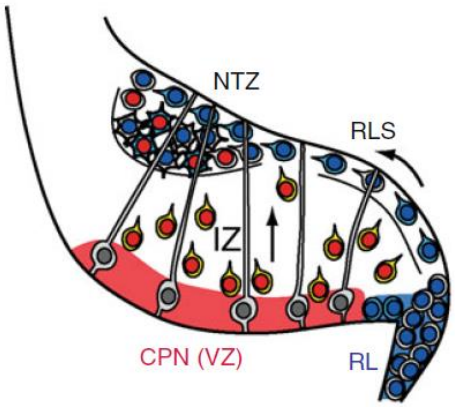

Fig. 34. Migration of cerebellar neurons from the germinative zones to their final positions, at the early stage of cerebellar development (E9 - E13). The figure is taken from the chapter 10 "Development of cerebellar nuclei (Elsen et al.)" of the book "Handbook of the cerebellum and the cerebellar disorders, 2013".

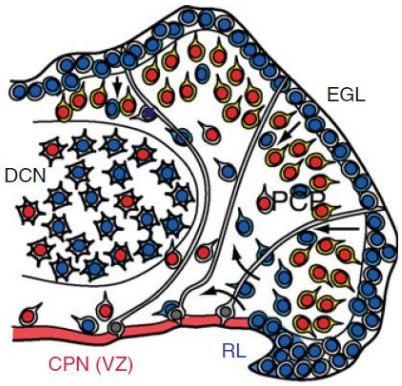

Fig. 35. Migration of cerebellar neurons from the germinative zones to their final positions, at the later stage of cerebellar development (E14-P20). The figure is taken from the chapter 10 "Development of cerebellar nuclei (Elsen et al.)" of the book "Handbook of the cerebellum and the cerebellar disorders, 2013".

E9 - E13: URL (blue nuclei) gives rise to glutamatergic neurons of the DCN. DCN migrate tangentially along the dorsal surface of the cerebellar anlage through the rostral *Rhombic Lip Migratory Stream* (RLS) and accumulate at NTZ. The early cerebellar VZ gives rise to GABAergic neurons of the DCN and PC. Both GABAergic neurons of DCN and PC migrate radially from the cerebellar VZ (red nuclei) of the *Cerebellar Plate Neuroepithelium* (CNP) along radial glial cells (gray) through the *Intermediate Zone* (IZ), toward the RLS and NTZ.

E14 - E18: RL gives rise to GrC precursors and UBC. GrC precursors migrate tangentially along the dorsal surface of the cerebellar anlage to form the EGL. UBCs migrate directly into the cerebellar anlage. The cerebellar VZ gives rise to precursors of GABAergic interneurons (GoC, SC and BC) which migrate radially from the cerebellar VZ. The PCP was formed, and the early RLS is replaced with the EGL. Cells from the EGL migrate radially inward through the PCP, UBCs migrate directly from the RL into the IZ. The DCN contain glutamatergic neurons derived from the NTZ.

Postnatal age: cf and mf development.

GrC: E11-E14 proliferation in RL; E15-P0 EGL cells formation and proliferation; P4 axon extension in the EGL; P4-P15 migration from EGL to IGL; P20 synaptogenesis in the IGL.

PC: E11-E13 proliferation in VZ; E14-E16 migration and axon extension; E16-P0 dendrites formation.

4.1.2.2 Axon and Dendrites Growth

Pathways of attractive and repulsive guidance molecules, in the extracellular environment, guide the axons to their targets to establish precise neural circuits. Axons and dendrites are provided, on their terminal parts, of a highly mobile and sensitive structure, the growth cone, which respond to specific sets of extracellular cues so to find the correct path toward their targets. Important axon guidance molecules are *Reelin, Netrins, Immunoglobulins, Semaphorins, Ephrins, Slits, Synapsins, Wnt-7a, Cadherins* (Dickson, 2002; Chilton, 2006). Classical axon guidance molecules such as *Semaphorins, Netrins, Ephrins, Reelin,* and *Slits* have their receptors expressed by PCs, at specific stages of postnatal cerebellar development, and are involved in PC axon guidance. Little is known

about the molecular cues that guide the nascent PC axons toward their nuclear targets. One receptor for *Netrin1, Unc5c* (also known as *Unc5h3*), is strongly expressed in DCN and in PC progenitors, and around E13.3 this receptor is expressed in PC axons, in an area close to NTZ. Unc5c is a repulsive receptor for Netrin1 and is expressed in the medial cerebellar neurons within the NTZ too (Tamada et al., 2008; Kim and Ackerman, 2011). Another receptor for Netrin1, called *DCC*, and members of the *Slit/Robo* guidance system, have been found to regulate the ventral guidance and midline crossing of precerebellar neurons and their axons (Bloch-Gallego et al., 1999; Causeret et al., 2002).

The Ca^{2+} signaling is important in axon guidance and dendrite growth. In the growth cone the Ca^{2+} ion is able to attach itself to the tubulin, which is a structural protein forming the microtubules and the main part of the cytoskeleton, and, if the Ca^{2+} concentration is above a certain threshold and in presence of magnesium, it is able to destabilize the microtubules formation and has effect on growth cone motility (O'Brien et al., 1997). Ca^{2+} signaling is involved in the control of dendritic development (Wu and Cline, 1998; Konur and Ghosh, 2005). Since this is a vast topic, more information can be found in other publications (Henley and Poo, 2004; Gomez and Zheng, 2006; Sutherland et al., 2014).

4.1.2.3 Synapses Formation during the Cerebellar Development

Mossy fibers from the PCN make excitatory synaptic contact with GrCs under the control of *Wnt7a*, which is released by GrCs. A similar system is used by GrCs, which connects to GoCs under control of contactin. The synapses between GrCs, IO to PCs are highly segregated. The GrCs can make a synapse on a single spine in a dendritic territory marked by the presence of Vglut-1, instead the cf can make multiple synapses along the non-spiny main dendritic trunk and only in a territory filled with Vglut-2 (Zhang et al., 2015). Another fundamental protein that has surged in importance in the last years is the receptor *GluD2* which, even though is part of the AMPA subunits, is nonfunctional as a channels but it mediate the interaction between pf and PC spines (Ichikawa et al., 2016).

The cfs, which are the collateral of the axons of the IO nuclei, are the strongest excitatory afferent fibers of the cerebellar cortex and are responsible for the transmission of the "error signal" coming from the sensory and motor systems. During neurogenesis, these fibers are the first to enter the cerebellum and they generate a series of synaptic connection with the soma of the newly formed PCs. At this point, each soma, receives more than one CF terminal (E17-P3, supernumerary CF innervations) and, as the time passes, only the CF able to elicit the right responses in PCs, NMDA dependent, is maintained as a mature CF afferent (P3-P10, early phase of pruning). This process is called pruning and is followed by the relocation of the winner CF from the soma to the main and proximal dendrites leaving the space to the incoming BC axons (P10-P20, late phase of pruning). The *Semaphorins* (*Sema3A, Sema7A*) are expressed in PCs and have a fundamental role during the CFs pruning, mediating retrograde signals for elimination of redundant cfs (Uesaka et al., 2014).

All the inhibitory neurons of the cerebellum share the same morphological characteristic: their dendritic trees are quite extensive on two axes, more for PC/GoC and less for the SC/BC, but all of them are little thick with a near planar disposition in the space. In the case of an axon reaching for

a pyramidal cell spine, they can make a synaptic connection with almost any angle whereas PC spines and the rest of the inhibitory interneurons can accept only vertical connection with aas and horizontal connection with pfs. This particular arrangement was analyzed and produces many different theories (Komuro et al., 2013), but none has been proved since it very difficult to understand which GrC will connect what part of a PC and why.

The interaction between the excitatory mfs with GrC dendrites and GoC axon/dendrites is achieved in a structure called "*glomerulus*". This is composed of the axonal termination of the mf, the dendrites of many GrCs, a single axon of a GoC and, eventually, by the dendrites of a GoC. The stabilization of the system is glial dependent and, the entire procedure, is completed after birth.

4.1.2.4 Electrical Neuronal Activity

Neurons generate electrical signals and with them, they transmit information to other interconnected neurons through chemical or electrical synapses. The ions accumulation on the opposite sides of the cellular membrane, in conjunction with polar proteins, generates the electrical gradient. The flow of the ions when a channel open generates an ionic current that can be recorded with specific experimental techniques. The opening, in a specific order, of the Na^+, K^+ and Ca^{2+} ionic channels is at the basis of the generation of the action potentials.

The ionic conductance is the measure of the ion quantity that flows across the single ionic channel. This data is used, during modelling, to define a current density, which represent the total current, of that specific ion type, that can be generated. Since the ion flows actively trough the channels, there were defined active properties, instead the membrane capacitance, resistance even though fundamental for the creation of the action potential, they do not change during the action potential generation and are called passive properties.

Neuronal differentiation and migration are guided mainly by genetic control and biochemical cues, but a primordial electrical activity can induce specific changes in the neuronal operation, above all for the massive presence of Ca^{2+} ion. When the system reaches a more stable and organized state, than the electrical activity supersedes the other components, generating the intrinsic properties and defining the interaction with other neurons, through the electrical and chemical synaptic connections.

Table 8. Main cerebellar biological processes.

Biological processes	**Highlighted mechanisms that can be modeled for the cerebellum**
Neuronal differentiation and migration	Genes Atoh1 and Ptfa1 Glial cells and interaction with Notch, growth factors as ErbB and FGFR, astrotactin, neuregulin Ca^{2+} signaling Shh factor Reelin factor
Axon and dendrites growth	Semaphorin, Netrin, Ephrins, Reelin factors Ca^{2+} signaling
Synapses formation	Semaphorin factor
Electrical activity	Neuronal morphology Passive properties: resistance, capacitance Active properties: ionic conductances

Table 8. The table summarizes the main biological processes that can be modeled for the cerebellar development network construction.

4.1.3 Cerebellar Development Models

In an evolving model of the cerebellum, the challenge is to integrate the different biological processes underlying cerebellar neurogenesis, such as neuronal differentiation and migration, axon and dendrites growth and synapses formation to construct a functional network. In this section, we review models of distinct biological processes scattered throughout the brain (**Table 9**) and we investigate different frameworks, which can be used in the reconstruct of a cerebellar network.

4.1.3.1 Cellular Differentiation and Migration

This subsection describes models of differentiation and migration reconstructing these processes from different parts of the SNC, which can be useful to plan a framework for the cerebellar network.

To model the differentiation of the cerebellar neurons, it is suitable to create a Gene Regulatory Network (GRN) showing the two factors that activate the cell differentiation into glutamatergic and

GABAergic progenitors. The factor Math1 is expressed in the GABAergic neurons, which are born from VZ and the factor Ptfa1, in the glutamatergic neurons, which are born from RL.

The most common mathematical modeling techniques for GRNs were ordinary differential equations, Boolean networks, Petri nets, Bayesian networks, stochastic and graphical Gaussian models (De Jong, 2002). To produce different cell types, in the 3D model of the cerebral cortex proposed by Zubler et al., 2013, was used a Boolean networks approach of simplified GRN composed of sequentially activated bi-stable switches. This pairs of self-enhancing and mutually inhibiting genes a_i and b_i coded for transcription factors that had differential distributions during division. Another example of Boolean networks was developed to study the dynamics of intestinal crypts (Graudenzi et al., 2014). More information about this topic can be found elsewhere (Schlitt and Brazma, 2007; Bernot et al., 2013).

For the cerebellum, it is relevant to model the differentiation of the neuronal progenitors, in the different types of neurons, with their respective neuronal migration. During the cellular migration, it is required to show the interaction with extracellular, intracellular factors and the glia interaction. Several critical factors that need to be modeled are the *Reelin* and the *Shh* since they control the GrC and PC migration. Other factors, useful to have a realistic reconstruction, are Notch, several growth factors including *ErbB* and *FGFR,* proteins such as *astrotactin, neuregulin* and gradients of Ca^{2+} ions that are involved in the glia interaction during the cellular movement.

The following models describe the neuronal migration of neurons in the SNC and their interaction with intrinsic and extrinsic signals that are fundamental during migration process.

A cerebral cortex model of neuronal migration was built to show the interaction between extracellular signaling cues, such as GABA neurotransmitter, Reelin protein and the intracellular factors, like the *Lissencephaly 1 (LIS1)* and *Doublecortin (DCX)*, mediating the interaction with the glia (Setty et al., 2011). In this model, the cells were represented as executable objects whose migration is determined by explicit interactions between molecular entities in 2D grid.

A method to simulate morphogenesis of the cerebellum (Shinbrot, 2006), defined each cell as spherical particle that can migrate, interact, divide and differentiate. The 2D model used two cell types, type P (progenitors), and type Q (daughters) and when cells of either types come into contact, they can attract or repel each other. The simulations showed inter-cellular interactions leading to the formation of progenitor monolayer beneath a volume of differentiated daughters during development.

The pre-natal neurogenesis was the most common model, but, in some other cases, the attention was focus on the adult neurogenesis. A model of adult neurogenesis in the olfactory bulb reproduced both the cellular differentiation and migration processes. The model simplifies the processes into a 2D mathematical representation with complex reactions and interactions described through partial differential equations (Ashbourn et al., 2012). The model describes three types of cells, Type-B cells stay in the SVZ, Type-C were transit-amplifying cells and Type-A were the

migratory neuroblasts, assuming that Type-B and Type-C cells were fixed in space and Type-A cells move under the influence of a single chemoattractant factor.

The reconstruction of a tissue can be carried out with a 2D approach and expanded into a more complex 3D space to achieve a more realistic reconstruction. A multiscale model of the cerebral cortex development was built in a 3D environment and each process was guided by a formal language, analogous to genomic instructions (Zubler et al., 2013). The process started with a single progenitor cell containing a common genome, which gives rise to distinct populations of neuronal precursors that migrated to form the cortical plate and then extended their dendrites and axons. The behaviors of the simulated cells were determined by intracellular molecular-gene-like code called G-code (Zubler et al., 2011). This language was based on a set of primitives defining the basic neuronal actions and were combined to form network of instructions, called G-machines.

The study of adult neurogenesis allowed obtaining more data for each experiments in respect to the embryo, since it was simpler to observe the processes. For example, with in vivo imaging techniques, it was possible to record many aspects of cell migration speeds, proliferation, specification and apoptosis rates, fundamental for the development of models. A model of adult neurogenesis was built for the hippocampus (Ziebell et al., 2014), an area of the brain showing adult neurogenesis. The neuronal differentiation was reconstructed with a multi-compartmental system of ordinary equations based on experimental data. The model was composed of five cellular compartments, stem cells (c_1), neural progenitors (c_2), neuroblasts (c_3), mature neurons (c_4) and astrocytes (c_5) described by the following equations:

$$\frac{dc_1}{dt} = (2a_1\theta_1 - 1)p_1c_1(t) \tag{12}$$

$$\frac{dc_2}{dt} = \theta_1 2(1 - a_1)kp_1c_1(t) + \big((2a_2\theta_2 - 1)p_2 - d_2\big)c_2(t) \tag{13}$$

$$\frac{dc_3}{dt} = \big((1 + \theta_2) - 2a_2\theta_2\big)p_2c_2(t) - p_3c_3(t) - d_3c(t) \tag{14}$$

$$\frac{dc_4}{dt} = p_3c_3(t) - d_4c_4(t) \tag{15}$$

$$\frac{dc_5}{dt} = (\theta_1 2(1 - a_1)(1 - k) + 1 - \theta_1)p_1c_1(t) - d_5c_5(t) \tag{16}$$

Where *Θ* was the probability of stem cell division, *p* denoted the proliferation rate, *a* reflected the probability that a daughter cell had the same fate as its parent cell and *k* was the probability that a neural progenitor was produced in an asymmetric division rather than an astrocyte.

Models of the cellular migration had to comply with many mechanisms permitting the movement of cells and their interaction with others cells and the *Extracellular Matrix* (ECM). The physical interaction between two spherical somata can be described as a function of their diameter, their relative distance and the expression of adherence molecules (Zubler and Douglas, 2009). A wide range of theoretical works were constructed to describe this complex process, including a model of actin intracellular dynamics (Mogilner and Edelstein-Keshet, 2002), a model of single-cell mechanics during migration (Zaman et al., 2005) and models of cell migration in 2D and 3D matrices describing the interaction of the cells with the ECM (Painter, 2009; Schlüter et al., 2012). The forces on a single cell consist of a drag force that is balanced by the total force generated by the cell through contact with the matrix fibers and a term accounting for underlying noise.

The equation of motion has the following form:

$$F_{drag} = \sum_{f} F_{fj} + f_j(t) \tag{17}$$

F_{fj} is the force generated by a single cell through contact with an individual matrix fiber, $\sum_f F_{fj}$ is calculated from the directions and number of matrix fibers that contact the cell, $f_j(t)$ is the term that describes the noise (Schlüter et al., 2012).

Recently, was published a differential equation-based model that describes the proliferation and the differentiation of GrCs during the cerebellum development. The proliferation is followed by the differentiation in the EGL, and when the GrCs show the extension of an axon move from the EGL to the IGL. The data to construct and validate the model were obtained from experiments performed on mice at different postnatal age (Leffler et al., 2016).

4.1.3.2 Dendritic and Axonal Growth Models

The dendrites are the neuronal structures involved in the transmission of signals from the synapses to the soma, instead the axons transmit the signal integrated in the soma to other neurons.

In recent years, a wide range of mathematical and computational approaches were employed to simulate important features of axonogenesis, such as axon elongation, guidance, growth cone motility, microtubule dynamics, and neurofilament transport, at different temporal and spatial scales. The two most common ways to solve the axon growth are based on two opposite starting points: one requires the interaction of the growing axon with specific biochemical gradients in the ECM (*Extracellular Mechanisms*) (Goodhill, 1998) and the other requires a mathematical description of intracellular events (*Intracellular Mechanisms*), like the assembly of the cytoskeleton with *Tubulin* and *Microtubule Associated Proteins* (MAPs) (Kiddie et al., 2005).

For the cerebellum, the most important axon guidance molecules are Semaphorins, Netrins, Ephrins and Reelin. Ca^{2+} signaling is involved in the control of dendritic development acting as the main intracellular mechanism, interacting with the tubulin in the growth cone and providing the formation of microtubules and the main part of cytoskeleton. The following mathematical descriptions of axon and dendrites growth through extracellular and intracellular mechanisms can be adapted for the cerebellar growth processes.

Extracellular Mechanisms

In the developing CNS, growing axons are guided to targets by concentration gradients of target-derived diffusible factors. Growth cones are capable of sensing and evaluating the gradient across their spatial extent, moving toward a location with higher concentration, if act as an attractant factor or way from it, if the substance acts as a repellent factor (Zubler and Douglas, 2009).

Several models describe axon growth and guidance as a function of their response to chemical cues in the external environment (Goodhill, 1998; Goodhill et al., 2004; Maskery and Shinbrot, 2005; Krottje and van Ooyen, 2007; Kobayashi et al., 2010; Nguyen et al., 2016). A simple mathematical framework can be used to predict the maximum distance over which guidance could be possible, but in order to calculate the size of the change in concentration and how it evolves with time, it is necessary to assume a particular method for the diffusion of a factor. The concentration of the factor, in 3D collagen-gel assay, was definited as the distance (r) away from the target and the amount of time (t) elapsed from the start of the factor production *C(r, t)*. The complete formula was defined as follow:

$$\mathrm{C(r,t)} = \frac{q}{4\pi Dr} erfc \frac{r}{\sqrt{4Dt}} \tag{18}$$

Where *erfc* is the complementary error function, *D* is the diffusion constant (cm^2/sec) of the factor through the substrate and q (moles/sec) is the rate of factor production by the target, into an infinite, spatially uniform three-dimensional volume. Depending on the parameters, it can predict that guidance can be possible at distance of several millimeters before the distribution of factor reaches equilibrium. The parameters used are the diffusion constant (*D)*, the production rate of factor q, growth cone diameter (*Δr)*, and minimum and maximum concentration for gradient detection (Goodhill, 1998). An approach used to grow dendritic and axonal trees, with well-defined bifurcation and elongation, was built with the gradient of a protein called Semaphorins (Zubler et al., 2013).

Intracellular Mechanisms

In this section we review some mathematical approaches about the morphological development of axonal and dendrites, including initiation, differentiation, elongation, pathfinding, branching and shape definition.

Neurite Differentiation

The neurite differentiation concerns the formation of generic neurites from an initially spherical neuronal cell. With the presence of specific substances, one of the neurites will mature into the axon whereas the rest will evolve into dendrites (Galiano et al., 2012).

Models of neurite initiation and differentiation were studied and assembled to investigate how small inhomogeneities in the cell surface trigger mechanisms that lead the initial neurite outgrowth (Hentschel et al., 1998). Ca^{2+} is assumed to be the morphogen that promotes cell outgrowth and has an important role in axon guidance (Sutherland et al., 2014). Ca^{2+} concentrations in growth cones are regulated both by Ca^{2+} influx through the plasma membrane and by intracellular Ca^{2+} stores. Small bulges in the cell surface produce focal depolarization leading to elevated Na^{+} and Ca^{2+} entry and heightened Ca^{2+}-dependent outgrowth of the bulge, eventually leading to neurite formation.

A theoretical model was used to model axon-dendrite differentiation (Toriyama et al., 2010) where *Shootin 1*, a key regulator of axon outgrowth, accumulated in neurite tip in a length-dependent manner, and how the dynamics of this protein caused one neurite, from a group of neurites of similar length, to outgrow its siblings. Shootin 1 is stochastically and actively transported from the cell body to the growth cone, from where it diffuses back to the cell body leading to preferential accumulation of Shootin 1 in long neurites. This was due to the retrograde diffusion becomes weaker with length when compared to the active anterograde transport.

Neurite Elongation

Neurites elongate and branch reaching lengths of tens to hundreds of µm to over a meter or more for long axons. In the following outgrowth model of neurites was assumed to be rate-limited by the availability of a particular, but unspecified chemical at each neurite tip (Graham and van Ooyen, 2006). This chemical was produced in the cell body, transported by diffusion and active transport to the end of each neurite emanating from the cell body. The system of ordinary differential equations (ODEs) was used to describe the chemical concentration in the cell body, c_0, in each of n neurites, c_1 to c_n, and the lengths of each neurite, l_1 to l_n:

$$T_i = DA\frac{c_0 - c_i}{l_i} + F\frac{dl_i}{dt}c_0 \tag{19}$$

$$\frac{dc_0}{dt} = \frac{1}{V_0}\left(S - \sum_{i=1}^{n} T_i\right) \tag{20}$$

$$\frac{dc_i}{dt} = \frac{1}{V_i}\left(T_i - G\frac{dl_i}{dt}\right) \tag{21}$$

$$\frac{dl_i}{dt} = ac_i \tag{22}$$

T_i is the transfer rate of chemical from the soma to a neurite tip; D is the diffusion constant; A is the cross-section area of a neurite; V_0 is the volume of the soma; V_i is the volume of a neurite tip; F is a growth-dependent active transport rate. The elongation rate of a neurite was proportional (α) to the concentration in the tip, c_i, and the chemical compound was consumed in the tip at a rate proportional G to the elongation rate. A dynamic instability emerged when one neurite had a larger initial growth rate. This factor leads to higher consumption of the chemical at this neurite tip than at the others. This leads to rapid growth generating the axon, while all others neurites showed a very slow growth becoming dendrites. These competitive effects between neurites were also described in similar ODE models of the growth of branched dendritic structures (Graham and van Ooyen, 2006).

The following model was constructed to be more realistic based on the intracellular dynamics of cytoskeleton construction, particularly of the microtubules that form the supporting scaffold in the neurites. Elongation was assumed to be a function of the amount of available free tubulin in the growth tip of the neurite, which was assembled into the microtubules that extend the internal cytoskeleton. The constraints to growth were the production rate of tubulin and its transport from the site of synthesis, the cell soma, to the neurite tip by diffusion and active transport. It was developed a continuum (PDE) model of tubulin-driven neurite elongation that allowed determination of tubulin concentration and transport along the length of the growing neurite (McLean et al., 2004; Graham et al., 2006).

The system of partial differential equations (PDEs) is:

$$\frac{\partial c}{\partial t} + a\frac{\partial c}{\partial x} = D\frac{\partial^2 c}{dx^2} - gc \tag{23}$$

$$\frac{dl}{dt} = r_g c_{x=1} - S_g \tag{24}$$

$$-\frac{\partial c}{\partial x} = \varepsilon_0 c_0 \; at \; x = 0 \tag{25}$$

$$-\frac{\partial c}{\partial x} = \varepsilon_l c - \zeta_l \; at \; x = l \tag{26}$$

The free tubulin concentration at a point x in the neurite at time t is given by $c\,(x, t)$. The length of the neurite at time t is given by $l(t)$. Space x lies in the domain 0 to l. Tubulin moved by active transport (a) and diffusion (D) and degrades with rate g. Synthesis of tubulin in the cell body at rate $\varepsilon_0 c_0$ results in a flux of tubulin across the boundary at $x = 0$. Assembly of tubulin into microtubules

results in a flux of tubulin across the boundary at $x = l$ (assembly flux ε_l and return flux ζ_l) and a change in length (assembly rate r_g and disassembly s_g).

The following model described neurite elongation and retraction as the result of respectively assembly and disassembly of microtubules (van Ooyen, 2011). This was a mono compartmental model of a neuron with n distinct neurites. The rates of change of L_i (neurite length), C_i (concentration of tubulin in the growth cone) and C_0 (concentration of tubulin in the cell body) were:

$$\frac{dL_i}{dt} = a_i C_i - b_i \tag{27}$$

$$\frac{dC_i}{dt} = b_i - a_i C_i + \frac{D}{L_i + k}(C_0 - C_i) + fC_0 - gC_i \tag{28}$$

$$\frac{dC_0}{dt} = s - \sum_{i=1}^{n} \frac{D}{L_i + K}(C_0 - C_i) - \sum_{i=1}^{n} fC_0 - gC_0 \tag{29}$$

Where s is the rate of production of tubulin in the cell body. The tubulin is transported into the growth cones of the different neurites by diffusion with diffusion constant D and by an active transport with a rate constant f. The rate constant a_i is for microtubules assembly and the rate constant b_i is for microtubules disassembly. The assembly of microtubules in the growth cone permits the elongation of the neurite, instead the disassembly of microtubules into tubulin causes the retraction of the neurite. g is the rate constant of the degradation of tubulin in the cell body and in the growth cone. k is the distance between the centers of the cell body and the growth cone compartment when $L_i = 0$.

Another model for tubulin-driven axonal growth, consisting in a set of partial differential equation (PDE) and two ordinary differential equations (ODE), describes the tubulin concentration along the axon, its diffusion and degradation, to permit the axonal elongation (Diehl et al., 2016).

To model the axonal growth, it is possible to define every step with a system of differential equations with the addition of stochastic element. This approach was able to define the direction of the growth cone based on the definition of the emerging point (x and y) and the initial growth angle (ϑ) into equations (Li et al., 2007; Borisyuk et al., 2008; Pearson, Yanthe E. Emilio Castronovo et al., 2011; Roberts et al., 2014).

The system of axon growth equations was:

$$x_{n+1} = x_n + \Delta \cos(\theta_n) \tag{30}$$

$$y_{n+1} = y_n + \Delta \sin(\theta_n) \tag{31}$$

$$\theta_{n+1} = (1-\gamma)\theta_n + \mu(\bar{\Upsilon} - \gamma_n) + \xi \quad (32)$$

The noise in the axon growth angle describes a random deviation of the current angle from the deterministic component and was represented by a random variable uniformly distributed in the interval (-α, α), where parameter α defines the boundary for the angle deviation. The noise was modeled by a uniformly distributed random variable with mean equal to zero and variance equal to $\alpha^2/3$. *n* is the iteration number which represented the current position of the tip of the growing axon; ξ is a random variable uniformly distributed in the interval [-α, α] (α typically is about 2-5°); Δ is the 1 μm distance grown in a single iteration; γ represents the tendency of an axon to turn towards an angle of 0°, towards the longitudinal growth; μ and $\bar{y}$ characterize the interaction between two opposing repulsive gradients, one pushing from the ventral side to the dorsal side and one pushing from the dorsal side to the ventral direction in the case of the spinal cord neurons, $\bar{y}$ is the position at which these processes cancel each other out, μ is the strength of the attraction towards $\bar{y}$.

Another way to define the growth of the axon cone was based on a much more physical approach in which parameters, like the force of the axon elongation, the adhesion mechanism with the external matrix or the viscoelastic characteristic, are used to characterize the axon growth (O'Toole et al., 2008).

Neurite Branching

In the model described by (Graham and van Ooyen, 2004) neurites branching depended on the concentration of a branching-determining substance in each terminal segment transported by active transport and diffusion to the terminals. The models revealed that transport-limited effects may give rise to the same modulation of branching as indicated by the stochastic BESTL model (van Pelt and Uylings, 2005). Different limitations arise if transport was dominated by active transport or by diffusion.

The equations of the model of Graham and van Ooyen (Graham and van Ooyen, 2004) are:

$$\frac{dC_0}{dt} = I - \gamma_0 C_0 - \frac{aA_1}{V_0} C_0 - \frac{DA_1}{L_1 V_0}(C_0 - C_1) \quad (33)$$

$$\frac{dC_i}{dt} = \frac{aA_i}{V_i} C_{i-1} - \frac{a(A_l + A_r)}{V_i} C_i + \frac{DA_i}{L_i V_i}(C_{i-1} - C_i) - \frac{DA_l}{L_l V_i}(C_i - C_l) - \frac{DA_r}{L_r V_i}(C_i - C_r) \quad (34)$$

$$\frac{dC_T}{dt} = -\gamma_T C_T + \frac{aA_T}{V_T} C_i + \frac{DA_T}{L_T V_T}(C_i - C_T) \quad (35)$$

that describe changes in the branch-determining substance concentration in cell body, C_0, in an intermediate segment, C_i and in the terminal segment, C_T. The branching probability of terminal segment *T* during a short time period *dt* is given by $p_T = k_b C_T dt$. The fixed branching rate, *kb*, and the

time interval *dt* are chosen so that *pT < 1*. A branch event results in a bifurcation of the terminal segment.

As with the BESTL model (van Pelt and Uylings, 2005), the previous model described dendritic growth as a stochastic process in which each terminal segment, in the growing tree, had a probability of branching to form two new daughter segments in any given short time period. The model of Van Pelt and Uylings (van Pelt and Uylings, 2005) with the following equation:

$$p_i = C2^{-S\gamma_i} n^{-E}(B/N) \tag{36}$$

p_i is the probability that the terminal segment *i* will branch to form two daughter terminal segments. *B/N* is a fixed probability factor for branching in any one of the *N* time bins of the growth period; *n* is the total number of terminals in the tree at the current time bin and *E* is the factor by which n affects the branching probability; γ_i is the centrifugal order of the terminal segment (number of branch points currently between the terminal segment and the cell body) and *S* is the factor by which γ_i affects the branching probability.

4.1.4 Synaptic Formation and Connectivity

The axons, once arrive in their target region, tend to form synaptic connections when they enter in contact with dendrites, soma and, sometime, axons of nearby neurons (local circuits) and only when specific transmembrane proteins are located on their membranes (Ichikawa et al., 2016). This is the simplest definition of the interaction to generate a synaptic contact, since most of the biochemical compounds involved are not yet well characterized (Roberts et al., 2014). The formation of synaptic connection was reproduced primarily with probabilistic connectivity: when an axon comes into close contact with a dendrite, a synapse is formed with a certain probability between the two elements (Stepanyants et al., 2002; Li et al., 2007; Roberts et al., 2014). In recent years it was proposed a more realistic approach based on the physical interaction between 3D reconstructed morphologies placed and oriented in a 3D environment (Markram et al., 2015). The resulting contact where converted into synapses and described with NMODL, a language derived from C programming language, contained in the NEURON simulator (Hines and Carnevale, 2001). Each synaptic type can be described with a different level of details ranging from the simplest biexponential approach to complex biochemical kinetic scheme (Destexhe et al., 1994, 1998; Tsodyks et al., 1998; Carnevale and Hines, 2006; Nieus et al., 2006). The details which can be added to a synapse are countless and, to further study the complex molecular level, it was used an approach based on the Monte Carlo algorithm. This approach can keep track of each single diffusing molecules and the receptors were built with a very high quantity of details (Stiles and Bartol, 2000). This method was used to model synapses and synaptic responses to instruct a machine learning system (Montes et al., 2013).

The number of synapses is not prefixed and during development, neurons and other target cells are often initially innervated by more axons than into adulthood. The process that leads to elimination of connections is referred to as axonal or synaptic competition. Models describing in detail the competition in the development of nerve connections were built taking in account the underlying

biochemistry of neurotrophic factors such as the Neurotrophin (van Ooyen and Willshaw, 1999; van Ooyen, 2003).

The synaptic activity can be modified by the specific activity applied to the presynaptic and post synaptic sides. These modifications were modelled with different approaches, ranging from on an input-output relationship between neuronal activity and synaptic plasticity (Luque et al., 2016), and the description at biophysical level (Brette et al. 2007).

4.1.5 Models of Electrical Activity

The models of electrical activity are the most common models concerning the cerebellar activity.

The theory developed by Lapique (Abbott, 1999; Brunel and van Rossum, 2007) was the base for the definition of the integrate-and-fire (IF) models, also defined spiking neuron models. These models describe a system composed of a resistance and a capacitance, mimicking the cell membrane behavior and one of the advantages is the simplicity and computational efficiency (Burkitt, 2006). Since that the IF models are simplified description of neurons, they do not describe any ionic channels, and therefore are able to reproduce only some behaviors, instead of the high degree of freedom that characterizes real neurons. The total current that flows through the membrane is defined by the following equation:

$$I(t) = \frac{u(t)}{R} + C\frac{du}{dt} \tag{37}$$

The driving current can be split into two components $I(t) = I_R + I_C$. The first component is the resistive current I_R that passes through the linear resistor R. It can be calculated from Ohm's law as $I_R = u/R$ where u is the voltage across the resistor. The second component I_C charges the capacitor C. From the definition of the capacity as $C = q/u$ (where q is the charge and u the voltage), we find a capacitive current $I_C = C\,\mathrm{d}u/\mathrm{d}t$.

The Hodgkin–Huxley (HH) model is a conductance-based model, developed by Hodgkin and Huxley's 1952 (Hodgkin and Huxley, 1952), which describes, with a system of ordinary differential equations (ODE), the behavior of each single channel and their interaction to generate and propagate action potentials. Ionic channel activity was usually modeled following the HH formulation where, in each compartment, membrane voltage was obtained as the time integral of the equation:

$$\frac{dV}{dt} = -\frac{1}{C_m} * \left\{\sum [g_i * (V - V_i)] + i_{inj}\right\} \tag{38}$$

Where V is the membrane potential, C_m membrane capacitance, g_i are the ionic conductances and V_i the E_{rev} (the subscript i indicates different channels), and i_{inj} is the injected current. Adjacent compartments communicating through an internal coupling resistance. For each ionic channel i, the conductance g_i is

$$g_i = Gmax_i * x_i^{zi} * y_i \tag{39}$$

where $Gmax_i$ is the maximum ionic conductance, x_i and y_i are state variables (probabilities ranging from 0 to 1) for a gating particle, and z_i is the number of such gating particle. The gating particles are part of the conformational structure of the ionic channel and control the ion flow through the channel. When the ion flow moves in response to a change of membrane voltage, causes conformational changes in the protein, opening and closing these gating particles.

Spiking Neuron Models (IF)

The IF approach is the most effective to reconstruct extensive network composed of hundred thousand neurons, to study network level problem without the geometrical limitations, or the huge computational impact of the conductance based (HH) approach. To mitigate some limitations of the original IF model, they were extended with the introduction of leak integrates and fire (LIF) models and the recent exponential integrate and fire (EIF), which can be used to generate simplified model capable of reproduction a good range of behaviors and, above all, integrate some parameters for the ionic channels (Barranca et al., 2014). With these tools a GrC EIF model (Bezzi et al., 2004) and a PCs EIF model (Lynch and Houghton, 2013) were developed.

Large-scale spiking networks of the cerebellum were created using *IF* models and simplified synapses, since the *IF* approach is the most effective to simulate huge network (Brette et al., 2007; D'Angelo et al., 2013; Garrido et al., 2013a; Kistler and De Zeeuw, 2003; Medina and Mauk, 2000; Medina et al., 2000), being suitable for studying the interaction properties of high-level functions, such as working memory (Del Giudice et al., 2003) or typical cerebellar behaviors, as the delayed eye blink conditioning (Yamazaki and Tanaka, 2009). To test the interactions between MLIs/PCs and their responses, was designed a network of IF neurons composed of PCs connected to MLIs, placed on a mono-dimensional grid. With this network model it was possible to study the recursive interaction of MLIs through gap junctions and their ability to inhibit other MLIs in the spatial neighborhood (Lennon et al., 2014).

Cerebellar network models become more and more complex adding biological details to describe carefully cerebellar processes and mechanisms, therefore GPUs are now used to accelerate neuronal simulations due to their ability to perform computations in parallel, showing significant improvement in execution time compared to CPUs. Several works performed on GPU were done to simulate cerebellar network models, composed of millions of neurons and synapses, which run in real-time. They consist of reproducing large-scale spiking network models of the cerebellum, used to study the role of the cerebellum as a learning machine. One of these extensive network reproduced, in real time, the delayed eye blink conditioning and was used to action a robotic arm with the ability to hit a ball, after a certain number of learning sessions (Yamazaki and Igarashi, 2013). Another large-scale network model reproduces the eye blink conditioning, a classical conditioning which is a form of sensory-motor learning depending of the cerebellum (Kim and Thompson, 1997; Li et al., 2013). The IF networks are suitable to be translated into system able to control robotic simulations and robotic hardware. These networks are endowed with multiple types of plasticity mechanism to obtain a wide range of synaptic behaviors (Luque et al., 2011; Garrido et al., 2013b; Casellato et al., 2014). The model of the IO network, which is responsible with the cerebellum for crucial sensorimotor integration functions in humans, was simulated on 4 different

GPU platforms (Du Nguyen et al., 2015). A model of a large-scale spiking network of the cerebellum, composed of more than 1 million neurons, was implemented to be executed on 4 GPUs simultaneously, achieving simulations in real-time, in order to study the neural mechanisms of memory consolidation in the brain (Gosui and Yamazaki, 2016).

More recently, accelerated neuromorphic hardware systems were utilized for the implementations of different computational neuronal models, reproducing the function of IF neurons in real time. In a silicon form, neuromorphic devices mimic the structure and emulate the function of biological neural networks. The neuromorphic approach is relevant for its high parallelism and acceleration (Bruederle et al., 2009; Indiveri et al., 2011; Pfeil et al., 2013). A new parallel chip multiprocessor that permits to simulate networks of 10^9 spiking neurons is Spinnaker (Galluppi et al., 2015)

Conductance-Based Models (HH)

The HH approach is used preferably to build single neuron model, for its high level of details and less for network models for their heavy computational impact. The detailed mathematical description of each ionic current allows understanding the ionic mechanisms underlying the neuronal activity, which, depending on the neuronal type, can have a different arrangement of ionic channels.

Models of Cerebellar Single Neurons

The HH approach was used to build several biophysically detailed models of neurons and synapses of the cerebellum and published on the database ModelDB (https://senselab.med.yale.edu/modeldb), the main model repository of this kind of models. The reconstruction of a biophysical realistic cell model begins with the acquisition of a 3D neuron morphology. If this is not available, an equivalent morphology, based on statistical data, can be reconstructed and used. The next step is the definition of the appropriate passive properties, resistance and membrane capacitance, and the active properties, the ionic conductances, of the ionic channels, which can be described with HH or the Markovian kinetic scheme approaches. The final step requires the testing of the modelling effort with specific protocols, similarly to the experimental procedure, to control the quality of the results. The most significant drawback of this approach is the high computational cost, since each part is described with sets of ODE.

In the past 20 years, many detailed models of cerebellar single neurons, were built starting with one of the most used, the PC (De Schutter and Bower, 1994a, 1994b; Bower, 2015) that was the base for a successive radical modification with the introduction of the AIS as its main compartment (Masoli et al., 2015). The PC model was built to reproduce the intrinsic properties of these complex neurons, such as the autorhythmic generation of action potential, the particular axonal transmission, the Ca^{2+} importance in dendrites and Na^{+} in the rest of the neuron. The GrC received a lot of attention at the end of the 90s and subsequent years, with a series of experimental study used in the reconstruction of several models. The GrC models reproduce the most important electroresponsive properties of the neuron such as the fast spiking, the presence of adaptation and the resonance frequency (D'Angelo et al., 2001; Diwakar et al., 2009; Nieus et al., 2006). The same principle was applied to the GoC, reproducing the spontaneous firing of the neuron, the fast spiking

response to steps of current injections, the post-inhibitory rebound and the resonance frequency (Solinas et al., 2007a, 2007b; Vervaeke et al., 2010; Szoboszlay et al., 2016). The model of the UBC reproduces the neuronal behavior, highlighting the neuronal adaptation and the delayed bursting. (Subramaniyam et al., 2014). The outside connections to the cerebellar network were also modelled reproducing the main electrical characteristics of the IO, with its slow spiking, Ca^{2+} spikes and subthreshold oscillations (De Gruijl et al., 2012; Torben-Nielsen et al., 2012), and of the DCNs with their fast spiking and the post-inhibitory rebound properties (Luthman et al., 2011; Steuber et al., 2011).

Cerebellar Network Models

One of the first examples of GCL network built with biophysical detailed mono-compartmental neurons was built in 1998 to test the inhibitory activity of the GoCs with respect to GrC, mf and pf excitatory input (Maex and De Schutter, 1998). With this model, it was possible to see a clock-like activity if the mfs were stimulated in a random way and this activity was cancelled when the mfs were way too much stimulated or when the activity was very low.

The large-scale networks, based on HH models and distributed in a 3D environment, are built using an extensive amount of information and incorporate neurons capable of responding with a wide range of behaviors to arbitrary input patterns. The 3D environment can be filled in two ways: 1) with mono and multi compartmental models based on equivalent morphologies, distributed in the space based on their densities and connected with synapses based on statistical information too (Solinas et al., 2010). 2) With a space filling algorithm capable of distributing in the space, using a process of juxtaposition, neurons reconstructed with realistic 3D morphology. This system was used to develop the neocortical micro circuitry (Markram et al., 2015) using the neuronal volume and cellular density as main parameters. This approach permits the generation of synaptic connections when two morphologies are in close proximity and only following specific rules such as distance and angle of contact.

4.1.6 Spatial Models

To reproduce a model of a biological system it is important to not overlook the concept of “spatial modeling”, however, this approach was never applied for the cerebellar network models to date. These models consider an area divided into a large number of similar units represented with squares or polygons and can be classified into two types, in-lattice (or grid)-models and off-lattice (or lattice-free) models (De Matteis et al., 2013).

An example of "in lattice" model is the Glazier–Graner–Hogeweg (GGH) or cellular Potts model (CPM) which has been defined as a cell sorting model in a 2D environment, and was propose to model and simulate differential adhesion pattern of cell disposition caused by cell adhesion molecules (Graner and Glazier, 1992; Glazier and Graner, 1993). The effective energy, *H*, which is the Hamiltonian of the system includes the interactions between cells, with specific individual cell properties, and the ECM. This is defined as an unconstrained area and interacts with the cells with specific rules. Some fundamental properties are the cell size, which can vary in a small range and dictate the spatial evolution of the tissue, the energetic states between different cell types and the

boundaries of the area usable by each cell for their expansion. The original 2D lattice representation has been extended to support 3D lattices in a straightforward way (Scianna and Preziosi, 2012; De Matteis et al., 2013).

Many 1D, 2D and 3D off-lattice models have been developed over the years and several variations were defined with topological and geometrical representations different than the usual simple lattice. The location in space, of a specific structure such as the nucleus, is the main reference point to derive all the other. This approach is defined as "Voronoi" representations and another, based on the representation of surfaces and volumes as specific features, is defined as the polyhedral representation. In the first application of “Voronoi” tessellation, the cells, on a 2D lattice free, are not fixated in specific location but they can move under the influence of attractive and repulsive forces (Meineke et al., 2001). The model can be extended with intracellular biochemical network and extracellular factors that control cell proliferation too. This approach can be expanded to define a 3D model where are taken into account the behaviors of the single cell and each cell is described as an agents able to respond, with a specific set of rules, to internal and external inputs (Smallwood et al., 2004; Walker et al., 2004). A 3D bio-mechanical model for tissue organization has been developed by Galle (Galle et al., 2006), where the cells are described as "deformable elastic bodies (keeping spherical shape) capable and free of moving, growing, dividing, differentiating and communicating with each other" (De Matteis et al., 2013). Schaller–Meyer-Hermann’s model (Schaller and Meyer-Hermann, 2005) is a hybrid 3D biomechanical agent-based "Voronoi–Delaunay" model of general multicellular systems. In this model, the single cell shape varies from "spherical in thin solutions to convex polyhedral in dense tissues" and likely to the Galle’s model, the interactions inside the cells can be of different types: "elastic cell–cell forces, cell–cell, cell–substrate adhesive forces, friction forces between cells and the cells and the substrate" (De Matteis et al., 2013).

Table 9. Models of Neuronal Development Processes.

	Model cerebellum		Model hippocampus
	Model cerebral cortex		Model olfactory bulb
	Model spinal cord		No specific area model

Main biological processes / References	Neuronal differentiation	Neuronal proliferation	Neuronal migration	Axonal growth elongation branching	Dendrite growth	Synapses connection	Synapses formation	Electrical activity	
(Setty et al., 2011)	X	x	x						
(Zubler et al., 2013)	X	x	x	X	x	X			
(Roberts et al., 2014)				X	x	X			
(Li et al., 2007)				X	x	X			
(Borisyuk et al., 2008)				X					
(Ziebell et al., 2014)	X	x	x						
(Ashbourn et al., 2012)	X	x	x						
(Shinbrot, 2006)	X	x	x						
(Graham and van Ooyen, 2004, 2006)				X					
(Diehl et al., 2016)				X					

Table 9. The table summarizes the different types of models that describe the different biological processes.

4.1.7 Perspectives for a Self-Organizing Cerebellar Network Model

The reconstruction and validation of a neuronal network can be achieved without taking into account the actual geometrical disposition or the morphologies of each neuron and the synaptic location can be statistically approximate. This approach requires less information, less overall complexity and less computational resources but, at the same time, the results are subjects to a series of compromises, which can reduce the degree of freedom and the overall richness attainable by a complete reconstruction.

To obtain a realistic cerebellar reconstruction and to have a better chance to generate a network with many functional emerging properties, there are two different approaches that can be pursued: 1) the reconstruction in 3D of each neuron which defined realistic apposition used to define the exact synapses location (HBP (Human Brain Project) approach (Markram et al., 2015)), 2) the generation of the neural tissue trough the imposition of the same biochemical and biophysical rules used in reality to define the progressive neuronal differentiation, migration, the generation of their morphologies and the connection of each part into the final circuit (NeuroGenetic approach (Zubler et al., 2013)).

The HBP approach can be proved very useful on different fronts: 1) the 3D reconstruction of the morphology of each neuron permits the validation of specific biophysical properties, like the absence of dendritic back propagation of PC neurons (Masoli et al., 2015) or the strict compartmentalization between the somatodendritic and the axosomatic sections, typical in many cerebellar neurons like PCs, GrCs (Diwakar et al., 2009) and SCs. The definition of a 3D space can be then populated by the 3D reconstruction making the generation of a network much more realistic, above all, in the definition of location for each synapse. The PC spines will prove to be a testing ground since they are not randomly formed through the interaction with the excitatory input but are present from the inception of the neuron (O'Brien and Unwin, 2006).

To build such a network requires a lot of information about each single neuron, both biophysical and biochemical, and for the overall geometrical structure. There are countless publications about the cerebellar neurons structure, physiological behaviors and overall activity with only small exception, for example the globular cell and a complete view of the richness of GoC types (Simat et al., 2007). The network, instead, received a lot of attention starting in the seventies with seminal work (Palay and Chan-Palay, 1974) and, except for some recent development (Ankri et al., 2015), has been clarified, from a geometrical and connectivity point of view, thanks to its modularity. Of course not all was elucidated with the same degree of clarity and some fundamental connectivity rules are still based on theories but, with the HBP approach, will be possible to test and explain one of the most known theory of the cerebellar network, involving the exact functional rules defining the interaction between aas, pfs and the PC vast dendritic tree (Bower, 2013).

This approach has many pros but, of course, it has some drawbacks too. Currently there are only three realistic 3D morphologies of cerebellar neurons which had been used in previous models of GrC (Diwakar et al., 2009), PC (De Schutter and Bower, 1994a, 1994b) and GoC (Vervaeke et al., 2010). Another limitation is the availability of enough information to define a complete ionic

channels setup for all the cells. The reconstruction of new morphologies will be the first step and it will have to be done for more than one 3D morphology for each neuronal types, in conjunction with more than one set of ionic conductances to provide a much needed richness of results. The synapses of the cerebellum are not only complex to locate, from a pure geometrical point of view, but they show an extensive richness of plasticity mechanism, such as cross talking, which was difficult to test and prove in reality, but which will be much easier to prove in a 3D environment where the synapses will be place correctly than with any non-geometrical approach.

This approach was proven to be feasible for the cortex and it will be feasible for the cerebellar cortex only if the software will be able to support a series of non-standard characteristics such as the fixed orientation of each neuron in the 3D environment or the ability to generate synapses between a multitude of parallel axons connecting single spines on a single neuron.

The NeuroGenetic approach can be used to generate a network similar to the one obtainable with the HBP approach but with two fundamental differences: 1) the network will grow to maturity without predetermined morphologies, synaptic arrangements or network definition but, it will be the result of a GRN and biochemical interaction. 2) Since the entire procedure is evolving with time, can be used to simulate different stages of a circuit instead of creating a crystallized reproduction like with the HBP approach. This is optimal to study both the physiological and the pathological conditions arising from normal or abnormal conditions in the genesis or during maturity.

This approach requires an impressive quantity of information than the other approaches since the acquisition of a complete knowledge is slower and goes from the single gene to complex biochemical reactions. Since the evolving tissue receives support and direction from glial cells, they cannot be under valuated, as in other approaches, but they need to be taken into account from the first moment. This require even more information, which can be a problem since glial cells have been studied but not with the same quality as the nearby neurons. A fundamental drawback of this approach, is the tremendous amount of computational power required since the system has no predetermine solutions and each simulation can account for dozens of millions of cells at the same time.

The advantage of this approach can repay many of the downsides with a functional reproduction of the tissue, completed with the formation of synapses and the reproduction of the functional connectivity between each neuron, as the result of the complete development. Since each neuron is free to define its own structure, it will be able to express some variability in the shape of the morphology and in the ionic channels, thanks to a degree of freedom generated by the GRN. The feasibility of this approach has been proved with the reconstruction of a small portion of the cerebral cortex and nothing prevents that the same cannot be done for the cerebellar cortex (**Fig.**).

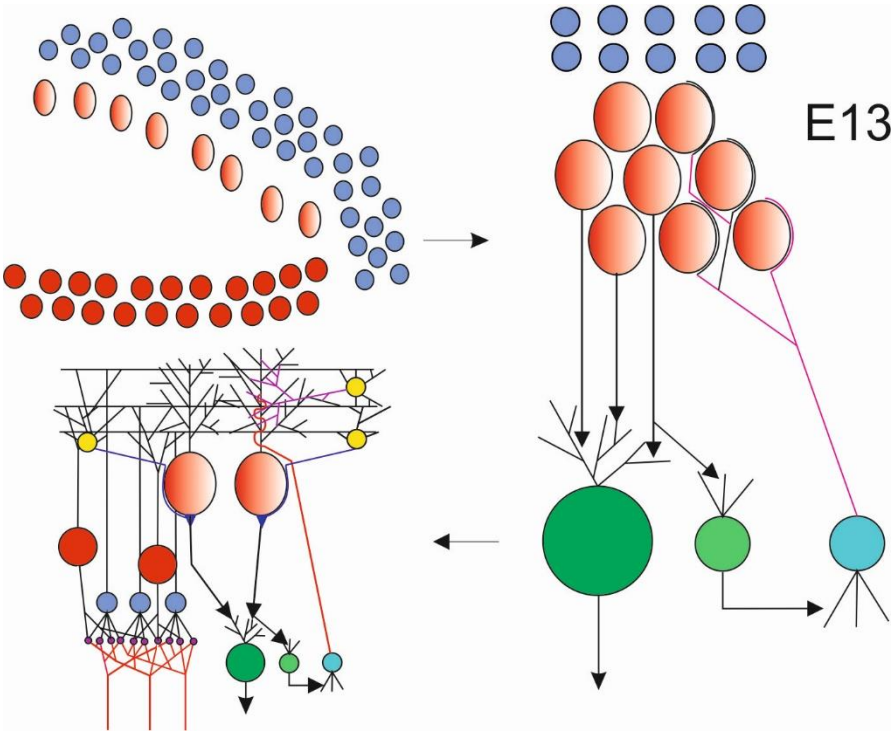

Fig. 36. Representation of the model of the cerebellar development network.

The schematic view shows the migration of the GoCs (red circles), PCs (pink ovals) and the GrCs (blue circles) and their connection with the DCN (green circle and green light circle), the IO (blue light circle) and the MLIs (yellow circles).

4.1.8 Tools

An overview of available tools for the simulation of the different neuronal characteristics is presented in this section (**Table 10**).

The most known computer simulation packages for the creation of electrical signaling models of neurons are NEURON (Hines and Carnevale, 2001) and GENESIS (Bower and Beeman, 2003). These simulators are capable of solving the biophysical properties, such as complex morphologies with dendritic and axonal trees composed of thousands of sections, fundamental membrane properties like axial resistance and membrane capacitance and ions channels interactions, to show specific behaviors in a time frame which, usually, last only seconds or minutes. These tools are unable, from a computational power requirement, to reproduce the development of behaviors on a day/week scale and the simulation of large networks. The fundamental limitation of these tools is that are unable to modify the morphological composition over time and they are not able to reproduce other complex biological processes such as cellular migration and axonal growth.

NEST (NEural Simulation Tool) is a tool to simulate spiking neuron networks composed of IF models, which can be associated in large-scale neuronal networks (Diesmann and Gewaltig, 2001; Eppler, 2008).

To show the potentiality of some of these tools was published a review in which these tools are used to simulate a spiking neuronal network in conjunction with specific synaptic plasticity properties, for example STDP (Spike-timing-dependent plasticity) (Brette et al., 2007).

BRIAN2 is an open source spiking neural network simulator written entirely in Python, is used to simulate single compartmental models but it is most suited for running networks with a large number of neurons (Goodman and Brette, 2008).

MOOSE (Multiphysics Object Oriented Simulation Environment) supports the generation of single cells as well as extensive networks and integrate a solver to add and simulate biochemical pathway in SBML format too (Ray and Bhalla, 2008).

STEPS (STochastic Engine for Pathway Simulation) is a tool for stochastic simulation of reaction-diffusion in 3D geometries based on Gillespie's SSA algorithm and expanded to permit the diffusion, on a 3D mesh, of molecules. The main feature is to simulate the biochemical pathways in dendrites and synaptic terminals but it can be used in a more generic way to study any kind of biochemical pathway. Another important point is the ability to adapt the simulation to morphologies and spatial gradients (Hepburn et al., 2012).

PSICS provides a way to build cell models with complex morphologies and ionic channels, as many other tools are able to, but, in this case, it provides an efficient way to specifies the location and number of each ionic channel (Cannon et al., 2010).

CX3D is a novel tool for simulating the growth of neuronal networks, in a physical 3D space. It is an open-source software written in Java and with this simulation tool is possible to model all stages of corticogenesis: cellular development that includes differentiation and migration processes, axonal and dendritic growth and formation of synaptic connections. Neurons are composed of discrete physical components such as spheres to reproduce the soma, cylinders for the neurites, and each neuron is located at a particular point in 3D space, where they interact to simulate physical and biological processes that occur in the tissues. To define the neighborhood relation is used a 3D Delaunay triangulation (Schaller and Meyer-Hermann, 2005). CX3D respects physical processes such as cell division, cell-cell interactions movement and chemical diffusion in 3D space (Zubler and Douglas, 2009). For the neurite outgrowth CX3D implements the model of Kiddie et al. (Kiddie et al., 2005) (Neurite Branching) (**Fig. 37**).

NETMORPH is a simulator where the network of neurons and their interaction trough synapses is obtained with the generation of the morphologies of each cell starting from the soma and creating dendrites and axons in a stochastic, phenomenological manner. This approach permits the generation of neurons with realistic dendrites and axons and their interaction generated synapses with realistic pattern (Koene et al., 2009).

CompuCell3D (CC3D) is an open source application which acts as a 3D framework environment providing tools to construct, run and simulate models based on the GGH scheme and, of course, visualize their results (Swat et al., 2012). The core part of the program is built with C++ but the environment provides two different languages to build models. The original CompuCell3D XML

syntax is useful to define many parameters of each simulation but it has a limitation when a simulation starts to become complex, above all, during the implementation of inter cell interaction or connections to the intracellular models. To resolve these limitations, the author of CC3D, decided to implement python, which is a very powerful script language. With this new language it is possible to define an entire simulation in a single file, define new steppers, energy functions, lattice monitors and the simulations themselves can benefit from the extensive number of modules available for python written mostly in C++. Since the environment is very user friendly, it can be used by programmers and biologist as well to create many different types of models ranging from angiogenesis, immune system, stem cell differentiation and, above all, morphogenesis of multicellular organisms where the cellular mechanisms interact with the gene regulatory networks to define basic cellular properties such as division, adhesion, differentiation and migration. The starting point for a simulation is the definition of a lattice and of the main GGH objects, a generalized cell, which, depending on what the modeller needs, can be a single cell, a subcellular compartment or a cluster of cells. When two or more generalized cells are bridge together they from subcells, which can be used to define complex shapes or specific compartments. Each generalized cell has a specific list of parameters like volume, cell types and so on. In the same way can be defined other specific properties like biochemical networks (Swat et al., 2012). CC3D is able to import biochemical pathway written in the SBML format too and integrate them in the models so to simulate intricate intra and extracellular biochemical reactions.

CHASTE (Cancer, Heart and Soft Tissue Environment) is a simulator that can be used, in a general way, to build and run multi-scale models of tissue with the capabilities of testing the electrophysiological properties. The two main targets are the creation of heart and cancer models but the simulator is flexible enough to permit the creation of many different types of tissues. The program is able to integrate in the simulation the data for biochemical and signaling pathways too. The main language to build the model is C++ but it can be also used the XML approach trough the CellML implementation (Pitt-Francis et al., 2009; Mirams et al., 2013). CHASTE has been used to model a single cortical neuron with realistic electrophysiological properties (Agudelo-Toro and Neef, 2013).

VIRTUAL CELL is a computational tool that permits the construction of complex spatial models of biological processes. All the molecules are simulated within specific compartments, which are geometrically defined and act as boundaries for the reactions (Loew and Schaff, 2001). Inside each compartment can be defined the initial conditions, speed of the reactions and diffusion protocols and, based on these data, the simulator can provide information about time responses, steady state and so on. The simulation environment is able to simulate the Ca^{2+} dynamics in a neuronal cell and has been used to simulate the interaction of many components of the intra cellular Ca^{2+} dynamics in the cerebellar ataxia (Brown et al., 2015).

CYTOSCAPE is a software platform for visualizing molecular interaction networks and integrating with the gene expression data (Shannon, 2003; Cline et al., 2007).

MCELL (Monte Carlo Cell) is a software to simulate biological reaction-diffusion systems that is able to reproduce 3D realistic cellular models in which the movement of the molecules and their reactions are computed with the Monte Carlo algorithms (Stiles and Bartol, 2001; Kerr et al., 2008).

Table 10. Tools.

	Biophysical simulators (IF-HH)		Morphogenesis simulators		Synaptic simulators
	Neurogenesis simulators		GRN simulators		

Biological process/ simulator	Neuronal differentiation proliferation	Neuronal migration	Axonal dendrite growth	Synapses formation	Single neuron	Neuronal network	Biochemical reactions	
NEURON					x	x		
GENESIS					x	x		
NEST					x	x		
BRIAN2					x	x		
STEPS							x	
MOOSE					x	x	x	
PSICS					x	x	x	
NETMORPH			x	x	x	x		
CX3D	x	x	x	x				
CC3D	x	x					x	
CHASTE	x	x			x		x	
VIRTUAL CELL							x	
CYTOSCAPE							x	
MCELL							x	

Table 10. The table summarizes the tool available to reconstruct models of the different biological processes.

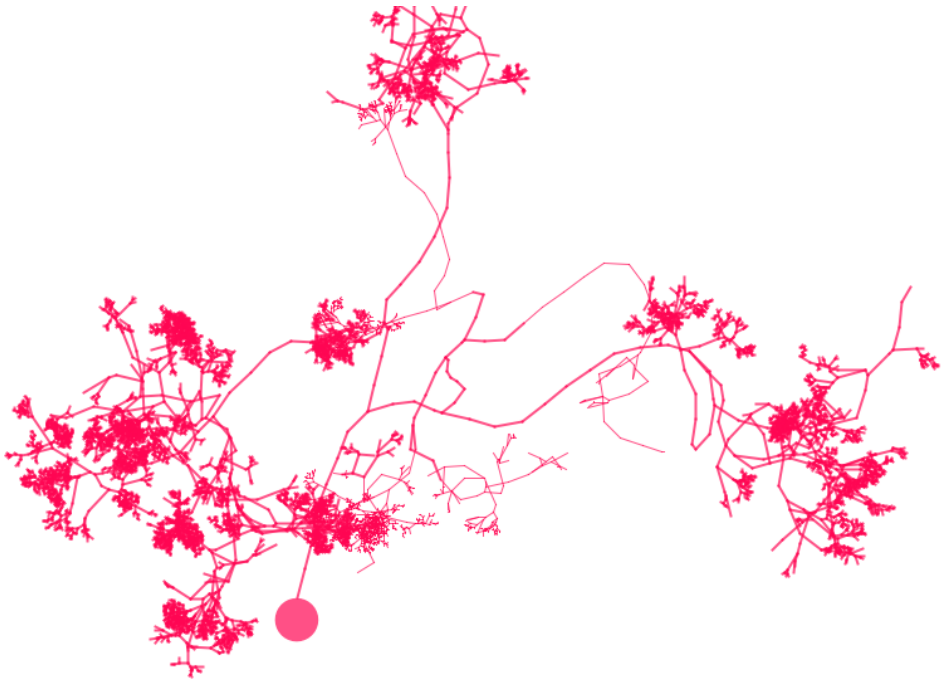

Fig. 37. The figure shows the result of a simulation with CX3D simulator. The simulation reproduces a neurite outgrowth. CX3D implements the model of Kiddie et al. (Kiddie et al., 2005).

4.1.9 Conclusions

The information provided in this review show the actual feasibility of the computational reconstruction of the cerebellar network. However, this approach is limited by three factors: I) The availability of experimental data for each step of the neurogenesis. The difficulty to obtain experimental data is due to technical limitations and to the fact that it is difficult to observe the neurogenesis in animal embryos. II) A tool flexible enough to reproduce the growth connected with the electrical behaviors of the neurons. The cerebellum requires a specific approach, since its shows critical morphological characteristics, particular connectivity rules resulting in electrical behaviors and network activity. The most common tools are designed to reproduce only the electrical activity, a few consider the neuronal morphogenesis and actually, there is not a tool capable to reproduce both processes. III) The definition of a large scale 3D environment filled, not only by neurons, but glial, vascular and ECM too.

Appendix

1. Review: “Modeling the Cerebellar Microcircuit: New strategies for a Long-Standing Issue”. Egidio D’Angelo, Alberto Antonietti, Stefano Casali, Claudia Casellato, Jesus A. Garrido, Niceto Rafael Luque, Lisa Mapelli, Stefano Masoli, Alessandra Pedrocchi, Francesca Prestori, **Martina Francesca Rizza**, and Eduardo Ros. Frontiers in Cellular Neuroscience, 2016 (D’Angelo et al., 2016).

2. Book Chapter: “Single-Neuron and Network Computation in Realistic Models of the Cerebellar Cortex” of the book: “The neuronal codes of the cerebellum”. Egidio D’Angelo, Stefano Masoli, **Martina Francesca Rizza**, Stefano Casali. Elsevier, 2016 (D’Angelo et al., 2016).

3. Paper: “Single Neuron Optimization as a Basis for Accurate Biophysical Modelling: the Case of Cerebellar Granule Cells”. Stefano Masoli, **Martina Francesca Rizza**, Martina Sgritta, Werner Van Geit, Felix Schürmann, Egidio D’Angelo. Frontiers in Cellular Neuroscience, 2016 (Masoli et al., 2017).

References

Abbott, L. (1999). Lapicque's introduction of the integrate-and-fire model neuron (1907). *Brain Research Bulletin*, *50*(5–6), 303–304. http://doi.org/10.1016/S0361-9230 (99)00161-6

Agudelo-Toro, A., & Neef, A. (2013). Computationally efficient simulation of electrical activity at cell membranes interacting with self-generated and externally imposed electric fields. *Journal of Neural Engineering*, *10*(2), 26019. http://doi.org/10.1088/1741-2560/10/2/026019

Akemann, W., & Knöpfel, T. (2006). Interaction of Kv3 potassium channels and resurgent sodium current influences the rate of spontaneous firing of Purkinje neurons. *The Journal of Neuroscience : The Official Journal of the Society for Neuroscience*, *26*(17), 4602–12. http://doi.org/10.1523/JNEUROSCI.5204-05.2006

Albus, J. S. (1971). A Theory of Cerebellar Function. *Mathematical Biosciences*, *10*(1/2), 25–61.

Alcami, P., & Marty, A. (2013). Estimating functional connectivity in an electrically coupled interneuron network. *Proceedings of the National Academy of Sciences*, *110*(49), E4798–E4807. http://doi.org/10.1073/pnas.1310983110

Altman, J., & Bayer, S. A. (1997). *Development of the Cerebellar System in Relation to its Evolution, Structure and Function.* (CRC Press). Boca Raton.

Anderson, D., Engbers, J. D. T., Heath, N. C., Bartoletti, T. M., Mehaffey, W. H., Zamponi, G. W., & Turner, R. W. (2013). The Cav3-Kv4 complex acts as a calcium sensor to maintain inhibitory charge transfer during extracellular calcium fluctuations. *The Journal of Neuroscience : The Official Journal of the Society for Neuroscience*, *33*(18), 7811–24. http://doi.org/10.1523/JNEUROSCI.5384-12.2013

Angelo, K., London, M., Christensen, S. R., & Hausser, M. (2007). Local and Global Effects of Ih Distribution in Dendrites of Mammalian Neurons. *Journal of Neuroscience*, *27*(32), 8643–8653. http://doi.org/10.1523/JNEUROSCI.5284-06.2007

Ankri, L., Husson, Z., Pietrajtis, K., Proville, R., Léna, C., Yarom, Y., Uusisaari, M. Y. (2015). A novel inhibitory nucleo-cortical circuit controls cerebellar Golgi cell activity. *eLife*, *4*, 1–26. http://doi.org/10.7554/eLife.06262

Anwar, H., Hong, S., & De Schutter, E. (2012). Controlling Ca2+-activated K+ channels with models of Ca2+ buffering in Purkinje cells. *Cerebellum (London, England)*, *11*(3), 681–93. http://doi.org/10.1007/s12311-010-0224-3

Armstrong, C. M. (1992). Voltage-dependent ion channels and their gating. *Physiol. Rev.* 72, S5–S13.

Armstrong, C. M., and Hille, B. (1998). Voltage-gated ion channels and electrical excitability. *Neuron* 20, 371–380. doi:10.1016/S0896-6273(00)80981-2.

Ascoli, G. A., Donohue, D. E., & Halavi, M. (2007). NeuroMorpho.Org: A Central Resource for Neuronal Morphologies. *Journal of Neuroscience*, *27*(35), 9247–9251. http://doi.org/10.1523/JNEUROSCI.2055-07.2007

Ashbourn, J. M. A., Miller, J. J., Reumers, V., Baekelandt, V., & Geris, L. (2012). A mathematical model of adult subventricular neurogenesis. *Journal of the Royal Society Interface*, *9*(75), 2414–2423. http://doi.org/10.1098/rsif.2012.0193

Baizer, J. S., Wong, K. M., Paolone, N. A., Weinstock, N., Salvi, R. J., Manohar, S., … Hof, P. R. (2014). Laminar and neurochemical organization of the dorsal cochlear nucleus of the human, monkey, cat, and rodents. *Anatomical Record (Hoboken, N.J. : 2007)*, *297*(10), 1865–84. http://doi.org/10.1002/ar.23000

Barbour, B. (2001). An Evaluation of Synapse Independence. 20, 7969–7984

Barranca, V. J., Johnson, D. C., Moyher, J. L., Sauppe, J. P., Shkarayev, M. S., Kovačič, G., & Cai, D. (2014). Dynamics of the exponential integrate-and-fire model with slow currents and adaptation. *Journal of Computational Neuroscience*, *37*(1), 161–180. http://doi.org/10.1007/s10827-013-0494-0

Barry, D. S., Pakan, J. M. P., & McDermott, K. W. (2014). Radial glial cells: key organisers in CNS development. *The International Journal of Biochemistry & Cell Biology*, *46*, 76–9. http://doi.org/10.1016/j.biocel.2013.11.013

Bastianelli, E. (2003). Distribution of calcium-binding proteins in the cerebellum. *Cerebellum (London, England)*, *2*(4), 242–62. http://doi.org/10.1080/14734220310022289

Beierlein, M., & Regehr, W. G. (2006). Local interneurons regulate synaptic strength by retrograde release of endocannabinoids. *The Journal of Neuroscience : The Official Journal of the Society for Neuroscience*, *26*(39), 9935–43. http://doi.org/10.1523/JNEUROSCI.0958-06.2006

Ben-Arie, N., Bellen, H. J., Armstrong, D. L., McCall, A. E., Gordadze, P. R., Guo, Q., … Zoghbi, H. Y. (1997). Math1 is essential for genesis of cerebellar granule neurons. *Nature*, *390*(6656), 169–72. http://doi.org/10.1038/36579

Bender, K. J., & Trussell, L. O. (2009). Axon initial segment Ca2+ channels influence action potential generation and timing. *Neuron*, *61*(2), 259–71. http://doi.org/10.1016/j.neuron.2008.12.004

Bernot, G., Comet, J.-P., Richard, A., Chaves, M., Gouzé, J.-L., & Dayan, F. (2013). Modeling and Analysis of Gene Regulatory Networks. In *Modeling in Computational Biology and Biomedicine*.

Bezzi, M., Nieus, T., J.-M. Coenen, O., & D'Angelo, E. (2004). An integrate-and-fire model of a cerebellar granule cell. *Neurocomputing*, *58–60*, 593–598. http://doi.org/10.1016/j.neucom.2004.01.100

Bialek, W., and Rieke, F. (1992). Reliability and information transmission in spiking neurons. *Trends Neurosci.* 15, 428–434. doi:10.1016/0166-2236(92)90005-S

Bloch-Gallego, E., Ezan, F., Tessier-Lavigne, M., & Sotelo, C. (1999). Floor plate and netrin-1 are involved in the migration and survival of inferior olivary neurons. *The Journal of Neuroscience : The Official Journal of the Society for Neuroscience*, *19*(11), 4407–4420.

Borisyuk, R., Cooke, T., & Roberts, A. (2008). Stochasticity and functionality of neural systems: Mathematical modelling of axon growth in the spinal cord of tadpole. *Biosystems*, *93*(1–2), 101–114. http://doi.org/10.1016/j.biosystems.2008.03.012

Bower, J. M., & Beeman, D. (2003). *The Book of GENESIS: Exploring Realistic Neural Models with the GEneral NEural SImulation System* (Internet E).

Bower, J. M. (2015). The 40-year history of modeling active dendrites in cerebellar Purkinje cells: emergence of the first single cell "community model". *Frontiers in Computational Neuroscience*, *9*(October), 129. http://doi.org/10.3389/fncom.2015.00129

Bower, J. M. (2013). Computational Structure of the Cerebellar Molecular Layer. In *Handbook of the Cerebellum and Cerebellar Disorders* (pp. 1359–1380). Dordrecht: Springer Netherlands. http://doi.org/10.1007/978-94-007-1333-8_60

Brette, R., Rudolph, M., Carnevale, T., Hines, M., Beeman, D., Bower, J. M., … Destexhe, A. (2007). Simulation of networks of spiking neurons: A review of tools and strategies. *Journal of Computational Neuroscience*, *23*(3), 349–398. http://doi.org/10.1007/s10827-007-0038-6

Brette, R., Rudolph, M., Carnevale, T., Hines, M., Beeman, D., Bower, J. M., Destexhe, A. (2007). Simulation of networks of spiking neurons: A review of tools and strategies. *Journal of Computational Neuroscience*, *23*(3), 349–398. http://doi.org/10.1007/s10827-007-0038-6

Brooke, R. E., Atkinson, L., Edwards, I., Parson, S. H., & Deuchars, J. (2006). Immunohistochemical localisation of the voltage gated potassium ion channel subunit Kv3.3 in the rat medulla oblongata and thoracic spinal cord. *Brain Research*, *1070*(1), 101–15. http://doi.org/10.1016/j.brainres.2005.10.102

Brown, D. A., & Passmore, G. M. (2009). Neural KCNQ (Kv7) channels. *British Journal of Pharmacology*, *156*(8), 1185–95. http://doi.org/10.1111/j.1476-5381.2009.00111.x

Brown, S.-A., McCullough, L. D., & Loew, L. M. (2015). Computational neurobiology is a useful tool in translational neurology: the example of ataxia. *Frontiers in Neuroscience*, *9*. http://doi.org/10.3389/fnins.2015.00001

Brown, T. H., Kairiss, E. W., & Keenan, C. L. (1990). Hebbian synapses: biophysical mechanisms and algorithms. *Annual Review of Neuroscience*, *13*, 475–511. http://doi.org/10.1146/annurev.neuro.13.1.475

Bruederle, D., Müller, E., Davison, A., Muller, E., Schemmel, J., & Meier, K. (2009). Establishing a Novel Modeling Tool: A Python-based Interface for a Neuromorphic Hardware System. *Frontiers in Neuroinformatics*, *3*. http://doi.org/10.3389/neuro.11.017.2009

Brunel, N., & van Rossum, M. C. W. (2007). Lapicque's 1907 paper: from frogs to integrate-and-fire. *Biological Cybernetics*, *97*(5–6), 337–9. http://doi.org/10.1007/s00422-007-0190-0

Brunel, N., & van Rossum, M. C. W. (2007). Lapicque's 1907 paper: from frogs to integrate-and-fire. *Biological Cybernetics*, *97*(5–6), 337–339. http://doi.org/10.1007/s00422-007-0190-0

Buffo, A., & Rossi, F. (2013). Origin, lineage and function of cerebellar glia. *Progress in Neurobiology*, *109*, 42–63. http://doi.org/10.1016/j.pneurobio.2013.08.001

Burkitt, A. N. (2006). A review of the integrate-and-fire neuron model: II. Inhomogeneous synaptic input and network properties. *Biological Cybernetics*, *95*(2), 97–112. http://doi.org/10.1007/s00422-006-0082-8

Cain, S. M., & Snutch, T. P. (n.d.). Contributions of T-type calcium channel isoforms to neuronal firing. *Channels (Austin, Tex.)*, *4*(6), 475–82. http://doi.org/10.4161/chan.4.6.14106

Cajal, S. R. (1911). *Histologie du Système Nerveux de l'Homme et des Vertébrés, vol. II.* (A. Maloine). Paris.

Cannon, R. C., O'Donnell, C., & Nolan, M. F. (2010). Stochastic ion channel gating in dendritic neurons: Morphology dependence and probabilistic synaptic activation of dendritic spikes. *PLoS Computational Biology*, *6*(8). http://doi.org/10.1371/journal.pcbi.1000886

Carletti, B., & Rossi, F. (2008). Neurogenesis in the cerebellum. *The Neuroscientist : A Review Journal Bringing Neurobiology, Neurology and Psychiatry*, *14*(1), 91–100. http://doi.org/10.1177/1073858407304629

Carnevale, N. T., & Hines, M. L. (2006). *The NEURON Book*. Cambridge: Cambridge University Press. http://doi.org/10.1017/CBO9780511541612

Carter, A. G., & Regehr, W. G. (2002). Quantal events shape cerebellar interneuron firing. *Nature Neuroscience*, *5*(12), 1309–1318. http://doi.org/10.1038/nn970

Carter, A. G., & Regher, W. G. (2000). Prolonged Synaptic Currents and Glutamate Spillover at the Parallel Fiber to Stellate Cell Synapse. *The Journal of Neuroscience*, *20*(12), 4423–4434.

Casellato, C., Antonietti, A., Garrido, J. A., Carrillo, R. R., Luque, N. R., Ros, E., … D'Angelo, E. (2014). Adaptive Robotic Control Driven by a Versatile Spiking Cerebellar Network. *PLoS ONE*, *9*(11), e112265. http://doi.org/10.1371/journal.pone.0112265

Causeret, F., Danne, F., Ezan, F., Sotelo, C., & Bloch-Gallego, E. (2002). Slit antagonizes netrin-1 attractive effects during the migration of inferior olivary neurons. *Developmental Biology*, *246*(2), 429–40. http://doi.org/10.1006/dbio.2002.0681

Cerminara, N. L., Lang, E. J., Sillitoe, R. V., & Apps, R. (2015). Redefining the cerebellar cortex as an assembly of non-uniform Purkinje cell microcircuits. *Nature Reviews Neuroscience*, *16*(2), 79–93. http://doi.org/10.1038/nrn3886

Chilton, J. K. (2006). Molecular mechanisms of axon guidance. *Developmental Biology*, *292*(1), 13–24. http://doi.org/10.1016/j.ydbio.2005.12.048

Chizhikov, V. V. (2013). Roof Plate in Cerebellar Neurogenesis. In *Handbook of the Cerebellum and Cerebellar Disorders*. http://doi.org/10.1007/978-94-007-1333-8_4

Choi, S., Yu, E., Kim, D., Urbano, F. J., Makarenko, V., Shin, H.-S., & Llinás, R. R. (2010). Subthreshold membrane potential oscillations in inferior olive neurons are dynamically regulated by P/Q- and T-type calcium channels: a study in mutant mice. *The Journal of Physiology*, *588*(Pt 16), 3031–43. http://doi.org/10.1113/jphysiol.2009.184705

Cline, M. S., Smoot, M., Cerami, E., Kuchinsky, A., Landys, N., Workman, C., Bader, G. D. (2007). Integration of biological networks and gene expression data using Cytoscape. *Nature Protocols*, *2*(10), 2366–82. http://doi.org/10.1038/nprot.2007.324

Collin, T., Chat, M., Lucas, M. G., Moreno, H., Racay, P., Schwaller, B., Llano, I. (2005). Developmental changes in parvalbumin regulate presynaptic Ca2+ signaling. *The Journal of Neuroscience : The Official Journal of the Society for Neuroscience*, *25*(1), 96–107. http://doi.org/10.1523/JNEUROSCI.3748-04.2005

Dahmane, N., & Ruiz i Altaba, A. (1999). Sonic hedgehog regulates the growth and patterning of the cerebellum. *Development (Cambridge, England)*, *126*(14), 3089–100.

D'Angelo, E., Nieus, T., Maffei, A., Armano, S., Rossi, P., Taglietti, V., Naldi, G. (2001). Theta-frequency bursting and resonance in cerebellar granule cells: experimental evidence and modeling of a slow k+-dependent mechanism. *The Journal of Neuroscience : The Official Journal of the Society for Neuroscience*, *21*(3), 759–70.

D'Angelo, E., Solinas, S., Garrido, J., Casellato, C., Pedrocchi, A., Mapelli, J., Prestori, F. (2013). Realistic modeling of neurons and networks: towards brain simulation. *Functional Neurology*, *28*(3), 153–66.

D'Angelo, E., Antonietti, A., Casali, S., Casellato, C., Garrido, J. A., Luque, N. R., et al. (2016a). Modeling the Cerebellar Microcircuit: New Strategies for a Long-Standing Issue. *Front. Cell. Neurosci.* 10, 176. doi:10.3389/fncel.2016.00176.

D'Angelo, E., Masoli, S., Rizza, M., and Casali, S. (2016b). *Single-Neuron and Network Computation in Realistic Models of the Cerebellar Cortex*. Elsevier Inc. doi:10.1016/B978-0-12-801386-1.00011-3.

De Gruijl, J. R., Bazzigaluppi, P., de Jeu, M. T. G., & De Zeeuw, C. I. (2012). Climbing fiber burst size and olivary sub-threshold oscillations in a network setting. *PLoS Computational Biology*, *8*(12), e1002814. http://doi.org/10.1371/journal.pcbi.1002814

De Matteis, G., Graudenzi, A., & Antoniotti, M. (2013). A review of spatial computational models for multi-cellular systems, with regard to intestinal crypts and colorectal cancer development. *Journal of Mathematical Biology*, *66*(7), 1409–62. http://doi.org/10.1007/s00285-012-0539-4

De Schutter, E., & Bower, J. M. (1994). An active membrane model of the cerebellar Purkinje cell. I. Simulation of current clamps in slice. *Journal of Neurophysiology*, *71*(1), 375–400.

De Schutter, E., & Bower, J. M. (1994). Simulated responses of cerebellar Purkinje cells are independent of the dendritic location of granule cell synaptic inputs. *Proceedings of the National Academy of Sciences of the United States of America*, *91*(11), 4736–40.

Deb, K., Pratap, A., Agarwal, S., and Meyarivan, T. (2002). A fast and elitist multiobjective genetic algorithm: NSGA-II. *IEEE Trans. Evol. Comput.* 6, 182–197. doi:10.1109/4235.996017

Del Giudice, P., Fusi, S., & Mattia, M. (2003). Modelling the formation of working memory with networks of integrate-and-fire neurons connected by plastic synapses. *Journal of Physiology Paris*, *97*(4–6), 659–681. http://doi.org/10.1016/j.jphysparis.2004.01.021

Destexhe, A., Mainen, Z. F., & Sejnowski, T. J. (1994). An Efficient Method for Computing Synaptic Conductances Based on a Kinetic Model of Receptor Binding. *Neural Computation*, *6*(1), 14–18. http://doi.org/10.1162/neco.1994.6.1.14

Destexhe, A., Mainen, Z., & Sejnowski, T. (1998). Kinetic models of synaptic transmission. In C. Koch & I. Segev (Eds.), *Methods in neuronal modeling* (MIT Press,).

Devor, A., Fritschy, J. M., & Yarom, Y. (2001). Spatial distribution and subunit composition of GABA(A) receptors in the inferior olivary nucleus. *Journal of Neurophysiology*, *85*(4), 1686–96.

Devor, A., & Yarom, Y. (2002). Electrotonic coupling in the inferior olivary nucleus revealed by simultaneous double patch recordings. *Journal of Neurophysiology*, *87*(6), 3048–58.

Dickson, B. J. (2002). Molecular mechanisms of axon guidance. *Science (New York, N.Y.)*, *298*(5600), 1959–64. http://doi.org/10.1126/science.1072165

Diehl, S., Henningsson, E., & Heyden, A. (2016). Efficient simulations of tubulin-driven axonal growth. *Journal of Computational Neuroscience*. http://doi.org/10.1007/s10827-016-0604-x

Diesmann, M., & Gewaltig, M.-O. (2002). NEST: An environment for neural systems simulations. *In T. Plesser and V. Macho (Eds.), Forschung Und Wisschenschaftliches Rechnen, Beitrage Zum Heinz-Billing-Preis 2001, Volume 58 of GWDG-Bericht*, 43–70.

Diwakar, S., Magistretti, J., Goldfarb, M., Naldi, G., & D'Angelo, E. (2009). Axonal Na+ channels ensure fast spike activation and back-propagation in cerebellar granule cells. *Journal of Neurophysiology*, *101*(2), 519–32. http://doi.org/10.1152/jn.90382.2008

Druckmann, S. (2007). A novel multiple objective optimization framework for constraining conductance-based neuron models by experimental data. *Frontiers in Neuroscience*, *1*(1), 7–18. http://doi.org/10.3389/neuro.01.1.1.001.2007

Druckmann, S., Berger, T. K., Hill, S., Schürmann, F., Markram, H., & Segev, I. (2008). Evaluating automated parameter constraining procedures of neuron models by experimental and

surrogate data. *Biological Cybernetics*, *99*(4–5), 371–379. http://doi.org/10.1007/s00422-008-0269-2

Druckmann, S., Berger, T. K., Schürmann, F., Hill, S., Markram, H., & Segev, I. (2011). Effective Stimuli for Constructing Reliable Neuron Models. *PLoS Computational Biology*, *7*(8), e1002133. http://doi.org/10.1371/journal.pcbi.1002133

Eccles, J. C. (1967). Circuits in the cerebellar control of movement. *Proceedings of the National Academy of Sciences of the United States of America*, *58*(1), 336–343. http://doi.org/10.1073/pnas.58.1.336

Eccles, J. C. (1973). The cerebellum as a computer: patterns in space and time. *The Journal of Physiology*, *229*(1), 1–32.

Eccles, J. C., Sabah, N. H., Schmidt, R. F., & Taborikova, H. (1972). Mode of operation of the cerebellum in the dynamic loop control of movement, *40*, 73–80.

Eppler, J. M., Helias, M., Muller, E., Diesmann, M., & Gewaltig, M.-O. (2008). PyNEST: A convenient interface to the NEST simulator. *Frontiers in Neuroinformatics*, *2*. http://doi.org/10.3389/neuro.11.012.2008

Eyre, M. D., & Nusser, Z. (2016). Only a Minority of the Inhibitory Inputs to Cerebellar Golgi Cells Originates from Local GABAergic Cells. *eNeuro*, *3*(3). http://doi.org/10.1523/ENEURO.0055-16.2016

Fan, W.-J., Li, X., Yao, H.-L., Deng, J.-X., Liu, H.-L., Cui, Z.-J., Deng, J.-B. (2016). Neural differentiation and synaptogenesis in retinal development. *Neural Regeneration Research*, *11*(2), 312–8. http://doi.org/10.4103/1673-5374.177743

Fortier, P. A. (2010). Detecting and estimating rectification of gap junction conductance based on simulations of dual-cell recordings from a pair and a network of coupled cells. *Journal of Theoretical Biology*, *265*(2), 104–114. http://doi.org/10.1016/j.jtbi.2010.03.048

Fujita, H., Aoki, H., Ajioka, I., Yamazaki, M., Abe, M., Oh-Nishi, A., Sugihara, I. (2014). Detailed expression pattern of aldolase C (Aldoc) in the cerebellum, retina and other areas of the CNS studied in Aldoc-Venus knock-in mice. *PloS One*, *9*(1), e86679. http://doi.org/10.1371/journal.pone.0086679

Galarreta, M., & Hestrin, S. (2001). Electrical synapses between Gaba-Releasing interneurons. *Nature Reviews Neuroscience*, *2*(6), 425–433. http://doi.org/10.1038/35077566

Galiano, M. R., Jha, S., Ho, T. S.-Y., Zhang, C., Ogawa, Y., Chang, K.-J., Rasband, M. N. (2012). A distal axonal cytoskeleton forms an intra-axonal boundary that controls axon initial segment assembly. *Cell*, *149*(5), 1125–39. http://doi.org/10.1016/j.cell.2012.03.039

Galle, J., Sittig, D., Hanisch, I., Wobus, M., Wandel, E., Loeffler, M., & Aust, G. (2006). Individual Cell-Based Models of Tumor-Environment Interactions. *The American Journal of Pathology*, *169*(5), 1802–1811. http://doi.org/10.2353/ajpath.2006.060006

Galluppi, F., Lagorce, X., Stromatias, E., Pfeiffer, M., Plana, L. A., Furber, S. B., & Benosman, R. B. (2015). A framework for plasticity implementation on the SpiNNaker neural architecture. *Frontiers in Neuroscience*, *9*(JAN), 1–20. http://doi.org/10.3389/fnins.2014.00429

Garrido, J. A., Luque, N. R., D'Angelo, E., & Ros, E. (2013). Distributed cerebellar plasticity implements adaptable gain control in a manipulation task: a closed-loop robotic simulation. *Frontiers in Neural Circuits*, *7*, 159. http://doi.org/10.3389/fncir.2013.00159

Garrido, J. A., Ros, E., & D'Angelo, E. (2013). Spike timing regulation on the millisecond scale by distributed synaptic plasticity at the cerebellum input stage: a simulation study. *Frontiers in Computational Neuroscience*, *7*, 64. http://doi.org/10.3389/fncom.2013.00064

Glazier, J. A., & Graner, F. (1993). Simulation of the differential adhesion driven rearrangement of biological cells. *Physical Review E*, *47*(3), 2128–2154. http://doi.org/10.1103/PhysRevE.47.2128

Goldowitz, D., & Hamre, K. (1998). The cells and molecules that make a cerebellum. *Trends in Neurosciences*, *21*(9), 375–82.

Gomez, T. M., & Zheng, J. Q. (2006). The molecular basis for calcium-dependent axon pathfinding. *Nature Reviews. Neuroscience*, *7*(2), 115–25. http://doi.org/10.1038/nrn1844

Goodhill, G. J. (1998). Mathematical guidance for axons. *Trends in Neurosciences*, *21*(6), 226–231. http://doi.org/10.1016/S0166-2236 (97)01203-4

Goodhill, G. J., Gu, M., & Urbach, J. S. (2004). Predicting Axonal Response to Molecular Gradients with a Computational Model of Filopodial Dynamics. *Neural Computation*, *16*(11), 2221–2243. http://doi.org/10.1162/0899766041941934

Goodman, D., & Brette, R. (2008). Brian: a simulator for spiking neural networks in python. *Frontiers in Neuroinformatics*, *2*(November), 5. http://doi.org/10.3389/neuro.11.005.2008

Gosui, M., & Yamazaki, T. (2016). Real-World-Time Simulation of Memory Consolidation in a Large-Scale Cerebellar Model. *Frontiers in Neuroanatomy*, *10*, 21. http://doi.org/10.3389/fnana.2016.00021

Graham, B. P., Lauchlan, K., & Mclean, D. R. (2006). Dynamics of outgrowth in a continuum model of neurite elongation. *J COMPUT NEUROSCI*.

Graham, B. P., & van Ooyen, A. (2006). Mathematical modelling and numerical simulation of the morphological development of neurons. *BMC Neuroscience*, *7 Suppl 1*, S9. http://doi.org/10.1186/1471-2202-7-S1-S9

Graham, B. P., & van Ooyen, A. (2004). Transport limited effects in a model of dendritic branching. *Journal of Theoretical Biology*, *230*(3), 421–32. http://doi.org/10.1016/j.jtbi.2004.06.007

Graudenzi, A., Caravagna, G., De Matteis, G., & Antoniotti, M. (2014). Investigating the Relation between Stochastic Differentiation, Homeostasis and Clonal Expansion in Intestinal Crypts via Multiscale Modeling. *PLoS ONE*, *9*(5), e97272. http://doi.org/10.1371/journal.pone.0097272

Guo, C., Witter, L., Rudolph, S., Elliott, H. L., Ennis, K. A., & Regehr, W. G. (2016). Purkinje Cells Directly Inhibit Granule Cells in Specialized Regions of the Cerebellar Cortex. *Neuron*, *91*(6), 1330–41. http://doi.org/10.1016/j.neuron.2016.08.011

Gutfreund, Y., Yarom, Y., & Segev, I. (1995). Subthreshold oscillations and resonant frequency in guinea-pig cortical neurons: physiology and modelling. *The Journal of Physiology*, *483 (Pt 3*, 621–40.

Gymnopoulos, M., Cingolani, L. A., Pedarzani, P., & Stocker, M. (2014). Developmental mapping of small-conductance calcium-activated potassium channel expression in the rat nervous system. *Journal of Comparative Neurology*, *522*(5), 1072–1101. http://doi.org/10.1002/cne.23466

Halavi, M., Polavaram, S., Donohue, D. E., Hamilton, G., Hoyt, J., Smith, K. P., & Ascoli, G. A. (2008). NeuroMorpho.Org Implementation of Digital Neuroscience: Dense Coverage and Integration with the NIF. *Neuroinformatics*, *6*(3), 241–252. http://doi.org/10.1007/s12021-008-9030-1

Harris, J., Moreno, S., Shaw, G., & Mugnaini, E. (1993). Unusual neurofilament composition in cerebellar unipolar brush neurons. *Journal of Neurocytology*, *22*(12), 1039–59.

Hatten, M. E., Alder, J., Zimmerman, K., & Heintz, N. (1997). Genes involved in cerebellar cell specification and differentiation. *Current Opinion in Neurobiology*, *7*(1), 40–7.

Häusser, M., & Clark, B. A. (1997). Tonic synaptic inhibition modulates neuronal output pattern and spatiotemporal synaptic integration. *Neuron*, *19*(3), 665–78.

Hay, E., Hill, S., Schürmann, F., Markram, H., & Segev, I. (2011). Models of Neocortical Layer 5b Pyramidal Cells Capturing a Wide Range of Dendritic and Perisomatic Active Properties. *PLoS Computational Biology*, *7*(7), e1002107. http://doi.org/10.1371/journal.pcbi.1002107

He, C., Chen, F., Li, B., & Hu, Z. (2014). Neurophysiology of HCN channels: From cellular functions to multiple regulations. *Progress in Neurobiology*, *112*, 1–23. http://doi.org/10.1016/j.pneurobio.2013.10.001

Hebb, D. O. (2002). *The Organization of Behavior: A Neuropsychological Theory* (New Ed). Psychology Press.

Helias, M., Kunkel, S., Masumoto, G., Igarashi, J., Eppler, J. M., Ishii, S., Diesmann, M. (2012). Supercomputers Ready for Use as Discovery Machines for Neuroscience. *Frontiers in Neuroinformatics*, *6*. http://doi.org/10.3389/fninf.2012.00026

Henley, J., & Poo, M. (2004). Guiding neuronal growth cones using Ca2+ signals. *Trends in Cell Biology*, *14*(6), 320–30. http://doi.org/10.1016/j.tcb.2004.04.006

Hentschel, H. G. E., Samuels, D., & Fine, A. (1998). Instabilities during the dendritic and axonal development of neuronal form. *Physica A: Statistical Mechanics and Its Applications*, *254*(1–2), 46–61. http://doi.org/10.1016/S0378-4371 (98)00011-9

Hepburn, I., Chen, W., Wils, S., & De Schutter, E. (2012). STEPS: efficient simulation of stochastic reaction–diffusion models in realistic morphologies. *BMC Systems Biology*, *6*(1), 36. http://doi.org/10.1186/1752-0509-6-36

Herculano-Houzel, S. (2010). Coordinated scaling of cortical and cerebellar numbers of neurons. *Frontiers in Neuroanatomy*, *4*(March), 12. http://doi.org/10.3389/fnana.2010.00012

Hines, M. L., & Carnevale, N. T. (2001). NEURON : A Tool for Neuroscientists. *The Neuroscientis*, *7*(2), 123–135.

Hines, M. L., & Carnevale, N. T. (2008). Translating network models to parallel hardware in NEURON. *Journal of Neuroscience Methods*, *169*(2), 425–55. http://doi.org/10.1016/j.jneumeth.2007.09.010

Hines, M. (2009). NEURON and Python. *Frontiers in Neuroinformatics*, *3*. http://doi.org/10.3389/neuro.11.001.2009

Hines, M. L., Eichner, H., & Schürmann, F. (2008). Neuron splitting in compute-bound parallel network simulations enables runtime scaling with twice as many processors. *Journal of Computational Neuroscience*, *25*(1), 203–210. http://doi.org/10.1007/s10827-007-0073-3

Hines, M. L., Morse, T. M., & Carnevale, N. T. (2007). Model Structure Analysis in NEURON (pp. 91–102). http://doi.org/10.1007/978-1-59745-520-6_6

Hines, M., Markram, H., & Schuermann, F. (2007). Fully implicit parallel simulation of single neurons. *BMC Neuroscience*, *8*(Suppl 2), P6. http://doi.org/10.1186/1471-2202-8-S2-P6

Hodgkin, A., & Huxley, A. (1952). A Quantitative Description of Membrane Current and Its Application To Conduction and Excitation in Nerve. *Journal of Physiology*, *117*, 500–544.

Hölldobler, B., & Wilson, E. O. (2008). *The Superorganism*. W. W. Norton & Company.

Holtzman, T., Rajapaksa, T., Mostofi, A., & Edgley, S. A. (2006). Different responses of rat cerebellar Purkinje cells and Golgi cells evoked by widespread convergent sensory inputs. *The Journal of Physiology*, *574*(2), 491–507. http://doi.org/10.1113/jphysiol.2006.108282

Hourez, R., Servais, L., Orduz, D., Gall, D., Millard, I., de Kerchove d'Exaerde, A., Schiffmann, S. N. (2011). Aminopyridines correct early dysfunction and delay neurodegeneration in a mouse model of spinocerebellar ataxia type 1. *The Journal of Neuroscience : The Official Journal of the Society for Neuroscience*, *31*(33), 11795–807. http://doi.org/10.1523/JNEUROSCI.0905-11.2011

Huguenard, J. R., & McCormick, D. A. (1992). Simulation of the currents involved in rhythmic oscillations in thalamic relay neurons. *Journal of Neurophysiology*, *68*(4), 1373–83.

Hull, C., & Regehr, W. G. (2012). Identification of an Inhibitory Circuit that Regulates Cerebellar Golgi Cell Activity. *Neuron*, *73*(1), 149–158. http://doi.org/10.1016/j.neuron.2011.10.030

Ichikawa, R., Sakimura, K., & Watanabe, M. (2016). GluD2 Endows Parallel Fiber-Purkinje Cell Synapses with a High Regenerative Capacity. *Journal of Neuroscience*, *36*(17), 4846–4858. http://doi.org/10.1523/JNEUROSCI.0161-16.2016

Indiveri, G., Linares-Barranco, B., Hamilton, T. J., Schaik, A. van, Etienne-Cummings, R., Delbruck, T., Boahen, K. (2011). Neuromorphic Silicon Neuron Circuits. *Frontiers in Neuroscience*, *5*. http://doi.org/10.3389/fnins.2011.00073

Indiveri, G., Linares-Barranco, B., Hamilton, T. J., Schaik, A. van, Etienne-Cummings, R., Delbruck, T., Boahen, K. (2011). Neuromorphic Silicon Neuron Circuits. *Frontiers in Neuroscience*, *5*. http://doi.org/10.3389/fnins.2011.00073

Ishikawa, Y., Yamamoto, N., Yoshimoto, M., & Ito, H. (2012). The Primary Brain Vesicles Revisited : Are the Three Primary Vesicles (Forebrain / Midbrain / Hindbrain) Universal in Vertebrates ? *2012*, 75–83. http://doi.org/10.1159/000334842

Ito, M. (2008). Control of mental activities by internal models in the cerebellum. *Nature Reviews. Neuroscience*, *9*(4), 304–13. http://doi.org/10.1038/nrn2332

Jacobs, B., Johnson, N. L., Wahl, D., Schall, M., Maseko, B. C., Lewandowski, A., Manger, P. R. (2014). Comparative neuronal morphology of the cerebellar cortex in afrotherians, carnivores, cetartiodactyls, and primates. *Frontiers in Neuroanatomy*, *8*. http://doi.org/10.3389/fnana.2014.00024

Jaeger, D., De Schutter, E., & Bower, J. M. (1997). The role of synaptic and voltage-gated currents in the control of Purkinje cell spiking: a modeling study. *The Journal of Neuroscience : The Official Journal of the Society for Neuroscience*, *17*(1), 91–106.

Jensen, P., Smeyne, R., & Goldowitz, D. (2004). Analysis of cerebellar development in math1 null embryos and chimeras. *The Journal of Neuroscience : The Official Journal of the Society for Neuroscience*, *24*(9), 2202–11. http://doi.org/10.1523/JNEUROSCI.3427-03.2004

Jörntell, H., Bengtsson, F., Schonewille, M., & De Zeeuw, C. I. (2010). Cerebellar molecular layer interneurons – computational properties and roles in learning. *Trends in Neurosciences*, *33*(11), 524–532. http://doi.org/10.1016/j.tins.2010.08.004

Jörntell, H., & Hansel, C. (2006). Synaptic memories upside down: bidirectional plasticity at cerebellar parallel fiber-Purkinje cell synapses. *Neuron*, *52*(2), 227–38. http://doi.org/10.1016/j.neuron.2006.09.032

Kampa, B. M., Clements, J., Jonas, P., and Stuart, G. J. (2004). Kinetics of Mg^{2+} unblock of NMDA receptors: implications for spike-timing dependent synaptic plasticity. *J. Physiol.* 556, 337–345. doi:10.1113/jphysiol.2003.058842

Kandel, E. R. et al. (2013). *Principles of Neural Science*. , ed. M.-H. Medical New York ; Toronto.

Kennedy, J., & Eberhart, R. (n.d.). Particle swarm optimization. In *Proceedings of ICNN'95 - International Conference on Neural Networks* (Vol. 4, pp. 1942–1948). IEEE. http://doi.org/10.1109/ICNN.1995.488968

Kerr, R. A., Bartol, T. M., Kaminsky, B., Dittrich, M., Chang, J.-C. J., Baden, S. B., Stiles, J. R. (2008). FAST MONTE CARLO SIMULATION METHODS FOR BIOLOGICAL REACTION-DIFFUSION SYSTEMS IN SOLUTION AND ON SURFACES. *SIAM Journal on Scientific Computing : A Publication of the Society for Industrial and Applied Mathematics*, *30*(6), 3126. http://doi.org/10.1137/070692017

Khaliq, Z. M., Gouwens, N. W., & Raman, I. M. (2003). The contribution of resurgent sodium current to high frequency firing in Purkinje neurons: an experimental and modeling study. *Journal of Neuroscience*, *23*(12), 4899–4912.

Khavandgar, S., Walter, J. T., Sageser, K., & Khodakhah, K. (2005). Kv1 channels selectively prevent dendritic hyperexcitability in rat Purkinje cells. *The Journal of Physiology*, *569*(2), 545–557. http://doi.org/10.1113/jphysiol.2005.098053

Kiddie, G., McLean, D., Van Ooyen, A., & Graham, B. (2005). Biologically plausible models of neurite outgrowth. *Progress in Brain Research*, *147*(SPEC. ISS.), 67–80. http://doi.org/10.1016/S0079-6123(04)47006-X

Kim, D., & Ackerman, S. L. (2011). The UNC5C netrin receptor regulates dorsal guidance of mouse hindbrain axons. *The Journal of Neuroscience : The Official Journal of the Society for Neuroscience*, *31*(6), 2167–79. http://doi.org/10.1523/JNEUROSCI.5254-10.2011

Kistler, W. M., & De Zeeuw, C. I. (2003). Time windows and reverberating loops: a reverse-engineering approach to cerebellar function. *Cerebellum (London, England)*, *2*(1), 44–54. http://doi.org/10.1080/14734220309426

Kobayashi, T., Terajima, K., Nozumi, M., Igarashi, M., & Akazawa, K. (2010). A stochastic model of neuronal growth cone guidance regulated by multiple sensors. *Journal of Theoretical Biology*, *266*(4), 712–722. http://doi.org/10.1016/j.jtbi.2010.07.036

Koch, C. (1998). *Biophysics of Computation: Information Processing in Single Neurons* (Oxford Uni). New York.

Koene, R. A., Tijms, B., van Hees, P., Postma, F., de Ridder, A., Ramakers, G. J. A., van Ooyen, A. (2009). NETMORPH: A Framework for the Stochastic Generation of Large Scale Neuronal Networks with Realistic Neuron Morphologies. *Neuroinformatics*, *7*(3), 195–210. http://doi.org/10.1007/s12021-009-9052-3

Komuro, Y., K. Fahrion, J., D. Foote, K., Fenner, Kathleen B. Kumada, T., Ohno, N., & Komuro, H. (2013). Granule Cell Migration and Differentiation. In *Handbook of the Cerebellum and Cerebellar Disorders*.

Konur, S., & Ghosh, A. (2005). Calcium signaling and the control of dendritic development. *Neuron*, *46*(3), 401–5. http://doi.org/10.1016/j.neuron.2005.04.022

Kosaka, T. (2005). Structural Organization of the Glomerulus in the Main Olfactory Bulb. *Chemical Senses*, *30*(Supplement 1), i107–i108. http://doi.org/10.1093/chemse/bjh137

Krottje, J. K., & van Ooyen, A. (2007). A mathematical framework for modeling axon guidance. *Bulletin of Mathematical Biology*, *69*(1), 3–31. http://doi.org/10.1007/s11538-006-9142-4

Kumar, V., and Minz, S. (2014). Multi-Objective Particle Swarm Optimization : An Introduction. 4. doi:10.6029/smartcr.2014.05.001

Lang, R. J., Harvey, J. R., McPhee, G. J., & Klemm, M. F. (2000). Nitric oxide and thiol reagent modulation of Ca2+-activated K+ (BKCa) channels in myocytes of the guinea-pig taenia caeci. *The Journal of Physiology*, *525 Pt 2*, 363–76.

Larkum, M. E., Nevian, T., Sandler, M., Polsky, A., & Schiller, J. (2009). Synaptic integration in tuft dendrites of layer 5 pyramidal neurons: a new unifying principle. *Science (New York, N.Y.)*, *325*(5941), 756–60. http://doi.org/10.1126/science.1171958

Larner, A. J. (1997). The cerebellum in Alzheimer's disease. *Dement. Geriatr. Cogn. Disord.* 8, 203–9.

Larouche, M., & Goldowitz, D. (2013). Genes and Cell Type Specification in Cerebellar Development. In *Handbook of the Cerebellum and Cerebellar Disorders* (pp. 301–317). Dordrecht: Springer Netherlands. http://doi.org/10.1007/978-94-007-1333-8_15

Lefaivre, S. C., Brown, M. J. N., and Almeida, Q. J. (2016). Cerebellar involvement in Parkinson's disease resting tremor. *Cerebellum & Ataxias* 3, 13. doi:10.1186/s40673-016-0051-5.

Leffler, S. R., Legué, E., Aristizábal, O., Joyner, A. L., Peskin, C. S., & Turnbull, D. H. (2016). A Mathematical Model of Granule Cell Generation during Mouse Cerebellum Development. *Bulletin of Mathematical Biology*. http://doi.org/10.1007/s11538-016-0163-3

Lennon, W., Hecht-Nielsen, R., & Yamazaki, T. (2014). A spiking network model of cerebellar Purkinje cells and molecular layer interneurons exhibiting irregular firing. *Frontiers in Computational Neuroscience*, *8*. http://doi.org/10.3389/fncom.2014.00157

Leroi, I., O'Hearn, E., Marsh, L., Lyketsos, C. G., Rosenblatt, A., Ross, C. A., Margolis, R. L. (2002). Psychopathology in patients with degenerative cerebellar diseases: a comparison to Huntington's disease. *The American Journal of Psychiatry*, *159*(8), 1306–14. http://doi.org/10.1176/appi.ajp.159.8.1306

Leto, K., Carletti, B., Williams, I. M., Magrassi, L., & Rossi, F. (2006). Different Types of Cerebellar GABAergic Interneurons Originate from a Common Pool of Multipotent Progenitor Cells. *Journal of Neuroscience*, *26*(45), 11682–11694. http://doi.org/10.1523/JNEUROSCI.3656-06.2006

Leto, K., Arancillo, M., Becker, E. B. E., Buffo, A., Chiang, C., Ding, B., Hawkes, R. (2016). Consensus Paper: Cerebellar Development. *Cerebellum (London, England)*, *15*(6), 789–828. http://doi.org/10.1007/s12311-015-0724-2

Li, W.-C., Cooke, T., Sautois, B., Soffe, S. R., Borisyuk, R., & Roberts, A. (2007). Axon and dendrite geography predict the specificity of synaptic connections in a functioning spinal cord network. *Neural Development*, *2*, 17. http://doi.org/10.1186/1749-8104-2-17

Li, W.-K., Hausknecht, M. J., Stone, P., & Mauk, M. D. (2013). Using a million cell simulation of the cerebellum: Network scaling and task generality. *Neural Networks*, *47*, 95–102. http://doi.org/10.1016/j.neunet.2012.11.005

Liu, Y., Savtchouk, I., Acharjee, S., & Liu, S. J. (2011). Inhibition of Ca2+-activated large-conductance K+ channel activity alters synaptic AMPA receptor phenotype in mouse cerebellar stellate cells. *Journal of Neurophysiology*, *106*(1), 144–52. http://doi.org/10.1152/jn.01107.2010

Llinas, R. (1988). The intrinsic electrophysiological properties of mammalian neurons: insights into central nervous system function. *Science*, *242*(4886), 1654–1664. http://doi.org/10.1126/science.3059497

Loew, L. M., & Schaff, J. C. (2001). The Virtual Cell: a software environment for computational cell biology. *Trends in Biotechnology*, *19*(10), 401–6. http://doi.org/10.1016/S0167-7799(01)01740-1

Loewenstein, Y., Mahon, S., Chadderton, P., Kitamura, K., Sompolinsky, H., Yarom, Y., & Häusser, M. (2005). Bistability of cerebellar Purkinje cells modulated by sensory stimulation. *Nature Neuroscience*, *8*(2), 202–211. http://doi.org/10.1038/nn1393

Lorincz, A., & Nusser, Z. (2008). Cell-type-dependent molecular composition of the axon initial segment. *The Journal of Neuroscience : The Official Journal of the Society for Neuroscience*, *28*(53), 14329–40. http://doi.org/10.1523/JNEUROSCI.4833-08.2008

Luján, R., Albasanz, J. L., Shigemoto, R., & Juiz, J. M. (2005). Preferential localization of the hyperpolarization-activated cyclic nucleotide-gated cation channel subunit HCN1 in basket cell terminals of the rat cerebellum. *European Journal of Neuroscience*, *21*(8), 2073–2082. http://doi.org/10.1111/j.1460-9568.2005.04043.x

Luque, N. R., Garrido, J. A., Carrillo, R. R., Tolu, S., & Ros, E. (2011). Adaptive Cerebellar Spiking Model Embedded in the Control Loop: Context Switching and Robustness against Noise. *International Journal of Neural Systems*, *21*(5), 385–401. http://doi.org/10.1142/S0129065711002900

Luque, N. R., Garrido, J. A., Naveros, F., Carrillo, R. R., D'Angelo, E., & Ros, E. (2016). Distributed Cerebellar Motor Learning: A Spike-Timing-Dependent Plasticity Model. *Frontiers in Computational Neuroscience*, *10*(March), 1–22. http://doi.org/10.3389/fncom.2016.00017

Luque, N. R., Garrido, J. A., Carrillo, R. R., Coenen, O. J.-M. D., & Ros, E. (2011). Cerebellarlike corrective model inference engine for manipulation tasks. *IEEE Transactions on Systems, Man,*

and Cybernetics. Part B, Cybernetics : A Publication of the IEEE Systems, Man, and Cybernetics Society, *41*(5), 1299–312. http://doi.org/10.1109/TSMCB.2011.2138693

Luthman, J., Hoebeek, F. E., Maex, R., Davey, N., Adams, R., De Zeeuw, C. I., & Steuber, V. (2011). STD-dependent and independent encoding of input irregularity as spike rate in a computational model of a cerebellar nucleus neuron. *Cerebellum (London, England)*, *10*(4), 667–82. http://doi.org/10.1007/s12311-011-0295-9

Lynch, E. P., & Houghton, C. J. (2013). Modelling cerebellar Purkinje cells with simple neuron models of the threshold type. *BMC Neuroscience*, *14*(Suppl 1), P174. http://doi.org/10.1186/1471-2202-14-S1-P174

Maex, R., & De Schutter, E. (1998). Synchronization of golgi and granule cell firing in a detailed network model of the cerebellar granule cell layer. *Journal of Neurophysiology*, *80*(5), 2521–37.

Mann-Metzer, P., & Yarom, Y. (1999). Electrotonic coupling interacts with intrinsic properties to generate synchronized activity in cerebellar networks of inhibitory interneurons. *The Journal of Neuroscience : The Official Journal of the Society for Neuroscience*, *19*(9), 3298–306.

Markram, H., Muller, E., Ramaswamy, S., Reimann, M. W., Abdellah, M., Sanchez, C. A. Schurrmann, F. (2015). Reconstruction and Simulation of Neocortical Microcircuitry. *Cell*, *163*(2), 456–492. http://doi.org/10.1016/j.cell.2015.09.029

Marr, B. Y. D. (1969). A theory of cerebellar cortex. *J Physiol*, *202*, 437–470.

Maskery, S., & Shinbrot, T. (2005). Deterministic and stochastic elements of axonal guidance. *Annual Review of Biomedical Engineering*, *7*, 187–221. http://doi.org/10.1146/annurev.bioeng.7.060804.100446

Masoli, S., Solinas, S., & D'Angelo, E. (2015). Action potential processing in a detailed Purkinje cell model reveals a critical role for axonal compartmentalization. *Frontiers in Cellular Neuroscience*, *9*. http://doi.org/10.3389/fncel.2015.00047

Masoli, S., Rizza, M. F., Sgritta, M., Van Geit, W., Schürmann, F., and D'Angelo, E. (2017). Single Neuron Optimization as a Basis for Accurate Biophysical Modeling: The Case of Cerebellar Granule Cells. *Front. Cell. Neurosci.* 11, 1–14. doi:10.3389/fncel.2017.00071

Masoli, S., and D'Angelo, E. (2017). Synaptic Activation of a Detailed Purkinje Cell Model Predicts Voltage-Dependent Control of Burst-Pause Responses in Active Dendrites. 11, 1–18. doi:10.3389/fncel.2017.00278

Maxeiner, S., Krüger, O., Schilling, K., Traub, O., Urschel, S., & Willecke, K. (2003). Spatiotemporal transcription of connexin45 during brain development results in neuronal expression in adult mice. *Neuroscience*, *119*(3), 689–700. http://doi.org/10.1016/S0306-4522 (03)00077-0

McKay, B. E., & Turner, R. W. (2005). Physiological and morphological development of the rat cerebellar Purkinje cell. *The Journal of Physiology*, *567*(Pt 3), 829–50. http://doi.org/10.1113/jphysiol.2005.089383

McLean, D. R., van Ooyen, A., & Graham, B. P. (2004). Continuum model for tubulin-driven neurite elongation. *Neurocomputing*, *58–60*, 511–516. http://doi.org/10.1016/j.neucom.2004.01.088

Medina, J. F., Garcia, K. S., Nores, W. L., Taylor, N. M., & Mauk, M. D. (2000). Timing mechanisms in the cerebellum: testing predictions of a large-scale computer simulation. *The Journal of Neuroscience : The Official Journal of the Society for Neuroscience*, *20*(14), 5516–25.

Medina, J. F., Garcia, K. S., Nores, W. L., Taylor, N. M., & Mauk, M. D. (2000). Timing mechanisms in the cerebellum: testing predictions of a large-scale computer simulation. *The Journal of Neuroscience : The Official Journal of the Society for Neuroscience*, *20*(14), 5516–5525. http://doi.org/20/14/5516 [pii]

Medina, J. F., & Mauk, M. D. (2000). Computer simulation of cerebellar information processing. *Nature Neuroscience*, *3 Suppl*, 1205–11. http://doi.org/10.1038/81486

Medina, J. F., & Mauk, M. D. (2000). Computer simulation of cerebellar information processing. *Nature Neuroscience*, *3 Suppl*, 1205–1211. http://doi.org/10.1038/81486

Meineke, F. A., Potten, C. S., & Loeffler, M. (2001). Cell migration and organization in the intestinal crypt using a lattice-free model. *Cell Proliferation*, *34*(4), 253–66.

Miceli, F., Vargas, E., Bezanilla, F., & Taglialatela, M. (2012). Gating currents from Kv7 channels carrying neuronal hyperexcitability mutations in the voltage-sensing domain. *Biophysical Journal*, *102*(6), 1372–1382. http://doi.org/10.1016/j.bpj.2012.02.004

Milligan, C. J., Edwards, I. J., & Deuchars, J. (2006). HCN1 ion channel immunoreactivity in spinal cord and medulla oblongata. *Brain Research*, *1081*(1), 79–91. http://doi.org/10.1016/j.brainres.2006.01.019

Mirams, G. R., Arthurs, C. J., Bernabeu, M. O., Bordas, R., Cooper, J., Corrias, A., Gavaghan, D. J. (2013). Chaste: An Open Source C++ Library for Computational Physiology and Biology. *PLoS Computational Biology*, *9*(3), e1002970. http://doi.org/10.1371/journal.pcbi.1002970

Mirdamadi, J. L. (2016). Cerebellar role in Parkinson's disease. *J. Neurophysiol.* 116, 917–919. doi:10.1152/jn.01132.2015.

Mogilner, A., & Edelstein-Keshet, L. (2002). Regulation of actin dynamics in rapidly moving cells: a quantitative analysis. *Biophysical Journal*, *83*(3), 1237–58. http://doi.org/10.1016/S0006-3495(02)73897-6

Molineux, M. L., Fernandez, F. R., Mehaffey, W. H., & Turner, R. W. (2005). A-type and T-type currents interact to produce a novel spike latency-voltage relationship in cerebellar stellate cells. *The Journal of Neuroscience : The Official Journal of the Society for Neuroscience*, *25*(47), 10863–73. http://doi.org/10.1523/JNEUROSCI.3436-05.2005

Montes, J., Gomez, E., Merchán-Pérez, A., DeFelipe, J., & Peña, J.-M. (2013). A Machine Learning Method for the Prediction of Receptor Activation in the Simulation of Synapses. *PLoS ONE*, *8*(7), e68888. http://doi.org/10.1371/journal.pone.0068888

Mugnaini, E., & Floris, A. (1994). The unipolar brush cell: a neglected neuron of the mammalian cerebellar cortex. *The Journal of Comparative Neurology*, *339*(2), 174–80. http://doi.org/10.1002/cne.903390203

Nguyen, H., Dayan, P., Pujic, Z., Cooper-White, J., & Goodhill, G. J. (2016). A mathematical model explains saturating axon guidance responses to molecular gradients. *eLife*, *5*. http://doi.org/10.7554/eLife.12248

Nieus, T. R., Mapelli, L., & D'Angelo, E. (2014). Regulation of output spike patterns by phasic inhibition in cerebellar granule cells. *Frontiers in Cellular Neuroscience*, *8*(August), 246. http://doi.org/10.3389/fncel.2014.00246

Nieus, T., Sola, E., Mapelli, J., Saftenku, E., Rossi, P., & D'Angelo, E. (2006). LTP regulates burst initiation and frequency at mossy fiber-granule cell synapses of rat cerebellum: experimental observations and theoretical predictions. *Journal of Neurophysiology*, *95*(2), 686–99. http://doi.org/10.1152/jn.00696.2005

O'Toole, M., Lamoureux, P., & Miller, K. E. (2008). A Physical Model of Axonal Elongation: Force, Viscosity, and Adhesions Govern the Mode of Outgrowth. *Biophysical Journal*, *94*(7), 2610–2620. http://doi.org/10.1529/biophysj.107.117424

O'Brien, E. T., Salmon, E. D., & Erickson, H. P. (1997). How calcium causes microtubule depolymerization. *Cell Motility and the Cytoskeleton*, *36*(2), 125–135. http://doi.org/10.1002/(SICI)1097-0169(1997)36:2<125::AID-CM3>3.0.CO;2-8

O'Brien, J., & Unwin, N. (2006). Organization of spines on the dendrites of Purkinje cells. *Proceedings of the National Academy of Sciences of the United States of America*, *103*(5), 1575–80. http://doi.org/10.1073/pnas.0507884103

Oldfield, C. S., Marty, A., & Stell, B. M. (2010). Interneurons of the cerebellar cortex toggle Purkinje cells between up and down states. *Proceedings of the National Academy of Sciences*, *107*(29), 13153–13158. http://doi.org/10.1073/pnas.1002082107

Orduz, D., & Llano, I. (2007). Recurrent axon collaterals underlie facilitating synapses between cerebellar Purkinje cells. *Proceedings of the National Academy of Sciences*, *104*(45), 17831–17836. http://doi.org/10.1073/pnas.0707489104

Painter, K. J. (2009). Modelling cell migration strategies in the extracellular matrix. *Journal of Mathematical Biology*, *58*(4–5), 511–43. http://doi.org/10.1007/s00285-008-0217-8

Palay, S. L., & Chan-Palay, V. (1974). *Cerebellar Cortex*. Berlin, Heidelberg: Springer Berlin Heidelberg. http://doi.org/10.1007/978-3-642-65581-4

Pan, Z., Kao, T., Horvath, Z., Lemos, J., Sul, J., Cranstoun, S. D., Cooper, E. C. (2006). A Common Ankyrin-G-Based Mechanism Retains KCNQ and Na V Channels at Electrically Active Domains of the Axon. *Cell*, *26*(10), 2599–2613. http://doi.org/10.1523/JNEUROSCI.4314-05.2006

Panda, S., and Padhy, N. P. (2008). Comparison of particle swarm optimization and genetic algorithm for FACTS-based controller design. *Appl. Soft Comput. J.* 8, 543–551

Park, Y.-G., Park, H.-Y., Lee, C. J., Choi, S., Jo, S., Choi, H., Kim, D. (2010). CaV3.1 is a tremor rhythm pacemaker in the inferior olive. *Proceedings of the National Academy of Sciences of the United States of America*, *107*(23), 10731–6. http://doi.org/10.1073/pnas.1002995107

Patel, R. R., Barbosa, C., Xiao, Y., & Cummins, T. R. (2015). Human Nav1.6 Channels Generate Larger Resurgent Currents than Human Nav1.1 Channels, but the Navβ4 Peptide Does Not Protect Either Isoform from Use-Dependent Reduction. *PLOS ONE*, *10*(7), e0133485. http://doi.org/10.1371/journal.pone.0133485

Pearson, Yanthe E. Emilio Castronovo, E., Lindsley, T. A., & Drew, D. A. (2011). Mathematical Modeling of Axonal Formation Part I: Geometry. In *Bulletin of Mathematical Biology*.

Perney, T. M., Marshall, J., Martin, K. A., Hockfield, S., & Kaczmarek, L. K. (1992). Expression of the mRNAs for the Kv3.1 potassium channel gene in the adult and developing rat brain. *Journal of Neurophysiology*, *68*(3), 756–66.

Pfeil, T., Grübl, A., Jeltsch, S., Müller, E., Müller, P., Petrovici, M. A.,Meier, K. (2013). Six networks on a universal neuromorphic computing substrate. *Frontiers in Neuroscience*, (7 FEB). http://doi.org/10.3389/fnins.2013.00011

Pitt-Francis, J., Pathmanathan, P., Bernabeu, M. O., Bordas, R., Cooper, J., Fletcher, A. G. Gavaghan, D. J. (2009). Chaste: A test-driven approach to software development for biological modelling. *Computer Physics Communications*, *180*(12), 2452–2471. http://doi.org/10.1016/j.cpc.2009.07.019

Porrill, J., Dean, P., & Anderson, S. R. (2013). Adaptive filters and internal models: Multilevel description of cerebellar function. *Neural Networks*, *47*, 134–149. http://doi.org/10.1016/j.neunet.2012.12.005

Pouzat, C., & Hestrin, S. (1997). Developmental regulation of basket/stellate cell-->Purkinje cell synapses in the cerebellum. *The Journal of Neuroscience : The Official Journal of the Society for Neuroscience*, *17*(23), 9104–12.

Pouzat, C., & Hestrin, S. (1997). Developmental regulation of basket/stellate cell-->Purkinje cell synapses in the cerebellum. *The Journal of Neuroscience : The Official Journal of the Society for Neuroscience*, *17*(23), 9104–12.

Quiroga, R. Q., & Panzeri, S. (2009). Extracting information from neuronal populations: information theory and decoding approaches. *Nat. Rev. Neurosci.* 10.3.

Raman, I. M., & Bean, B. P. (1999). Ionic currents underlying spontaneous action potentials in isolated cerebellar Purkinje neurons. *The Journal of Neuroscience : The Official Journal of the Society for Neuroscience*, *19*(5), 1663–74.

Raman, I. M., & Bean, B. P. (2001). Inactivation and recovery of sodium currents in cerebellar Purkinje neurons: evidence for two mechanisms. *Biophysical Journal*, *80*(2), 729–737.

Ramirez, J. E., & Stell, B. M. (2016). Calcium Imaging Reveals Coordinated Simple Spike Pauses in Populations of Cerebellar Purkinje Cells. *Cell Reports*, *17*(12), 3125–3132. http://doi.org/10.1016/j.celrep.2016.11.075

Ray, S., & Bhalla, U. S. (2008). PyMOOSE: Interoperable Scripting in Python for MOOSE. *Frontiers in Neuroinformatics*, *2*(December), 6. http://doi.org/10.3389/neuro.11.006.2008

Reyes-Sierra, M., and Coello, C. A. C. (2006). Multi-Objective Particle Swarm Optimizers : A Survey of the State-of-the-Art. *Int. J. Comput. Intell. Res.* 2, 287–308. doi:10.5019/j.ijcir.2006.68

Roberts, A., Conte, D., Hull, M., Merrison-Hort, R., Al Azad, A. K., Buhl, E., Soffe, S. R. (2014). Can simple rules control development of a pioneer vertebrate neuronal network generating behavior? *The Journal of Neuroscience : The Official Journal of the Society for Neuroscience*, *34*(2), 608–21. http://doi.org/10.1523/JNEUROSCI.3248-13.2014

Rosenmund, C., Feltz, a, and Westbrook, G. L. (1995). Synaptic NMDA receptor channels have a low open probability. *J. Neurosci.* 15, 2788–2795

Rossi, D. J., Hamann, M., & Attwell, D. (2003). Multiple modes of GABAergic inhibition of rat cerebellar granule cells. *The Journal of Physiology*, *548*(Pt 1), 97–110. http://doi.org/10.1113/jphysiol.2002.036459

Rossi, P., Sola, E., Taglietti, V., Borchardt, T., Steigerwald, F., Utvik, J. K., et al. (2002). NMDA receptor 2 (NR2) C-terminal control of NR open probability regulates synaptic transmission and plasticity at a cerebellar synapse. *J Neurosci* 22, 9687–9697. doi:22/22/9687

Rowan, M. J. M., Tranquil, E., & Christie, J. M. (2014). Distinct Kv channel subtypes contribute to differences in spike signaling properties in the axon initial segment and presynaptic boutons of cerebellar interneurons. *The Journal of Neuroscience : The Official Journal of the Society for Neuroscience*, *34*(19), 6611–23. http://doi.org/10.1523/JNEUROSCI.4208-13.2014

Ruppersberg, J. P., Kitzing, E. v., and Schoepfer, R. (1994). The mechanism of magnesium block of NMDA receptors. *Semin. Neurosci.* 6, 87–96. doi:10.1006/smns.1994.1012

Saftenku, E. È. (2005). Modeling of slow glutamate diffusion and AMPA receptor activation in the cerebellar glomerulus. *J. Theor. Biol.* 234, 363–382. doi:10.1016/j.jtbi.2004.11.036

Sassoè-Pognetto, M., & Patrizi, A. (2013). Development of Glutamatergic and GABAergic Synapses. In *Handbook of the Cerebellum and Cerebellar Disorders* (pp. 237–255). Dordrecht: Springer Netherlands. http://doi.org/10.1007/978-94-007-1333-8_12

Sato, T., Joyner, A. L., & Nakamura, H. (2004). How does Fgf signaling from the isthmic organizer induce midbrain and cerebellum development? *Development, Growth & Differentiation*, *46*(6), 487–94. http://doi.org/10.1111/j.1440-169x.2004.00769.x

Schaller, G., & Meyer-Hermann, M. (2005). Multicellular tumor spheroid in an off-lattice Voronoi-Delaunay cell model. *Physical Review E*, *71*(5), 51910. http://doi.org/10.1103/PhysRevE.71.051910

Schaller, K., & Caldwell, J. (2003). Expression and distribution of voltage-gated sodium channels in the cerebellum. *The Cerebellum*, *2*(1), 2–9. http://doi.org/10.1080/14734220309424

Schlitt, T., & Brazma, A. (2007). Current approaches to gene regulatory network modelling. *BMC Bioinformatics*, *8*(Suppl 6), S9. http://doi.org/10.1186/1471-2105-8-S6-S9

Schlüter, D. K., Ramis-Conde, I., & Chaplain, M. A. J. (2012). Computational Modeling of Single-Cell Migration: The Leading Role of Extracellular Matrix Fibers. *Biophysical Journal*, *103*(6), 1141–1151. http://doi.org/10.1016/j.bpj.2012.07.048

Schonewille, M., Khosrovani, S., Winkelman, B. H. J., Hoebeek, F. E., De Jeu, M. T. G., Larsen, I. M., … De Zeeuw, C. I. (2006). Purkinje cells in awake behaving animals operate at the upstate membrane potential. *Nature Neuroscience*, *9*(4), 459–461. http://doi.org/10.1038/nn0406-459

Schweighofer, N., Arbib, M. A., & Kawato, M. (1998). Role of the cerebellum in reaching movements in humans. I. Distributed inverse dynamics control. *The European Journal of Neuroscience*, *10*(1), 86–94.

Scianna, M., & Preziosi, L. (2012). Multiscale Developments of the Cellular Potts Model. *Multiscale Modeling & Simulation*, *10*(2), 342–382. http://doi.org/10.1137/100812951

Seeley, T. D. (1989). The Honey Bee Colony as a Superorganism. *American Scientist*, *77*(6), 546.

Seok, J., Warren, H. S., Cuenca, A. G., Mindrinos, M. N., Baker, H. V., Xu, W., Tompkins, R. G. (2013). Genomic responses in mouse models poorly mimic human inflammatory diseases. *Proceedings of the National Academy of Sciences*, *110*(9), 3507–3512. http://doi.org/10.1073/pnas.1222878110

Serôdio, P., & Rudy, B. (1998). Differential expression of Kv4 K+ channel subunits mediating subthreshold transient K+ (A-type) currents in rat brain. *Journal of Neurophysiology*, *79*(2), 1081–91.

Setty, Y., Chen, C.-C., Secrier, M., Skoblov, N., Kalamatianos, D., & Emmott, S. (2011). How neurons migrate: a dynamic in-silico model of neuronal migration in the developing cortex. *BMC Systems Biology*, *5*(1), 154. http://doi.org/10.1186/1752-0509-5-154

Setty, Y., Cohen, I. R., Dor, Y., & Harel, D. (2008). Four-dimensional realistic modeling of pancreatic organogenesis. *Proceedings of the National Academy of Sciences of the United States of America*, *105*(51), 20374–9. http://doi.org/10.1073/pnas.0808725105

Setty, Y., Dalfó, D., Korta, D. Z., Hubbard, E. J. A., & Kugler, H. (2012). A model of stem cell population dynamics: in silico analysis and in vivo validation. *Development (Cambridge, England)*, *139*(1), 47–56. http://doi.org/10.1242/dev.067512

Shannon, P. (2003). Cytoscape: A Software Environment for Integrated Models of Biomolecular Interaction Networks. *Genome Research*, *13*(11), 2498–2504. http://doi.org/10.1101/gr.1239303

Shinbrot, T. (2006). Simulated morphogenesis of developmental folds due to proliferative pressure. *Journal of Theoretical Biology*, *242*(3), 764–773. http://doi.org/10.1016/j.jtbi.2006.04.021

Sillitoe, R. V., Chung, S.-H., Fritschy, J.-M., Hoy, M., & Hawkes, R. (2008). Golgi Cell Dendrites Are Restricted by Purkinje Cell Stripe Boundaries in the Adult Mouse Cerebellar Cortex. *Journal of Neuroscience*, *28*(11), 2820–2826. http://doi.org/10.1523/JNEUROSCI.4145-07.2008

Simat, M., Parpan, F., & Fritschy, J.-M. (2007). Heterogeneity of glycinergic and gabaergic interneurons in the granule cell layer of mouse cerebellum. *The Journal of Comparative Neurology*, *500*(1), 71–83. http://doi.org/10.1002/cne.21142

Simms, B. A., and Zamponi, G. W. (2014). Neuronal voltage-gated calcium channels: Structure, function, and dysfunction. *Neuron* 82, 24–45. doi:10.1016/j.neuron.2014.03.016

Sjöbeck, M., and Englund, E. (2001). Alzheimer's disease and the cerebellum: a morphologic study on neuronal and glial changes. *Dement. Geriatr. Cogn. Disord.* 12, 211–8. doi:51260

Smallwood, R. H., Holcombe, W. M. L., & Walker, D. C. (2004). Development and validation of computational models of cellular interaction. *Journal of Molecular Histology*, *35*(7), 659–65. http://doi.org/10.1007/s10735-004-2660-1

Söhl, G., Maxeiner, S., & Willecke, K. (2005). Expression and functions of neuronal gap junctions. *Nature Reviews. Neuroscience*, *6*(3), 191–200. http://doi.org/10.1038/nrn1627

Solinas, S., Forti, L., Cesana, E., Mapelli, J., De Schutter, E., & D'Angelo, E. (2007). Computational reconstruction of pacemaking and intrinsic electroresponsiveness in cerebellar Golgi cells. *Frontiers in Cellular Neuroscience*, *1*, 2. http://doi.org/10.3389/neuro.03.002.2007

Solinas, S., Forti, L., Cesana, E., Mapelli, J., De Schutter, E., & D'Angelo, E. (2007). Fast-reset of pacemaking and theta-frequency resonance patterns in cerebellar golgi cells: simulations of their impact in vivo. *Frontiers in Cellular Neuroscience*, *1*, 4. http://doi.org/10.3389/neuro.03.004.2007

Solinas, S., Nieus, T., & D'Angelo, E. (2010). A realistic large-scale model of the cerebellum granular layer predicts circuit spatio-temporal filtering properties. *Frontiers in Cellular Neuroscience*, *4*, 12. http://doi.org/10.3389/fncel.2010.00012

Sotelo, C., Llinás, R., Port-royal, H. De, Animale, L. D. B., Sciences, F., & City, I. (1972). Specialized membrane junctions between neurons in the vertebrate cerebellar cortex. *The Journal of Cell Biology*, *53*(2), 271–89. http://doi.org/10.1083/jcb.53.2.271

Sotelo, C. (2004). Cellular and genetic regulation of the development of the cerebellar system. *Progress in Neurobiology*, *72*(5), 295–339. http://doi.org/10.1016/j.pneurobio.2004.03.004

Sotelo, C., & Rossi, F. (2013). Purkinje Cell Migration and Differentiation. In *Handbook of the Cerebellum and Cerebellar Disorders* (pp. 147–178). Dordrecht: Springer Netherlands. http://doi.org/10.1007/978-94-007-1333-8_9

Stepanyants, A., Hof, P. R., & Chklovskii, D. B. (2002). Geometry and structural plasticity of synaptic connectivity. *Neuron*, *34*(2), 275–288. http://doi.org/10.1016/S0896-6273 (02)00652-9

Steuber, V., Mittmann, W., Hoebeek, F. E., Silver, R. A., De Zeeuw, C. I., Häusser, M., & De Schutter, E. (2007). Cerebellar LTD and Pattern Recognition by Purkinje Cells. *Neuron*, *54*(1), 121–136. http://doi.org/10.1016/j.neuron.2007.03.015

Steuber, V., Schultheiss, N. W., Silver, R. A., De Schutter, E., & Jaeger, D. (2011). Determinants of synaptic integration and heterogeneity in rebound firing explored with data-driven models of deep cerebellar nucleus cells. *Journal of Computational Neuroscience*, *30*(3), 633–58. http://doi.org/10.1007/s10827-010-0282-z

Stiles, J., & Bartol, T. (2001). Monte Carlo methods for simulating realistic synaptic microphysiology using MCell. In E. De Schutter (Ed.), *Computational Neuroscience: Realistic Modeling for Experimentalists* (CRC Press, pp. 87–127).

Stocker, M., & Pedarzani, P. (2000). Differential distribution of three Ca(2+)-activated K(+) channel subunits, SK1, SK2, and SK3, in the adult rat central nervous system. *Molecular and Cellular Neurosciences*, *15*(5), 476–493. http://doi.org/10.1006/mcne.2000.0842

Stonehouse, a H., Pringle, J. H., Norman, R. I., Stanfield, P. R., Conley, E. C., & Brammar, W. J. (1999). Characterisation of Kir2.0 proteins in the rat cerebellum and hippocampus by polyclonal antibodies. *Histochemistry and Cell Biology*, *112*(6), 457–465. http://doi.org/10.1007/s004180050429

Subramaniyam, S., Solinas, S., Perin, P., Locatelli, F., Masetto, S., & D'Angelo, E. (2014). Computational modeling predicts the ionic mechanism of late-onset responses in unipolar brush cells. *Frontiers in Cellular Neuroscience*, *8*, 237. http://doi.org/10.3389/fncel.2014.00237

Sutherland, D. J., Pujic, Z., & Goodhill, G. J. (2014). Calcium signaling in axon guidance. *Trends in Neurosciences*, *37*(8), 424–32. http://doi.org/10.1016/j.tins.2014.05.008

Swat, M. H., Thomas, G. L., Belmonte, J. M., Shirinifard, A., Hmeljak, D., & Glazier, J. A. (2012). Multi-scale modeling of tissues using CompuCell3D. *Methods in Cell Biology*, *110*, 325–66. http://doi.org/10.1016/B978-0-12-388403-9.00013-8

Swensen, A. M., & Bean, B. P. (2005). Robustness of burst firing in dissociated purkinje neurons with acute or long-term reductions in sodium conductance. *The Journal of Neuroscience : The Official Journal of the Society for Neuroscience*, *25*(14), 3509–20. http://doi.org/10.1523/JNEUROSCI.3929-04.2005

Szapiro, G., & Barbour, B. (2007). Multiple climbing fibers signal to molecular layer interneurons exclusively via glutamate spillover. *Nature Neuroscience*, *10*(6), 735–42. http://doi.org/10.1038/nn1907

Szoboszlay, M., Lőrincz, A., Lanore, F., Vervaeke, K., Silver, R. A., & Nusser, Z. (2016). Functional Properties of Dendritic Gap Junctions in Cerebellar Golgi Cells. *Neuron*, *90*(5), 1043–1056. http://doi.org/10.1016/j.neuron.2016.03.029

Tamada, A., Kumada, T., Zhu, Y., Matsumoto, T., Hatanaka, Y., Muguruma, K., … Murakami, F. (2008). Crucial roles of Robo proteins in midline crossing of cerebellofugal axons and lack of their up-regulation after midline crossing. *Neural Development*, *3*(1), 29. http://doi.org/10.1186/1749-8104-3-29

Torben-Nielsen, B., Segev, I., & Yarom, Y. (2012). The generation of phase differences and frequency changes in a network model of inferior olive subthreshold oscillations. *PLoS Computational Biology*, *8*(7), e1002580. http://doi.org/10.1371/journal.pcbi.1002580

Toriyama, M., Sakumura, Y., Shimada, T., Ishii, S., & Inagaki, N. (2010). A diffusion-based neurite length-sensing mechanism involved in neuronal symmetry breaking. *Molecular Systems Biology*, *6*. http://doi.org/10.1038/msb.2010.51

Tsodyks, M., Pawelzik, K., & Markram, H. (1998). Neural networks with dynamic synapses. *Neural Computation*, *10*(4), 821–835. http://doi.org/10.1162/089976698300017502

Tsodyks, M., Uziel, a, and Markram, H. (2000). Synchrony generation in recurrent networks with frequency-dependent synapses. *J. Neurosci.* 20, RC50. doi:Artn Rc50

Turner, R. W., & Zamponi, G. W. (2014). T-type channels buddy up. *Pflügers Archiv : European Journal of Physiology*, *466*(4), 661–75. http://doi.org/10.1007/s00424-013-1434-6

Tyrrell, T., & Willshaw, D. (1992). Cerebellar cortex: its simulation and the relevance of Marr's theory. *Philosophical Transactions of the Royal Society of London. Series B, Biological Sciences*, *336*(1277), 239–57. http://doi.org/10.1098/rstb.1992.0059

Uesaka, N., Uchigashima, M., Mikuni, T., Nakazawa, T., Nakao, H., Hirai, H., Kano, M. (2014). Retrograde semaphorin signaling regulates synapse elimination in the developing mouse brain. *Science (New York, N.Y.)*, *344*(6187), 1020–3. http://doi.org/10.1126/science.1252514

Valera, A. M., Binda, F., Pawlowski, S. A., Dupont, J.-L., Casella, J.-F., Rothstein, J. D., Isope, P. (2016). Stereotyped spatial patterns of functional synaptic connectivity in the cerebellar cortex. *eLife*, *5*. http://doi.org/10.7554/eLife.09862

Van Der Giessen, R. S., Maxeiner, S., French, P. J., Willecke, K., & De Zeeuw, C. I. (2006). Spatiotemporal distribution of Connexin45 in the olivocerebellar system. *The Journal of Comparative Neurology*, *495*(2), 173–184. http://doi.org/10.1002/cne.20873

Van Geit, W., De Schutter, E., & Achard, P. (2008). Automated neuron model optimization techniques: a review. *Biological Cybernetics*, *99*(4–5), 241–51. http://doi.org/10.1007/s00422-008-0257-6

Van Geit, W., Achard, P., & De Schutter, E. (2007). Neurofitter: A parameter-tuning package for a wide range of electrophysiological neuron models. *Frontiers in Neuroinformatics*, *1*. http://doi.org/10.3389/neuro.11.001.2007

Van Geit, W., Gevaert, M., Chindemi, G., Rössert, C., Courcol, J.-D., Muller, E. B., Markram, H. (2016). BluePyOpt: Leveraging Open Source Software and Cloud Infrastructure to Optimise Model Parameters in Neuroscience. *Frontiers in Neuroinformatics*, *10*. http://doi.org/10.3389/fninf.2016.00017

Van Geit, W. (2015). BlueBrainProject. eFEL. Available on line at: https://github.com/BlueBrain/eFEL (AccessedFebruary16,2016)

van Ooyen, A., & Willshaw, D. J. (1999). Competition for neurotrophic factor in the development of nerve connections. *Proceedings. Biological Sciences / The Royal Society*, *266*(1422), 883–92. http://doi.org/10.1098/rspb.1999.0719

van Ooyen, A. (2011). Using theoretical models to analyse neural development. *Nature Reviews. Neuroscience*, *12*(6), 311–326. http://doi.org/10.1038/nrn3031

van Ooyen, A. (2003). *Modeling Neural Development* (The MIT Pr).

van Pelt, J., & Uylings, H. (2005). Natural Variability in the Geometry of Dendritic Branching Patterns. In *Modeling in the Neurosciences*. CRC Press. http://doi.org/10.1201/9780203390979.ch5

Vervaeke, K., LÖrincz, A., Gleeson, P., Farinella, M., Nusser, Z., & Silver, R. A. (2010). Rapid Desynchronization of an Electrically Coupled Interneuron Network with Sparse Excitatory Synaptic Input. *Neuron*, *67*(3), 435–451. http://doi.org/10.1016/j.neuron.2010.06.028

Walker, D. C., Hill, G., Wood, S. M., Smallwood, R. H., & Southgate, J. (2004). Agent-based computational modeling of wounded epithelial cell monolayers. *IEEE Transactions on Nanobioscience*, *3*(3), 153–63.

Wang, V. Y., & Zoghbi, H. Y. (2001). Genetic regulation of cerebellar development. *Nature Reviews. Neuroscience*, *2*(7), 484–91. http://doi.org/10.1038/35081558

Wassef, M. (2013). Specification of the Cerebellar Territory. In *Handbook of the Cerebellum and Cerebellar Disorders,*. http://doi.org/0.1007/978-94-007-1333-8_4,

Weiser, M., Vega-Saenz de Miera, E., Kentros, C., Moreno, H., Franzen, L., Hillman, D., Rudy, B. (1994). Differential expression of Shaw-related K+ channels in the rat central nervous system. *The Journal of Neuroscience : The Official Journal of the Society for Neuroscience*, *14*(3 Pt 1), 949–72.

Weisheit, G., Gliem, M., Endl, E., Pfeffer, P. L., Busslinger, M., & Schilling, K. (2006). Postnatal development of the murine cerebellar cortex: formation and early dispersal of basket, stellate and Golgi neurons. *The European Journal of Neuroscience*, *24*(2), 466–78. http://doi.org/10.1111/j.1460-9568.2006.04915.x

White, J. J., & Sillitoe, R. V. (2013). Development of the cerebellum: from gene expression patterns to circuit maps. *Wiley Interdisciplinary Reviews: Developmental Biology*, *2*(1), 149–164. http://doi.org/10.1002/wdev.65

Wingate, R. J., & Hatten, M. E. (1999). The role of the rhombic lip in avian cerebellum development. *Development (Cambridge, England)*, *126*(20), 4395–404.

Wolpert, D. M., Miall, R. C., & Kawato, M. (1998). Internal models in the cerebellum. *Trends in Cognitive Sciences*, *2*(9), 338–347. http://doi.org/10.1016/S1364-6613(98)01221-2

Wu, G., & Cline, H. T. (1998). Stabilization of Dendritic Arbor Structure in Vivo by CaMKII. *Science*, *279*(5348), 222–226. http://doi.org/10.1126/science.279.5348.222ù

Wu, T., and Hallett, M. (2013). The cerebellum in Parkinson's disease. *Brain* 136, 696–709. doi:10.1093/brain/aws360

Xie, C., Bondarenko, V. E., Morales, M. J., & Strauss, H. C. (2009). Closed-state inactivation in Kv4.3 isoforms is differentially modulated by protein kinase C. *AJP: Cell Physiology*, *297*(5), C1236–C1248. http://doi.org/10.1152/ajpcell.00144.2009

Xu, H., Yang, Y., Tang, X., Zhao, M., Liang, F., Xu, P., Fan, X. (2013). Bergmann Glia Function in Granule Cell Migration during Cerebellum Development. *Molecular Neurobiology*, *47*(2), 833–844. http://doi.org/10.1007/s12035-013-8405-y

Xu, J., & Clancy, C. E. (2008). Ionic Mechanisms of Endogenous Bursting in CA3 Hippocampal Pyramidal Neurons: A Model Study. *PLoS ONE*, *3*(4), e2056. http://doi.org/10.1371/journal.pone.0002056

Xu, S., & Rahmat-Samii, Y. (2007). Boundary Conditions in Particle Swarm Optimization Revisited. *IEEE Transactions on Antennas and Propagation*, *55*(3), 760–765. http://doi.org/10.1109/TAP.2007.891562

Yamada, W. M., Koch, C., & Adams, P. R. (1989). Multiple channels and calcium dynamics. In *Methods in neuronal modeling* (pp. 97–133). MIT Press Cambridge, MA, USA.

Yamazaki, T., & Igarashi, J. (2013). Realtime cerebellum: a large-scale spiking network model of the cerebellum that runs in realtime using a graphics-processing unit. *Neural Networks : The Official Journal of the International Neural Network Society*, *47*, 103–11. http://doi.org/10.1016/j.neunet.2013.01.019

Yamazaki, T., & Tanaka, S. (2009). Computational models of timing mechanisms in the cerebellar granular layer. *Cerebellum (London, England)*, *8*(4), 423–32. http://doi.org/10.1007/s12311-009-0115-7

Yarrow, S., Challis, E., and Seriès, P. (2012). Fisher and Shannon Information in Finite Neural Populations. *Neural Comput.* 24, 1740–1780. doi:10.1162/NECO_a_00292

Yartsev, M. M., Givon-Mayo, R., Maller, M., & Donchin, O. (2009). Pausing Purkinje cells in the cerebellum of the awake cat. *Frontiers in Systems Neuroscience*, *3*. http://doi.org/10.3389/neuro.06.002.2009

Yu, F. H., Yarov-Yarovoy, V., Gutman, G. A., & Catterall, W. A. (2005). Overview of molecular relationships in the voltage-gated ion channel superfamily. *Pharmacological Reviews*, *57*(4), 387–95. http://doi.org/10.1124/pr.57.4.13

Zaman, M. H., Kamm, R. D., Matsudaira, P., & Lauffenburger, D. A. (2005). Computational Model for Cell Migration in Three-Dimensional Matrices. *Biophysical Journal*, *89*(2), 1389–1397. http://doi.org/10.1529/biophysj.105.060723

Zhang, B., Chen, L. Y., Liu, X., Maxeiner, S., Lee, S., Gokce, O., & Südhof, T. C. (2015). Neuroligins Sculpt Cerebellar Purkinje-Cell Circuits by Differential Control of Distinct Classes of Synapses. *Neuron*, *87*(4), 781–796. http://doi.org/10.1016/j.neuron.2015.07.020

Zhang, L., & Goldman, J. E. (1996). Generation of cerebellar interneurons from dividing progenitors in white matter. *Neuron*, *16*(1), 47–54.

Zhou, H., Lin, Z., Voges, K., Ju, C., Gao, Z., Bosman, L. W., Schonewille, M. (2014). Cerebellar modules operate at different frequencies. *eLife*, *3*, e02536. http://doi.org/10.7554/eLife.02536

Ziebell, F., Martin-Villalba, A., & Marciniak-Czochra, A. (2014). Mathematical modelling of adult hippocampal neurogenesis: effects of altered stem cell dynamics on cell counts and bromodeoxyuridine-labelled cells. *Journal of the Royal Society Interface*, *11*(94), 20140144–20140144. http://doi.org/10.1098/rsif.2014.0144

Zitzler, E., and Künzli, S. (2004). “Indicator-Based Selection in Multiobjective Search,” in *PPSN V: Proceedings of the 5th International Conference on Parallel Problem Solving from Nature*, 832–842. doi:10.1007/978-3-540-30217-9_84

Zubler, F., & Douglas, R. (2009). A framework for modeling the growth and development of neurons and networks. *Frontiers in Computational Neuroscience*, *3*. http://doi.org/10.3389/neuro.10.025.2009

Zubler, F., Hauri, A., Pfister, S., Bauer, R., Anderson, J. C., Whatley, A. M., & Douglas, R. J. (2013). Simulating Cortical Development as a Self-Constructing Process: A Novel Multi-Scale Approach Combining Molecular and Physical Aspects. *PLoS Computational Biology*, *9*(8). http://doi.org/10.1371/journal.pcbi.1003173

Zubler, F., Hauri, A., Pfister, S., Whatley, A. M., Cook, M., & Douglas, R. (2011). An Instruction Language for Self-Construction in the Context of Neural Networks. *Frontiers in Computational Neuroscience*, *5*(December), 1–15. http://doi.org/10.3389/fncom.2011.00057